

# Topics On Nondestructive Evaluation

---

## **Topics on Nondestructive Evaluation Series**

B. Boro Djordjevic and Henrique Dos Reis, Series Editors

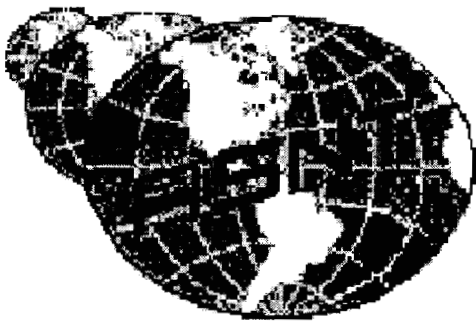
---

### **Volume 4**

## **Automation, Miniature Robotics and Sensors for Nondestructive Testing and Evaluation**

Yoseph Bar-Cohen, Technical Editor

---



**The American Society for Nondestructive Testing, Inc.**

# Table of Contents

## PREFACE

## CHAPTER 1 - INTRODUCTION - Y. Bar-Cohen, JPL

## CHAPTER 2 - ROBOTICS

2.1 Robotic Systems and Control - E. Baumgartner, JPL

2.2 Robotics Critical Technologies - Mel Siegel, CMU

## CHAPTER 3 - CRAWLERS AND PORTABLE SCANNERS

3.1 Background -Y. Bar-Cohen, JPL

3.2 Robotic crawler with open architecture -Y. Bar-Cohen and P. Backes, JPL

3.3 Inspection Crawlers - M. Siegle, CMU

3.4 Wall-climbing crawlers - T. Sattar, South Bank University, London

## CHAPTER 4 – NDE SENSORS

4.1 Overview on sensors - Y. Bar-Cohen, JPL

4.2 Optical Sensors for Enhanced Visual NDT - David Forsyth and Jerzy Komorowski, NRC, Canada

4.3 Tap Testing - M. Siegel, CMU

4.4 Eddy Current and Dielectric Imaging Sensor Arrays - Neil Goldfine and Andrew Washabaugh, Jentek Sensors

4.5 MOI Technology and Automated-Scanning Using Small Robot-Crawlers - G. L. Fitzpatrick, C. Knisely, D. K. Thome, R.L. Skaugset and W.C. L. Shih, PRI

4.6 Ultrasonic sensors for robotics and field operation - David Hsu, Iowa State University

4.7 Sensors to Monitor Manufacturing of Advanced Materials for Process Control - Suresh M. Menon, XXsys Technologies Inc., San Diego, CA

## CHAPTER 5 - ACTUATORS

5.1 Conventional motors, Shape memory alloys and ElectroRheological fluids - D. Mavroidis, C. Pfeiffer, and M. Mosley, Rutgers U.

5.2 Ultrasonic Materials, Actuators and Motors (USM) - Stewart Sheritt Y. Bar-Cohen, and Xiaoqi Bao, JPL

5.3 Electroactive polymer (EAP) Actuators - Y. Bar-Cohen, and S. Leary, JPL

## CHAPTER 6 - MINIATURIZATION AND MEMS TECHNOLOGY - C. Liu, UIUC

## CHAPTER 7 - SIGNAL PROCESSING, SENSOR FUSION AND DATA/ INFORMATION MANAGEMENT

7.1 Intelligent Sensor Models with Learning Capabilities - Ajay Mahajan, Southern Illinois University at Carbondale, Carbondale, IL

7.2 Applications of Artificial Intelligence Techniques in NDE - David Forsyth, NRC, Ottawa, Canada

7.3 Neural-Net Processing of Characteristic Patterns - Arthur J. Decker, NASA-Glenn Research Center at Lewis Field, Cleveland, Ohio

7.4 Neural Network algorithms for visual detection of cracks and corrosion - Mel Siegel, CMU

## CHAPTER 8 - DATA COMMUNICATION, DISPLAY AND REAL TIME IMAGING

- 8.1 Image processing for Non destructive Testing & Evaluation - Shaun Lawson, University of Surrey, Guildford, Surrey, England
- 8.2 Miniature Cordless/Wireless Communications - William C.L. Shih, Reza Rofougaran, PRI Research & Development Corp., Torrance, CA

## CHAPTER 9 - APPLICATIONS TO MANUFACTURING, SERVICE, FIELD AND OTHER AREAS

- 9.1 Automated NDE Systems in Aerospace Applications - Jim Chern, NASA-GSFC
- 9.2 Robotic System for Aircraft Wing Skin Inspection - Ser Yong Lim, Gintic Institute of Manufacturing Technology, Singapore, Brian Stephen Wong and Liang Mong Koh, *Nanyang Technological University, Nanyang Avenue, Singapore*
- 9.3 Robotics NDE of Steel Highway Structures and Bridges -Margarit G. Lozev, Virginia Transportation Research Council, Charlottesville, VA
- 9.4 Application of Automated NDT in Nuclear and Steel Plants - Tariq P. Sattar, South Bank University, London, England

## Chapter 10: FUTURE TRENDS IN ROBOTICS AND AUTOMATED NDE

- 10.1 ROBOTICS AND AUTOMATIC NDE - Yoseph Bar-Cohen, JPL, Pasadena, CA
- 10.2 BIOLOGICALLY INSPIRED (BI) SYSTEMS - Brett Kennedy, JPL, Pasadena, CA
- 10.3 HAPTIC INTERFACES - Yoseph Bar-Cohen, JPL, Constantinos Mavroidis, & Charles Pfeiffer, Rutgers U. and Christopher Culbert & Darby F. Magruder, NASA-JSC, TX

# CHAPTER 1: INTRODUCTION

Yoseph Bar-Cohen,  
JPL, Caltech, 4800 Oak Grove Dr., Pasadena, CA 90740  
818-354-2610, fax 818-393-4057, [yosi@jpl.nasa.gov](mailto:yosi@jpl.nasa.gov)

CHAPTER 1: INTRODUCTION.....	1
1.1 BACKGROUND.....	1
1.2 MECHANISMS OF ACQUIRING NDE DATA.....	2
1.3 THE EVOLUTION OF AUTOMATION IN NDT.....	3
1.4 MAKING AN AUTOMATIC NDT SYSTEM.....	6
1.5 AUTOMATIC INSPECTION SUPPORT TECHNOLOGIES.....	7
1.5.1 Internet - Information Highway.....	8
1.5.2 Inspection Simulation.....	8
1.5.3 Miniaturization.....	10
1.5.4 Testbed for Validation of New NDE Techniques.....	11
1.6 SUMMARY.....	11
1.7 REFERENCES.....	12

## 1.1 BACKGROUND

The development of NDE techniques has always been driven by the ongoing need for low-cost, rapid, user friendly, reliable and efficient methods of detecting and characterizing flaws as well as determining material properties. The need for such capability is relevant to the whole life cycle of components, structures, products and systems from production through service. The application of most NDE methods is easier in lab and shop conditions and is subject to great constraints when used in field conditions. Manual field inspection is labor-intensive, time consuming, demands great attention to details by the inspectors and it is subject to human errors. The interpretation of the data depends critically on the inspectors' experience, competence, attentiveness and meticulous dedication. For instance, rivet crack inspection using eddy current is known to be a mundane and painstaking task, which can lead to a significant decrease in the inspector attention during a long inspection session. Disassembly of structures for inspection in laboratory conditions offer a greater reliability of the test results, however it is costly and, in many cases, is not a practical approach. The limitations of field inspection are hampering the growth in usage of composite structures for construction of aircraft since they require more often inspection of large areas. This is due to the fact that composite structures are sensitive to impact damage, which can occur at any point and any time.

In recent years, scanners were introduced to overcome the limitations of field NDE methods, where the inspection can be performed automatically and rapidly scanning large complex-shape structures. For military aircraft, in addition to the desire to increase the speed and reliability of the inspection, there is a need in some applications to operate at harsh, hostile and/or remote conditions (extreme temperature, battlefield, remote expertise, etc.). While field inspection is associated with large structures that automation can make the process faster and more reliable, production inspection may be involved with a large volume of parts that need to be inspected

efficiently and quickly at low cost. The various issues associated with the application of automation, robotics and sensors will be discussed in this book.

## 1.2 MECHANISMS OF ACQUIRING NDE DATA

Generally, the concept of automatic NDE systems has been used in practice for many years. The term automation referred to the non-manual inspection of either a single or a plurality of parts. The contribution of automation and robotics to the various NDE methods depends on the specific technique that is involved and the associated data acquisition process. NDE methods are distinguished by the size of the area covered in a single shot data acquisition. Three groups of data acquisition can be identified and examples of sensors and inspection methods in each group as described in Table 1,

- Stationary sensing - A transducer or a probe is placed next or inside the test material and acquires data.
- Manual inspection - An operator uses remote or contact type sensors that are coupled to the test part and acquire information in the form of an A-scan.
- Scanning - This approach is involved with the covering of a test area to produce an image showing its integrity.

Visual, Radiography, Thermography, Shearography, Magnetic Particles and Liquid Penetrants are providing information about defects over the test area, where the defects size and location are presented without the need for mechanical scanning. On the other hand, sensor-base methods that include ultrasonics and eddy-current are requiring scanning in order to create a map showing the spatial distribution of defects. Otherwise, the data represents the specific location where the test was conducted and it covers a region that is the size of the probe active surface or less. For a limited area of several centimeters in size, transducer arrays can be used, which are scanned electronically for rapid imaging. Such imaging is widely used in medical ultrasonics and is not highly practical for large structures, where mechanical scanners are the preferred choice.

**Table 1:** Methods of extracting NDE information from test structures.

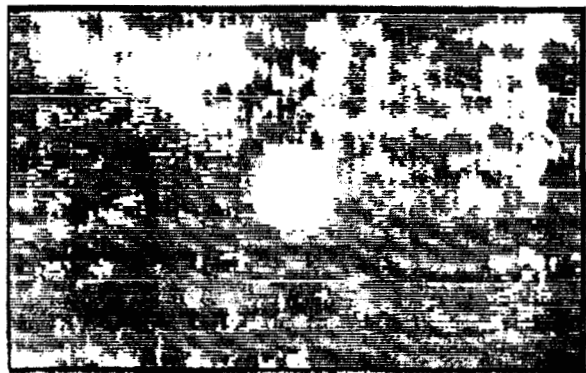
Approach	Test Method or Mechanism
Stationary sensing	<ul style="list-style-type: none"> <li>• Remote sensors - Eddy current, magnetic, visual, etc.</li> <li>• Attached sensors - Cracking fuse, resistance gauging, strain gage, acoustic emission, ultrasonic, eddy current and fiber optics.</li> <li>• Sensitive coating - Bruising paint indicator, brittle coating, liquid crystals</li> <li>• Imbedded sensors - Fiber optics, dielectric, eddy current, magnetic, ultrasonics</li> </ul>
Manual inspection	<ul style="list-style-type: none"> <li>• Most widely used methods are visual and tap testing</li> <li>• Inspector operates an NDE instrument at the test site producing the equivalent of A-Scan.</li> </ul>
Scanning	<ul style="list-style-type: none"> <li>• Imaging/viewing - Visual inspection of large area using CCD</li> <li>• Illumination - Infrared, shearography, reflection/enhancement screen (e.g., D-Sight)</li> <li>• Beam sweepers - Laser induced ultrasonic scanning</li> <li>• Mechanical scanner - Manual and mechanical B- or C-scanners</li> </ul>

- |  |  |
|--|--|
|  | <ul style="list-style-type: none"><li>● Crawlers - Miniature rover crawling over the structure</li></ul> |
|--|--|

### 1.3 THE EVOLUTION OF AUTOMATION IN NDT

Over the last four decades, scanners were developed to support ultrasonic inspections producing B-scan and C-scan images. Scanners provided detailed images of flaws size and location and they made the biggest impact on the wide use of ultrasonics. During the early days of the C-scan technology, the recorded images provided limited information that was related to the variation in amplitude of the received signals. In Figure 1-1 an example of a C-scan is shown for a graphite/epoxy laminate with a controlled 2.5-cm diameter delamination. While the delamination is visualized in a go/no-go recording format, other indications are identified and there is no sufficient data to identify the source of these indications. Further, when a scan was made with test parameters that did not provide the necessary resolution or sensitivity the inspector had to repeat the test with various conditions until acceptable recording conditions were obtained. The evolution of the computer technology that started in the 70's led to a significant improvement in data acquisition, evaluation and recording capabilities. C-scans systems in the early 80's already had the ability to process the recorded data and the image without the need to repeat the inspection, and the data included flaw depth information. The use of color graphics as well as gray scale added a great enhancement feature for flaw detection and identification. An example of a C-scan presentation in colors is shown in Figure 1-2, where an impact damage in a graphite/epoxy laminate is presented and the colors identify the depth information. Data manipulation allowed the rotation of the image in such a way that the depth distribution of the impact damage is easily visible.

**Figure 1-1:** C-scan performed in the early 70's is showing controlled flaws (middle white circle) and unexplained indications (other white areas).



**Figure 1-2:** A C-scan image produced in mid 80's showing an impact damage in a composite laminate.

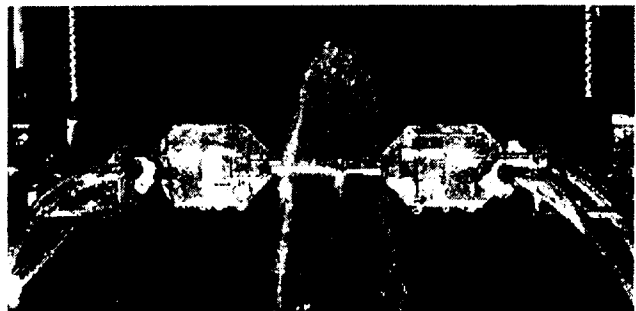


The colors provide depth information about the damage profile as illustrated by data rotation.

Since the introduction of microprocessors, various types of portable scanners were developed using such NDE methods as visual, eddy currents, ultrasonics, shearography, radiography and thermography. While most scanners have been dedicated to a single inspection method, there is an overall trend to combine the capability of more than one inspection method. Increasingly such a multi-mode option is becoming commercially available and systems, such as the MAUS (Boeing, St. Louis, MO), are offering interchangeable components to perform more than one test method [Bar-Cohen and Backes, 1999]. While not applied simultaneously yet, the leading NDE methods that are used include mostly eddy current and ultrasonics. Efforts are being made to add also visual inspection capability.

Scanners offered a form of documenting test results, providing consistent data acquisition, and automating the determination process of acceptance or rejection. Current control software allows to record data at any ratio including 1:1 as well as the examination of various ultrasonic parameters and angle views as well as enhancement of the images for better flaw detectability. The emergence of microprocessors enabled to make lab systems that are capable of contour-following complex shapes of structures and address the sensitivity of ultrasonic tests to having the beam normal to the surface. Combining precision control capability and effective squirters, which provide effective ultrasonic coupling through a water column, allowed the rapid inspection of large and complex shape structures. An example of a through transmission arrangement of water columns from squirters is shown in Figure 1-3. Such systems were made to operate in concurrence with detailed CAD drawings and to inspect as large structures as a full wing of an aircraft as shown in Figure 1-4. For a long time, the automated inspection capability of C-scans was limited to lab or shop conditions while field inspection was performed manually. As will be discussed later in this book, significant development was made in this area leading to the availability of portable field scanners. At the end of the 80's, the capability of C-scan systems as emerged in the form of eddy current scanners. Further, automatic inspection of full structures was not confined to ultrasonics and other NDE methods were automated including Neutron-Radiography and X-ray radiography. An example of such a radiographic system at the McClellan Air Force Base facility of aircraft maintenance is shown in Figure 1-5. As can be seen in this Figure, a robotic manipulator arm is maintaining the alignment of X-ray source and detector while scanning a complete aircraft wing.

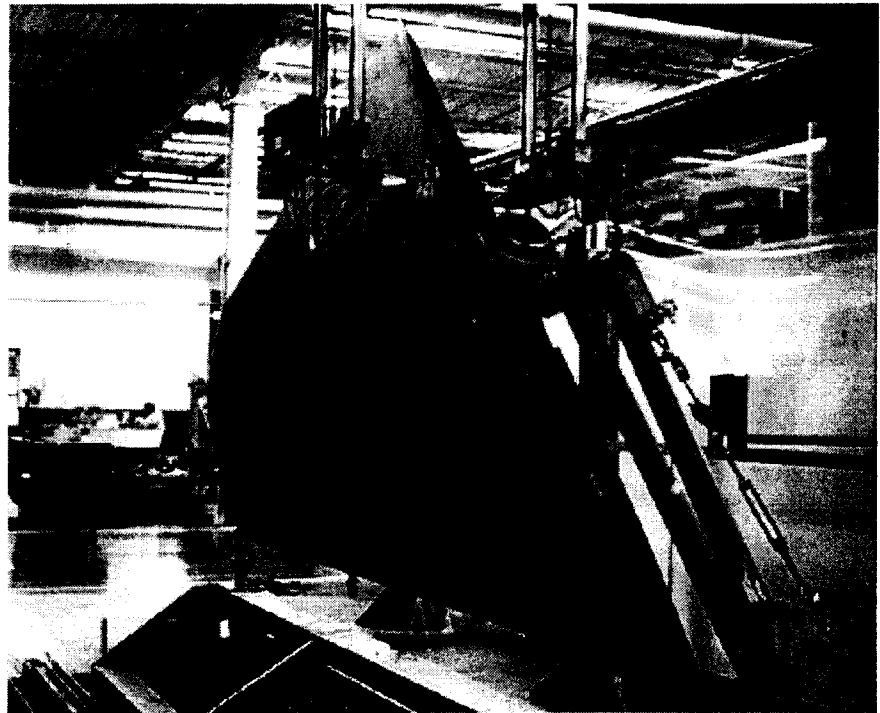
**Figure 1-3:** A set of squirters aligned to form a water fan (courtesy of CalData Systems).



For many years, wide spread usage of automatic NDE was precluded by cost factors. However, as a result of increased demand for rapid, reliable, and often remote inspections a growing number of industries such as aircraft, nuclear power, petrochemical, etc. are seeking to use such

capably. Fortunately, this demand coincided with the evolution of powerful, miniature and inexpensive computer technology as well as an enormous development in microelectronics. The growing need, the significant increase in capability and growing affordability are helping in wide spread application of automated inspection technology. Most automatic NDE are still conducted in lab or industrial setting where the system is placed at a fixed location and the parts are being brought to the test setup. Because of the relatively small market, automated systems for inspection of large structures were developed by a very small number of manufacturers, mostly as custom units (e.g., a system that was installed at McClellan Air Force Base). For aerospace, large automated commercial systems were developed in the early 70's and 80's by McDonnell Douglas (currently Boeing) and General Dynamics. In recent years, as the result of the decrease in the investment cost associated with the production of such systems, a growing numbers of small manufacturers are making large systems. As an example, SDI (Simi Valley, CA) is making an 8-foot diameter scanner turntable for large tubing inspection.

**Figure 1-4:** A large scanner testing a full wing of an aircraft at Boeing Aircraft, St. Louis, MO.



**Figure 1-5:** An automatic X-ray inspection of a full aircraft wing of an F-18 aircraft during maintenance at McClellan Air Force Base, CA (Courtesy of Thomas Ducharme, 1999)



## 1.4 MAKING AN AUTOMATIC NDT SYSTEM

An automated inspection system can have five general functions including (1) accurately positioning of the transducer(s) and if relevant also the receiver(s); (2) data acquisition; (3) data processing and analysis; (4) interpretation in relation to a preset criteria; and (4) presentation of the test results. The inspection can be conducted with high reliability and with great repeatability of the test parameters. Automation eliminates concerns to the human operators when performing tests at harsh, hazardous or constrained areas. Further, automation reduces the difficult associated with training inspector as involved with manual inspection and decision making.

The construction of an automated inspection system requires attention to the following issues:

- Structure size - The size of the scanned area and its percentage of the full structure.
- Part geometry - For scanning of structures with complex geometry using ultrasonics, contour following capability is required. Real-time configuration sensing capability or CAD data that describes the part are highly desirable to support such capability.
- Recording or scanning format - Required recording format, including A-, B- and C-scans. If storage of the A-scan data of every scanned point is necessary significantly larger amount of data storage and computing power is needs.
- Recording - To assist inspectors with the evaluation of the test results it is essential to be able to record the results in various ratios in relation to the test part. To compress images of large structures over small hardcopy a high ratio is needed, whereas to assess the location and the effect of defects 1:1 ratio can be very helpful.

To perform rapid inspection, efficiently and reliability, seven automation elements need to be harmoniously integrated (see Table 2).

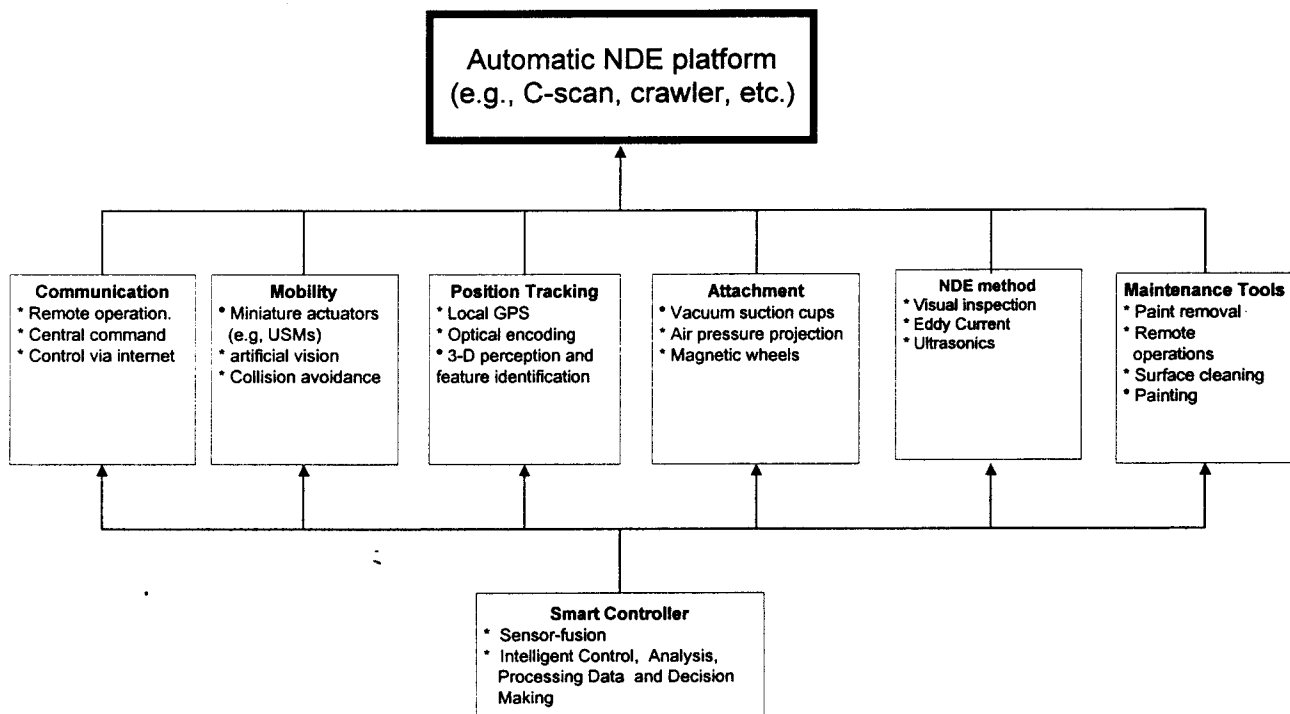
**TABLE 2:** General elements of automatic inspection systems

Element	Function
System structure	Automatic systems have a main frame that is designed according to the task requirements and serves as the housing and support structure of the system. For example a lab C-scan consist of a scanning tank with water immersion bath.
Motion control	The control of the location of the system transducer(s) is done with the aid of a series of actuators and motion controllers that allow positioning the transducer at the desired locations and perform the programmed scan patterns.
Electronic hardware	The control of the system operation, as well as the data acquisition, processing, presentation and recording are performed by the system hardware.
Software	A series of computer instructions define the specific sequence of functions that include data acquisition, analysis, recording and display.
Transmitter and receiver	A transmitter generates the desired signal characteristics and the receiver assures sufficient signal-to-noise ratio to assure a reliable signal analysis.
Transducer	Transducer(s) is(are) used to induce the required form of energy into the component and to receive the signal that interacted with the test material.
Display	The acquired and processed data is presented in a format that inspectors can

use to determine the soundness of the test structure.

Accepting the reality that no single method can provide all the necessary NDE information, efforts are being made to integrate several methods. The complimenting capabilities offer greater detectability and the overlapping ones enhance the inspection reliability. Data fusion techniques [Gros, 1996] are being developed to allow effective data-acquisition and processing as well as provide a sound interpretation of the test parameters in relation to the material integrity (see more details in Chapter 7). Instruments are now commercially available that can be used to perform ultrasonic and eddy current tests using a core hardware and interchangeable transducers and modules. Also, to support such systems capability, commercial software packages are available to process data obtained from various NDE methods. Once data is acquired, the image can be analyzed and manipulated using a common set of software features.

When constructing an automatic NDE platform, a series of multidisciplinary technologies are needed. A block diagram of the required technologies is shown in Figure 1-6. This book covers some the key technologies that are shown in this figure.



**Figure 1-6:** Components of an automatic NDE platform

## 1.5 AUTOMATIC INSPECTION SUPPORT TECHNOLOGIES

The increased processing speed and improvement in hardware capability is allowing real-time imaging of all the wave-base NDE methods including radiography, ultrasonics, shearography, etc. Using analytical tools, finite element analysis as well as computer hardware and software, test procedures can be developed graphically by interactive process simulation. Moreover, progress in microelectronics led to the development of miniature portable instruments that are pocket size. Some of the technologies that support automatic inspection include the internet (information highway), inspection simulation and miniaturization technology. New techniques

and devices can be tested at a testbed that was established by Federal Aviation Administration (FAA) in Albuquerque, New Mexico, and it consists of aging aircraft with very well characterized flaws.

### **1.5.1 Internet - Information Highway**

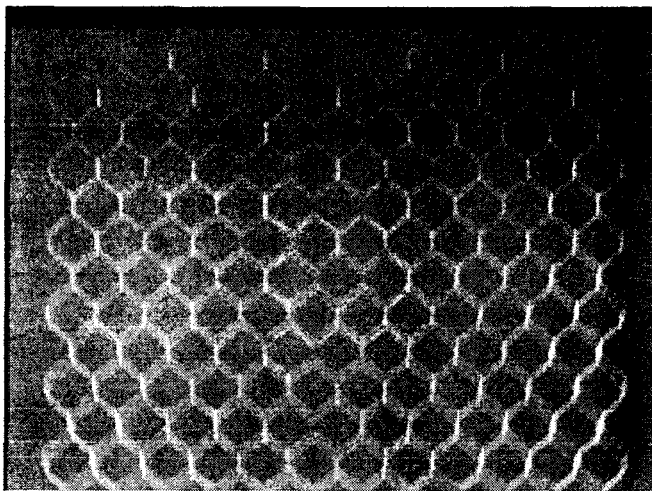
In the relatively short time since Internet became the world-wide-web as we know it, this information highway contributed greatly to the advancement of many fields including NDE [Bar-Cohen, et al, 1996]. Internet is now the information communication tool of choice for multimedia (data, files, text, programs, drawings, pictures, video and sound) at speeds, efficiency and content that cannot be matched by any other known method. NDE experts around the world rapidly recognized the power of Internet as a forum of information exchange and archival. The technology is simplifying and helping to rapidly develop international standards and process specifications. Further, it is enabling the centralization and easing access of information achieves and databases. Formed in 1995, the global NDE Newsgroup [nde@coqui.ccf.swri.edu], which is maintained on a server at South West Research Institute, is widely used by NDE experts around the world as an electronic bulletin board. Subscribers are added electronically and they receive via e-mail inquiries, data, information and announcements of general interest. Global efforts and initiatives of individuals and companies are contributing greatly to the field. As an example, the electronic publishing forum, *NDT.net*, is a highly active and effective website that combines an electronic journal, information archive and monthly technical forums of information exchange [<http://www.ndt.net/newsweb/newsweb.htm>]. To take advantage of the various web capabilities the author formed the JPL's NDEAA webhub [<http://ndeaa.jpl.nasa.gov/>] with clickable animation to aid understanding various mechanisms and with hotlinks to downloadable recent publications. Moreover, to quickly find and access the growing number of homepages of international technical societies, the author formed the Global NDT Internet Superhub (GNIS) with clickable countries on a globe map [<http://eis.jpl.nasa.gov/ndeaa/nasa-nde/gnis/gnis.htm>]. The technology reached a point where "companies do not exist unless they have a homepage". To find some of the major homepage addresses, one can use the NTIAC webpage that has links to several hundreds of NDE sites [<http://www.ntiac.com/>]. Through its homepages, ASNT is offering society information such as various services, conferences, and other relevant activity and announcements [<http://www.asnt.org/>].

Beside information archive, communication and exchange, internet can be used to control automatic scanners, to download update programs from the manufacturer as well as perform maintenance and repairs that can be handled by software. Using encryption techniques and passwords, the access to the system can be limited to authorized personal only. Simultaneously, many individuals can view the system setup and inspection results in a teleconference format allowing rapid decision making by remotely located experts.

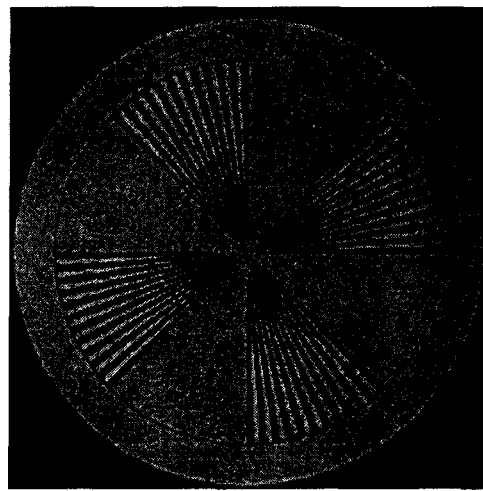
### **1.5.2 Inspection Simulation**

Ray tracing has been a well-established tool for investigating the travel path of waves. With the progress and increased speed of computer graphics it became feasible to use ray tracing for the development of inspection procedures using rapid interactive simulation. Simulation software can perform 3D ray tracing, and examine the wave interaction with the test structure geometry while accounting for the material that is involved. Effective tools were developed by such

research institutes as the Center for NDE at Iowa State University and the Canadian National Research Council as well as commercially by UTEX (Ontario, Canada). Computer models were used to develop user-friendly accurate and rapid simulation of such methods as radiography, ultrasonics, and eddy current. Numerous test parameters were included in the models, e.g., for X-ray simulation (see example in Figure 1-7) some of the parameters are X-ray source, film type, part geometry, setup distances, exposure value, material absorption, etc. The part structure can be described using 3-D CAD models, and many types of defects can be inserted anywhere into the model to form a realistic simulation of the test process. In the case of modeling ultrasonics, the reflected, transmitted and refracted waves can be used to produce simulated A-, B-, and C-scans. Further, for eddy current the real and imaginary components of the impedance-plane output as a function of the probe position can be simulated in response to crack-like defects.



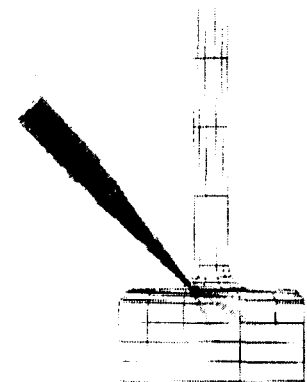
a. A honeycomb sandwich.



b. A penetrameter gauge

**Figure 1-7:** Simulated radiographs using computer code and interactive graphics ((Iowa State University).

Ultrasonic test procedures can be developed and transferred to the computer that automatically test the structure using complex real-world parts (see example in Figure 1-8). A complete ultrasonic inspection can be simulated including the test results; difficult problems can be anticipated and diagnosed by confirming the source of the returning echoes; the sound paths in the part can be visualized; the sound field of the transducer can be evaluated to make an effective choice of the transducer; and inspectors can be easily and effectively be trained. Specifically, A-scan displays for various angles of incidence can be simulated to assist inspectors in developing ultrasonic test procedures. Longitudinal and shear mode conversions can be identified by the operator and assist in explaining the origin of echoes that appear on an A-scan display. Moreover, simulated B-scans can display how stray sound modes and part geometry might accidentally shadow flaws. If fixturing is required, the simulation software provides the necessary information for the probe angulation, spacing, delay line or water-path distances. Transducer modeling features can simulate both contact and immersion coupling using various frequencies and bandwidths as well as various focal geometries (circular, elliptical or rectangular). Tests can be



viewed in both pulse echo and pitch catch and the transducer can be manipulated to follow the part surface at a fixed distance and/or inspection angle.

**Figure 1-8:** Simulation of the interaction of ultrasonic wave with a complex configuration using ray tracing and computer graphics [Iowa State University, <http://www.cnde.iastate.edu/staff/mgarton/mgarton.html>].

### 1.5.3 Miniaturization

Progress in microelectronics enabled the miniaturization of NDE hardware and the production of portable instruments that can be carried to the field and reach difficult to access areas. Pocket size ultrasonic thickness gauges are commercially available from most of the leading manufacturers of ultrasonic instruments. The technology is leading to reduction in cost as well as in instrumentation weight and size with a great enhancement of the capability. Data acquisition cards that can be plugged into a laptop computer have been available for several years (e.g., Wesdyne International, California) and credit card size plug-in that conform to the PCMCIA type 2 standard is one of the forms in which this progress is expressed. This type of cards allow making a laptop to a small ultrasonic pulser/receiver and with appropriate software it can be operated as a complete ultrasonic data acquisition and imaging system. Such cards can be used as motion control (encoder) interfaces, high-resolution A/D converters and signal processors for portable scanners. The systems are battery operated and increasingly they are employing wireless communication capabilities.

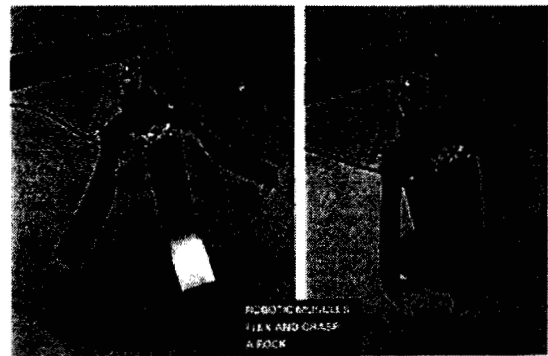
The technology of miniaturization made an impact also on the size of sensors and their support electronics. For over ten years, the trucking industry has been using tires with imbedded sensors that wirelessly communicate every several minutes the individual tires' identity and pressure. Using effective power management, these sensors can operate for periods of more than 8 years without needing to change battery. This technology is intended to help truck drivers to avoid tragic and costly accidents that can result from a flat tire. Another area of automotive that benefited from the miniaturization technology is impact sensing and activation mechanism of airbags. Further, insects such as bees are commonly tracked with the aid of miniature transmitters that are installed as backpacks. Such capabilities can be transitioned to the field of acoustic emission and other NDE if miniature wireless stick-on sensors are used. The size of electronics has become so small that insects can be instrumented to perform tasks that used to be view as science fiction. Example is shown in Figure 1-9, where a spider at the University of Tokyo, Japan, was instrumented as a locomotive to carry a backpack of wireless electronics. Development in actuation technology is expected to lead to insect-like robots that can be launched into hidden areas like aircraft engine and perform inspection and maintenance tasks. Beside miniaturization of conventional actuators, such as motors, electroactive polymers are being developed to offer the closest emulation of biological muscles. In Figure 1-10 an example is shown where bending electroactive polymer fingers are operated similar to human hand

grabbing a rock. This gripper is being developed for potential use as an end-effector of a miniature robotic arm supporting planetary exploration tasks [Bar-Cohen, et al, 1998].

**Figure 1-9:** An instrumented spider at the University of Tokyo illustrates the potential to NDE in terms of mobile sensors [<http://www.leopard.t.u-tokyo.ac.jp/>].



**Figure 1-10:** A gripper with bending Electroactive Polymer fingers lifting a rock similar to a human hand. Potentially, this type of materials will be used similar to biological muscles to drive insect-like robots.



#### 1.5.4 Testbed for Validation of New NDE Techniques

The need for a testbed to demonstrate new NDE techniques and instruments hampered their transition to a practical use. In August 1991, FAA center for NDE was formed at Albuquerque, New Mexico, to offer a validation testbed consisting of aging aircraft with known flaws. This Sandia National Laboratories' Airworthiness Assurance Nondestructive Inspection Validation Center (AANC) was facilitated with a series of aging civilian aircraft and a library of structural parts with documented flaws [<http://www.sandia.gov/aanc/pubs.htm>, Smith & Shurtleff, 1997 and Shurtleff, et al, 1997]. The center arose out of the Aviation Safety Act of 1988, passed by Congress, after the midair structural failure of the Aloha Airlines Boeing 737. Sandia's role has since been expanded to other areas covering aircraft overall safety system design such as fire protection, information system management, and accident investigation support. A view of one of the aircraft that is available at the AANC facility is shown in Figure 1-11.

#### 1.6 SUMMARY

NDE have evolved significantly in recent years as a result of development in the field as well as the enhancement in instrumentation capability. Automation is essential to assuring inspection reliability and speed and can lead to lower cost of operation. Automation can be applied to various levels of inspection from batch and large volume production parts to one of a kind complex geometry structure. This book covers the various aspects of automatic or robotic inspection including robotic systems, crawlers, actuators, sensors, miniaturized hardware or micro-electro-mechanical systems (MEMS), signal processing, communication and display. The

book is concluded with examples of applications as well as expected view of future development based on the trend in robotics and other related fields.

**Figure 1-11:** An aging aircraft with well-documented flaws at AANC (Sandia National Labs).



### ACKNOWLEDGEMENT

This chapter was written at the Jet Propulsion Laboratory, California Institute of Technology, under a contract with the National Aeronautics and Space Administration.

### 1.7 REFERENCES

- Bar-Cohen Y., and P. Backes, " Open-architecture robotic crawlers for NDE of aircraft structures," Materials Evaluation, Vol. 57, No. 3 (1999) pp.361-366.
- Bar-Cohen Y., R. Diederichs, M. Jones and M. Onoe, "International NDT Technical Collaboration Using the Internet," Proceedings of the 96' ASNT Fall Conference, Seattle, Washington, Oct. 14-18, (1996), pp. 224-226.
- Bar-Cohen Y., T. Xue, M. Shahinpoor, J. O. Simpson, and J. Smith, " Low-mass muscle actuators using electroactive polymers (EAP), " Proceedings of the SPIE International Smart Materials and Structures Conf., SPIE Paper No. 3324-32, San Diego, CA, 1-6 March 1998.
- Gros X.E., NDT Data Fusion, <http://www.riam.kyushu-u.ac.jp/fracture/xav16.htm> ISBN: 0340676485 Arnold, London, UK (1996)
- Shurtleff, W., Roach, D., and Valley, M., "Overview of Composite Projects at the FAA Airworthiness Assurance Validation Center", International Conference on Composite Materials, July 1997.
- Smith, C. and Shurtleff, W., "Validation and Technology Transfer of NDI Techniques for Corrosion Quantification and Small Crack/Disbond Detection", First Joint DoD/FAA/NASA Conference on Aging Aircraft, Ogden, Utah, July 8-10, 1997.

## CHAPTER 2.1: ROBOTIC SYSTEMS AND CONTROL

Eric T. Baumgartner

JPL, Caltech, 4800 Oak Grove Dr., Pasadena, CA 90740

818 354-4831, fax 818-393-4057, [Eric.T.Baumgartner@jpl.nasa.gov](mailto:Eric.T.Baumgartner@jpl.nasa.gov)

CHAPTER 2.1: ROBOTIC SYSTEMS AND CONTROL .....	1
2.1.1 INTRODUCTION .....	1
2.1.2 ROBOT TYPES .....	1
2.1.2.1 Fixed-base Manipulators.....	1
2.1.2.2 Mobile Systems.....	2
2.1.3 ROBOT CONTROL.....	2
2.1.3.1 Joint level control.....	3
2.1.3.2 Trajectory control .....	3
2.1.3.3 Positioning for manipulation systems .....	6
2.1.3.4 Mobile robot localization and control.....	7
2.1.4 APPLICATIONS: PLANETARY SURFACE ROBOTICS FOR MARTIAN EXPLORATION .....	10
2.1.5 REFERENCES.....	12

### 2.1.1 INTRODUCTION

For some years now, robots have been envisioned for use in many environments – from factory floors to planet surfaces. While the use of robots has not been as widespread as some might have expected, the number of robots utilized in industrial settings has grown steadily. In 1997, the population of robots in the United States was approximately 80,000, in Japan approximately 400,000, and in Western Europe approximately 120,000. Since 1992, annual robot shipments from U.S. manufacturers have increased by 172% and annual revenues have increased by 136% [Robotic Industries Association, 1998]. Primarily due to cost constraints but also due to fundamental technology shortfalls, robotic systems have not made inroads into the household market and we are still many years from the development of a robotic assistant in the home. On the other hand, during NASA's Pathfinder mission that included the little rover, Sojourner, the public was greatly inspired by a robotic device that was designed to explore the Martian planet. This chapter is meant to provide a brief, but broad, overview of the issues related to the general use of robots today. For more detailed discussions of robotics, the reader is encouraged to review the many robotics textbooks available today.

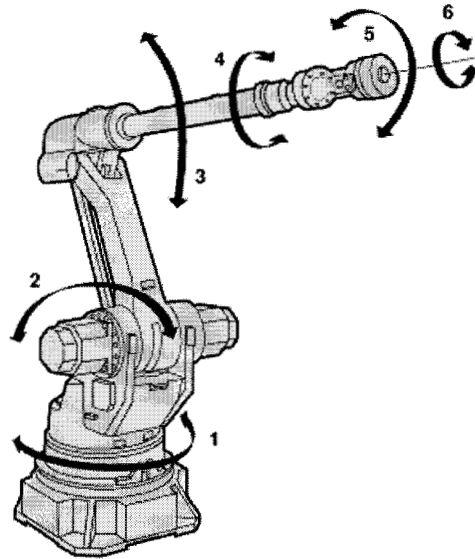
### 2.1.2 ROBOT TYPES

#### 2.1.2.1 Fixed-base Manipulators

The majority of robots in use today are found on factory floors carrying out operations such as spot welding, spray painting, part assembly, pallet stacking, component pick-and-place, etc. These manipulators are typically fixed-based systems in that they are fixed to operate in one location. Robot manipulation systems are controlled by a number of actuators that each produces either rotary or linear motion. Actuators are connected to one another by the links of the robot. Each actuator is called a degree-of-freedom and, depending on the particular task to be performed by the robot, the number of degrees-of-freedom associated with the robot may vary from two to six. Located at the end of the final link of the robot is the robot's end-effector or tool that is used to interact with the robot's environment. It is typically the requirement of the robotic

system to position and orient the robot's end-effector with respect to a particular target so that the desired operation can be carried out. If the robotic task requires the positioning of the end-effector in a 3D space without regard to the orientation of the end-effector with respect to the target, then a three degree-of-freedom robot system is required. If both positioning and orientation of the robot's end-effector with respect to the target is required, then this task requires a six degree-of-freedom manipulation system. Such a six degree-of-freedom robot arm is shown in Figure 2.1.

**Figure 2.1:** Six degree-of-freedom industrial manipulator



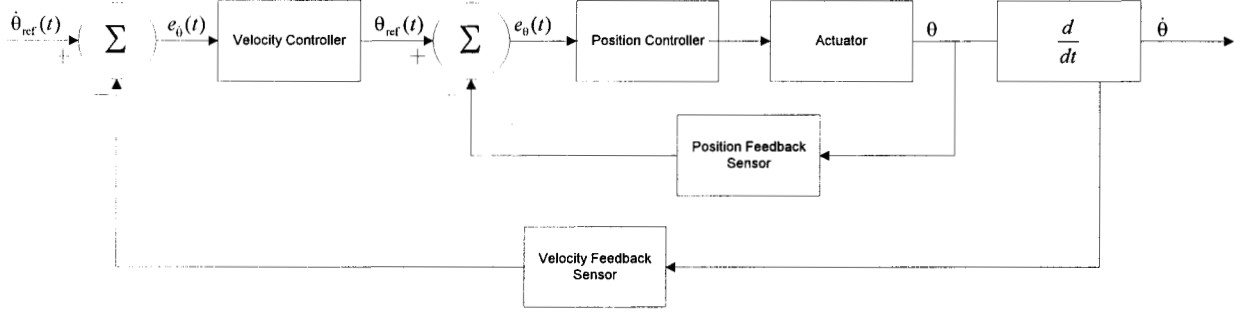
### 2.1.2.2 Mobile Systems

For other robot applications, the robot cannot remain fixed to a particular location but instead is required to move from location to location and perform various tasks at each location. Such mobile robots are much less common in industrial settings primarily due to the unique challenges associated with the control of a mobile or wheeled system (see discussion in Section 2.2.2). Some mobile robots are controlled through the use of tracks (e.g. visual, magnetic, or electric tracks) embedded in the floor so that the robot moves along a particular path at all times. In this way, the robot can be utilized as an automatic system for the transport of goods from one location to another. Other systems do not rely on guide tracks but instead determine the current location of the mobile robot through the sensing of bar-coded markers or through the sensing of known environmental markers such as walls, doorways, etc. One of the most successful mobile robot systems in use today is the Helpmate robot [Helpmate Robotics, Inc., 1997]. This robot is utilized within hospital environments to transport meals and medicines and to deliver these items to hospital patients. Another successful mobile robot system is the Sojourner rover (discussed in Section 2.3) which was used to explore the surface of Mars in July of 1997. Many academic research efforts are currently being conducted in the area of mobile robot design and control, however, most of these efforts have not been realized in industrial use today. In addition, non-traditional mobility techniques (e.g., walking systems [Wettergreen, 1995]) are studied primarily in academic settings.

### 2.1.3 ROBOT CONTROL

This section focuses on increasing levels of control for robot systems starting from the basic closed-loop control of robot actuators. Next, trajectory control techniques for fixed-base manipulators (holonomic systems) using inverse kinematics and for mobile systems (non-

holonomic systems) using path planning techniques are discussed. In addition, the control of the interactions between a robot and its surrounding environment are discussed in the context of the use of sensory feedback (e.g. proximity, force, and vision). Finally, issues related to the determination of a mobile robot's location within its environment will be discussed and the use of this information for the control of the robot's motion and positioning.



**Figure 2.2:** Closed-loop motor controller

### 2.1.3.1 Joint level control

At the heart of any robotic system is the actuation sub-system that is used to control the degrees-of-freedom of the robot device. Traditionally, linear or rotary drive systems are utilized for producing the required motion through the use of servomotors. These servomotors are typically brushed or brushless DC motors that include feedback devices that sense the position and/or velocity of the motor shaft. This feedback is then used in a closed-loop control approach that controls the actuator to follow a desired position or velocity profile. In addition to a position control system, many robotic systems also require the velocity control of the actuators. Typically an actuator is required to follow a specific velocity profile as a function of time such as a trapezoidal velocity profile or a higher-level velocity profile. An example of a closed-loop position and velocity controller is shown in Figure 2.2.

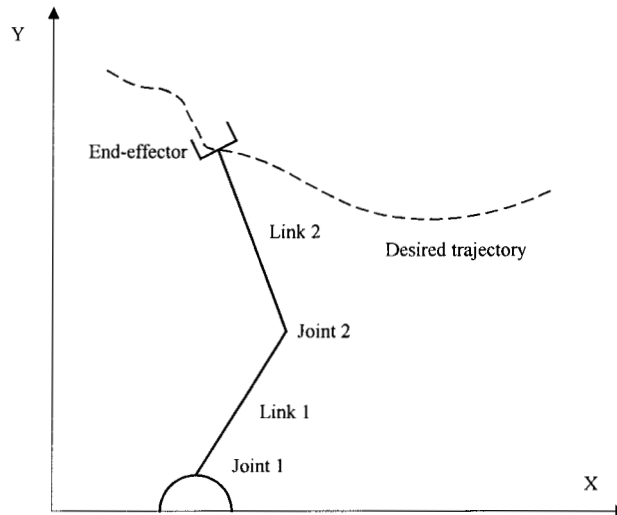
The most common feedback controller utilized in robotic systems is the Proportional-Integral-Derivative (PID) controller that takes the following form:

$$u(t) = k_p e(t) + k_d \frac{de(t)}{dt} + k_i \int e(t) dt \quad (2.1)$$

where  $u$  represents the control variable,  $e(t)$  is the error signal and  $k_p$ ,  $k_i$ , and  $k_d$  represent the gains associated with the proportional, integral, and derivative terms of  $e(t)$ . These gains are determined through knowledge of the plant dynamics and through standard controller design techniques (e.g., root locus plots, Bode plots, etc). Other feedback controllers include state-space controllers, optimal controllers (LQR, LQG, etc), and robust controllers (H- $\infty$ ).

### 2.1.3.2 Trajectory control

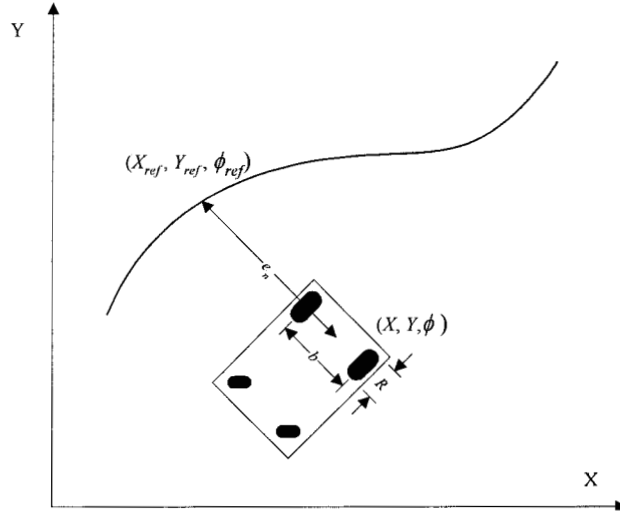
For fixed-base robot manipulation systems, a high-level controller is used to coordinate the joint-level motion associated with each actuator. In this way, the specific trajectory of a point on the robot can be followed precisely via the coordinated joint motion. To accomplish a trajectory control system, the forward and inverse kinematics of the manipulator must be described.



**Figure 2.3:** Two degree-of-freedom manipulator

Typically, the kinematics of a fixed-base manipulator are characterized by a series of parameters known as the Denavit-Hartenberg (D-H) parameters. These parameters include the link lengths, the joint offset distances, and the orientation of each joint coordinate reference frame with respect to the previous joint coordinate reference frame. The means for determining a robot's D-H parameters is described in [Craig, 1989]. In general terms, the forward kinematics of a fixed-base manipulator is given by a series of transformation matrices that describe the tip or end-effector position and orientation of the robot arm with respect to the base coordinate reference frame of the robot arm. In this way, with knowledge of the manipulator's joint angles, the end-effector position and orientation is known at all times. A fixed-base manipulator is said to be a holonomic system since the output of the system (e.g., end-effector position and orientation) is an algebraic function of the input to the system (e.g., joint angles). Thus, for a given set of joint angles, the manipulator's end-effector position and orientation is known through the algebraic forward kinematics and the path the robot arm takes to a given set of joint angles always yields the same end-effector position and orientation.

For the trajectory control of a robot arm, the inverse kinematics of the robot arm must be determined. The inverse kinematics are the set of equations that determine the joint angles required to yield a desired end-effector position and orientation. In general, the inverse kinematics are more difficult to derive as opposed to the forward kinematics since multiple solutions exist that yield the same end-effector position and orientation. Typically geometric or algebraic techniques are used to determine a manipulator's inverse kinematics [Craig, 1989]. With the inverse kinematics in hand, a desired end-effector trajectory can be followed by solving for the internal joint angles at each point along the trajectory (see Figure 2.3 for an example of a two degree-of-freedom manipulator following a 2D trajectory).



**Figure 2.4:** Mobile robot path tracking

In contrast to fixed-base manipulators, mobile robot systems are described by a differential relationship between the mobile robot's pose (i.e. position and orientation with respect to some coordinate reference frame) and the internal joint angles of the robot's wheels. Such a system is called a non-holonomic system where the output of the system is differentially related to the input to the system. For example, consider a two-wheeled mobile robot shown in Figure 2.4 where the two wheels are used to both drive and steer the rover. The back wheels consist of caster wheels that are not actively controlled. The forward kinematics of this mobile robot system can be described by the following equations:

$$\frac{d\mathbf{x}(\alpha)}{d\alpha} = \begin{bmatrix} \frac{dX(\alpha)}{d\alpha} \\ \frac{dY(\alpha)}{d\alpha} \\ \frac{d\phi(t)}{d\alpha} \end{bmatrix} = \begin{bmatrix} R \cos \phi(t) \\ R \sin \phi(t) \\ \frac{R}{b} u(t) \end{bmatrix} = \mathbf{f}(\mathbf{x}(t), u(t)) \quad (2.1)$$

where  $\mathbf{x} = [X \ Y \ \phi]^T$  is the rover state (position and orientation) in a planar space,  $\alpha$  is an independent variable associated with the measured wheel rotations, and  $u$  is the control variable. In this case,  $\alpha$  is defined as

$$\alpha = \frac{\theta_l + \theta_r}{2} \quad (2.2)$$

and

$$u = \frac{d\theta_l - d\theta_r}{d\theta_l + d\theta_r} \quad (2.3)$$

where  $\theta_l$  and  $\theta_r$  represent the left and right wheel rotations, respectively, and  $d\theta_l$  and  $d\theta_r$  represent the differentials of the left and right wheel rotations. As seen in Equation 2.2, the output planar position and orientation of the mobile robot is related to the input degrees-of-

freedom (e.g. wheel rotations) via a set of differential equations. Unlike the fixed-base holonomic manipulation system, the end pose of the mobile robot is dependant on the particular sequence of joint angles used as the input to the system. In this way, the means for tracking a particular path are more involved than simply solving the inverse kinematics of the fixed-base robot arm.

As an example, consider the tracking of a path shown in Figure 2.4 where a point on the mobile robot specified by  $(X, Y, \phi)$  is required to follow a given path. One technique that can be utilized for tracking this path is through the determination of the error in position and orientation with respect to the path. With this error determined, the control variable,  $u$  (in this case the differential velocities of the two drive wheels as in equation (2.3)), can be computed by passing this error through a PID control law:

$$u(\alpha) = k e_n(\alpha) + k_2 \int_0^\alpha e_n(\alpha) d\alpha + k_3 \frac{de_n(\alpha)}{d\alpha} + k_4 e_\phi(\alpha) + k_5 \int_0^\alpha e_\phi(\alpha) d\alpha + k_6 \frac{de_\phi(\alpha)}{d\alpha} \quad (2.4)$$

where  $e_n(\alpha)$  is the error in the normal direction between the mobile robot and the path and  $e_\phi(\alpha) = \phi(\alpha) - \phi_{ref}(\alpha)$  is the orientation error. Note that this path tracking controller is time independent and the speed of the mobile robot as it traverses the path is not actively controlled for path following.

### 2.1.3.3 Positioning for manipulation systems

For manipulation systems, interaction with the robot's environment requires knowledge of the position of the robot's end-effector relative to the desired object to be manipulated. The use of robotic manipulation techniques in industrial settings typically has been limited to two distinct applications. The first is the case where the object that interacts with the robot arm can be fixtured or tightly constrained to a particular reference frame. In this application, the robot arm operates in a "teach-repeat" mode where the specific joint trajectory that carries out the desired operation is taught to the system and then repeated for each additional object (e.g. assembly-line spot welding operations). If uncertainty exists between the position and orientation of an object and the reference frame of the manipulator, then typically a vision system that is coupled to the manipulator's reference frame is required. For most vision-based industrial robot applications, the problem is cast as a two-dimensional (2D) operation in order to simplify calibration issues associated with the manipulator and the vision system (e.g. robotic pick-and-place conveyor operations). In both cases presented above, there is *a priori* knowledge given to the robotic system so that the desired operation is achieved. In the case of the teach-repeat robot, the location of the fixtured object is known to within some tolerance while, for the vision-based robotic system, the application is constrained so that both camera and manipulator calibration issues are minimized. If direct contact between the manipulator and the target is required, proximity sensors such as contact switches, sonar sensors, or laser range finders can be utilized to gage the distance from the robot's end-effector to the target. However, for 3D applications, range to the target does not fully determine the means by which the robot's end-effector is required to be positioned or orientated so that the positioning task can be completed.

For some applications, the robot arm is required to interact with objects whose location (position and orientation) with respect to the manipulator's reference frame is by definition not known *a priori*. Therefore, the manipulation system must rely on visual feedback in order to position the end-effector relative to targets of interest. A common technique for conducting this manipulation task utilizes a calibrated stereo imaging system for determination of the 3D

location of the target objective [Gennery, 1991]. Once the 3D target location is specified, the internal joint angles that position the arm's end-effector at this 3D location are computed via the manipulator's inverse kinematics [Tsi, 1987]. Using this approach, a well-calibrated manipulator/imaging system can achieve positioning accuracy on the order of 1-2 cm [Schenker et al., 1997].

The difficulty with a calibrated manipulation system is, of course, the lack of robustness to any changes in the system after the calibration has been completed. For space applications, various factors such as launch vibrations, landing impacts, and thermal expansion and contraction of mechanical components may cause the calibration of the manipulation system to degrade, thereby, reducing the achieved positioning accuracy. As an alternative to the calibrated manipulation system described above, robotic researchers have aggressively pursued visual feedback techniques that reduce the reliance on calibration to achieve increased robustness with respect to absolute positioning. Two such technologies that have emerged in the field of visual feedback techniques are visual servoing and camera-space manipulation.

Visual servoing (Hutchinson et al., 1996) is a technique in which the terminal maneuver of a robot arm is actively controlled within the reference frame of the participating camera or cameras without regard to an absolute reference frame. This approach utilizes the sensed error between the image-plane location of the target goal and the image-plane appearance of features on the manipulator, and attempts to drive this error to a zero state via a continuous feedback control approach. Visual servoing techniques rely on the image Jacobean that relates differential motion of features in a camera's image-plane to differential motion of a manipulator's joints. Difficulties with this approach include the need to continuously sense the image-plane error between the target features and the manipulator features. During the final terminal maneuver, the ability to sense the image-plane error may become problematic due to an obscuration of the target by the manipulator.

An alternative visual feedback technology, known as Camera Space Manipulation or CSM (Skaar et al., 1990), utilizes an estimation-based approach to the problem as opposed to the continuous feedback approach of visual servoing. In CSM, a minimum of two widely separated, stationary cameras are used to view the workspace associated with the manipulator. Independently for each participating camera, the relationship between the internal joint configuration of the robot arm and the image-plane (or camera-space) appearance of end-effector features is estimated via a six-parameter model. This model is refined throughout the maneuver so that an accurate representation is realized within the vicinity of the maneuver termination. The manipulator's joint configuration that achieves the desired terminal location is determined by minimizing a squared-error performance index. This performance index is specified relative to each of the participating camera's image plane so that the entire maneuver is achieved in "camera-space" without regard to any physical reference space. This technique has been successfully demonstrated for a variety of challenging applications and has achieved absolute positioning accuracy on the order of 1 mm. Recently CSM has been demonstrated for a Mars Polar Lander mission scenario using a lander-mounted robot arm prototype (Baumgartner and Schenker, 1996).

#### **2.1.3.4 Mobile robot localization and control**

During the Pathfinder mission (see Section 2.4.1), the Sojourner rover utilized the sensed wheel rotations and known rover kinematics to determine the rover's pose (position and orientation) relative to a lander-fixed reference frame. Estimates of the rover's pose that are

generated based on wheel rotation information alone are known as dead-reckoned estimates. These estimates are quite prone to errors during rover traverses due to factors such as wheel slippage in soft soil, wheel hang-up on obstacles, or varying kinematic parameters. For example, Sojourner's wheels incorporated cleats that were 10 mm in height above the nominal wheel surface. Depending on the encountered wheel/soil interaction, the rover's effective wheel radius varied as a function of the type of soil (hard or soft) over which the rover traversed and, therefore, led to significant dead-reckoning errors. To overcome the buildup of these errors, the high-resolution stereo imager on the Pathfinder lander was used periodically to update the position and orientation of the rover with respect to the lander's reference frame. The updated pose information was then passed along to the rover. Since ground operators commanded the rover within the reference of Pathfinder's stereo imager and since the rover only operated within the vicinity of the lander, the pose updates were adequate for maintaining accurate knowledge of the rover's location.

In contrast to the Sojourner rover mission, future Mars exploration missions will require the rover to venture out beyond the view of a lander and, therefore, no external updates of the rover's pose will be forthcoming. Thus, the rover must make use of its available sensory resources to maintain accurate estimates of its position and orientation relative to a particular reference frame in order to carry out the rover's science operations. For example, future Mars rovers will carry on-board stereo vision sensors, a sun sensor, and an inertial navigation package. Along with wheel rotation information, these sensory inputs can be fused together to produce "optimal" estimates of the rover's pose.

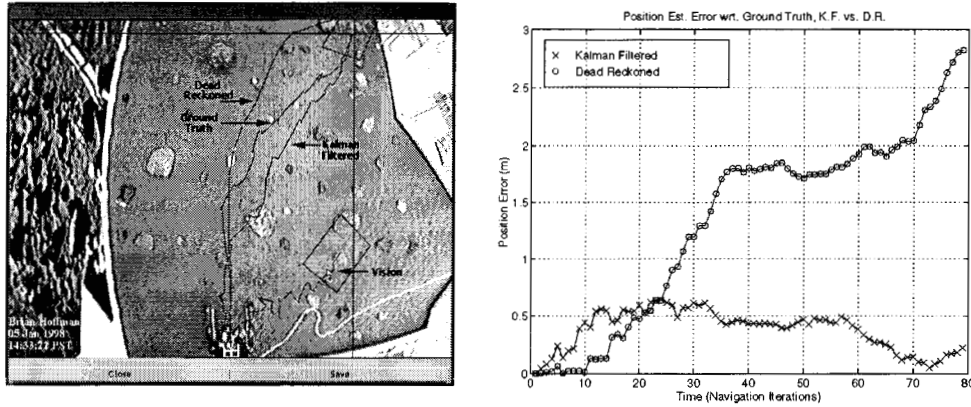
Robotic researchers that have investigated the use of sensor fusion techniques for the generation of optimal rover pose estimates include Cox [1991], Leonard and Durrant-Whyte [1991], and Baumgartner and Skaar [1994]. In each case, algorithms were developed to combine wheel rotation information with external sensory information (laser ranging, sonar sensing, vision sensing) to determine accurate estimates. Both Leonard and Durrant-Whyte as well as Baumgartner and Skaar pursued the use of a state estimation technique known as the extended Kalman filter [Gelb, 1974] as the framework for conducting sensor fusion. Within this framework, the state equations of the robotic vehicle can be written as:

$$\frac{d\mathbf{x}(\alpha)}{d\alpha} = \begin{bmatrix} dX(\alpha)/d\alpha \\ dY(\alpha)/d\alpha \\ d\phi(\alpha)/d\alpha \end{bmatrix} = \mathbf{f}(\mathbf{x}(\alpha), u(\alpha), \alpha) + \mathbf{w}(\alpha) \quad (2.5)$$

where  $\mathbf{x} = [X \ Y \ \phi]^T$  is the rover state (position and orientation) in a planar space,  $\alpha$  is an independent variable associated with the measured wheel rotations, and  $u$  is the control variable. The variable  $\mathbf{w}(\alpha)$  represents a Gaussian-distributed, white noise process that captures the uncertainty associated with the state equations due to factors such as wheel slippage. Any external measurement of the state can be written as a nonlinear algebraic function of the state:

$$\mathbf{z}(\alpha) = \mathbf{h}(\mathbf{x}(\alpha), u(\alpha)) + \mathbf{v}(\alpha) \quad (2.6)$$

where  $\mathbf{z}(\alpha)$  is the measurement vector and  $\mathbf{v}(\alpha)$  is a Gaussian-distributed, white noise process that captures the noise associated with the external measurements.



**Figure 2.5:** Sensor fusion results for planetary rovers.

With the state equations cast as in equation (1) and the measurement equations cast as in equation (2), the extended Kalman filter can be applied to this problem to produce “optimal” estimates of the rover’s state. In practice, the dead-reckoned estimates are determined in real-time via the sensing of the wheel rotations and the numerical integration of (1). As measurements become available, the measurement vector in (2) is utilized to update and correct the on-going state estimates. This sensor fusion framework has been proven through numerous applications to be a flexible approach to the determination of accurate rover state estimates.

One such application of this technique to a terrestrial setting is the development of an autonomous wheelchair for the disabled [Yoder et al., 1996]. In this application, wheel rotation information is fused together with the visual sensing of “cues” placed at discrete locations within the wheelchair’s environment. The image-plane location of these visual cues as detected by on-board cameras is related to the current state of the wheelchair and provides an independent piece of information about the wheelchair’s pose within its environment. The estimates produced by the extended Kalman filter provide the basis for path teaching as well as the tracking of these taught paths during autonomous wheelchair operations. This system has been demonstrated successfully within a large number of realistic settings (i.e. apartment and tight office setting) and has reliably produced accurate state estimates (less than 5 cm absolute error) throughout long wheelchair traverses.

This sensor fusion technique has recently been applied to the planetary rover navigation problem [Hoffman et al., 1998]. This research has focused on localizing the rover with respect to terrain features within the rover’s environment (e.g. rocks). Using the visual appearance of these features in the rover’s stereo hazard avoidance imager, the relative motion of the rover between successive stereo image pairs can be determined. The computation of the frame-to-frame translation and rotation of the rover is accomplished by registering the successive terrain maps using a least-squared-error approach. This measurement of the rover’s relative movement then can be combined with knowledge of the rover’s wheel rotations via the extended Kalman filter framework. The results of this work indicate that accurate rover state estimates can be maintained despite significant wheel slip and terrain variability. Figure 4 illustrates the rover

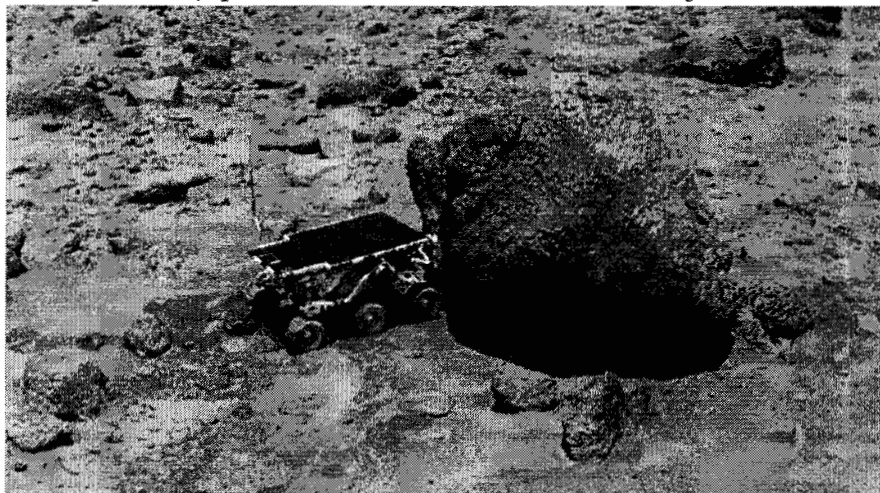
state estimates produced using this approach for a rover traverse through a soft-soil/rock-filled terrain environment.

#### **2.1.4 APPLICATIONS: PLANETARY SURFACE ROBOTICS FOR MARTIAN EXPLORATION**

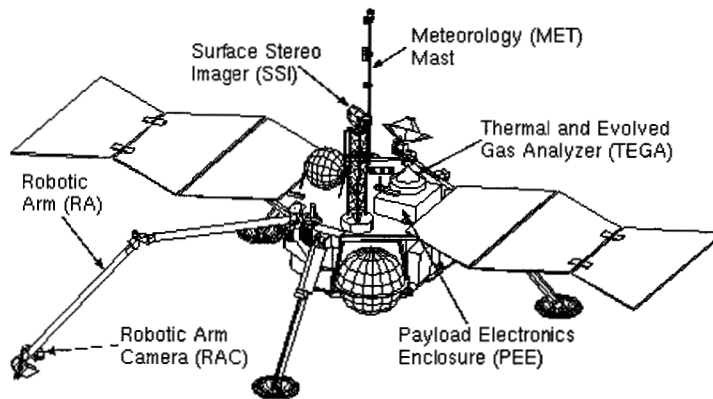
One of the most challenging requirements for any robotic system is operation within an unstructured or unknown environment. To date, the use of robots in industry have been restricted to environments that are well modeled and well understood. However, for NASA's planned exploration of the surfaces of solar system bodies, robots have been used and will be used for the scientific exploration of Mars as well as for asteroids. These robotic devices face the difficult challenge of operating within an environment that may be completely unknown prior to landing on the surface. In addition, all information that is learned about the environment after landing must be collected using sensory information on-board the robotic device.

On July 4, 1997, NASA successfully landed the Pathfinder mission on the Martian surface. One day after the arrival of the Pathfinder lander, later re-named the Carl Sagan Memorial Station, the micro-rover named Sojourner (Figure 2.6) rolled off the deployment ramps and on to the Martian soil. Sojourner [Shirley and Matijevic, 1995; Bickler, 1998] utilized a unique mobility system known as the six-wheeled, rocker-bogie suspension system that allowed the rover to safely traverse over hazards (e.g. rocks) which are at a height of 1.5 times the rover's wheel diameter. The rover also utilized a laser-based hazard detection and avoidance system that allowed the rover to safely complete autonomous traverses from one user-specified waypoint to another. A ground-based rover science and navigation team designated these rover traverses so that the rover visited various science sites and conducted soil mechanics experiments. Sojourner carried a single science instrument, the Alpha Proton X-Ray Spectrometer or APXS, which was successfully deployed and placed on rocks and soil by the rover.

The flight team that designed and built the Sojourner rover faced considerable challenges in the development of the mechanical, electro-mechanical, electronic, and computing environment. These challenges included the strict mass and volume constraints associated with the Pathfinder spacecraft and the operation of the rover within the harsh environmental conditions (low pressure, low temperature) present on the Martian surface. Sojourner's mission to Mars was



**Figure 2.6:** Sojourner rover

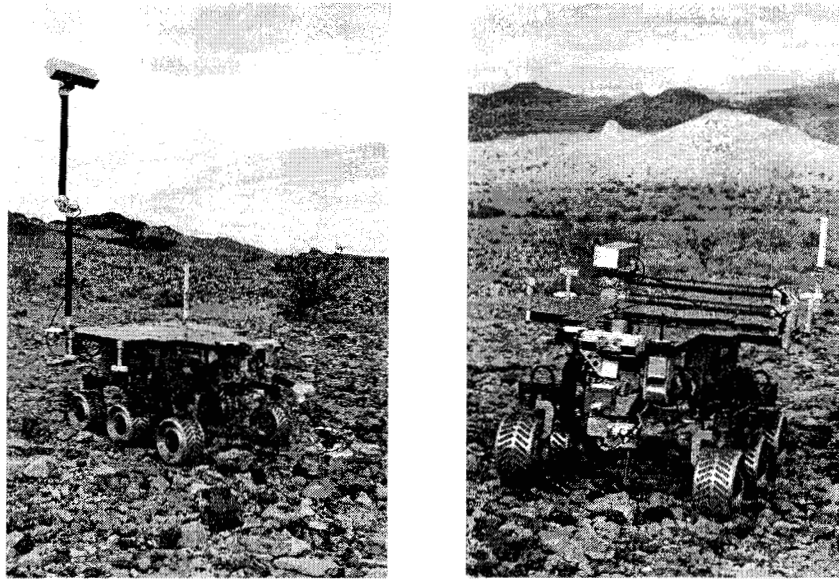


**Figure 2.7:** Mars Polar Lander and MVACS.

scheduled to last just seven days, but in fact lasted for three months at which time communication with the lander (the rover's communication link to Earth) was lost. For all we know "the little rover that could" is still circling the Pathfinder lander patiently waiting for its instructions from Earth.

In January of 1999, NASA will launch its next surface exploration mission to the polar region of Mars (80° S latitude). Known as the Mars Polar Lander, this mission will primarily consist of a lander-mounted science package that will utilize a robot arm for assisting with the mission's science investigations. Unlike the Pathfinder mission, which used an airbag system for achieving a soft landing, the Mars Polar Lander will use an active propulsion system for controlling the descent and placement of the lander on the planet surface. The lander-mounted robotic arm is part of the science payload known as MVACS or the Mars Volatiles and Climate Surveyor [Paige et al., 1996] and is illustrated in Figure 2.7. The arm is a four degree-of-freedom design with an actuated scoop for digging and trenching the Martian surface and for collecting and depositing soil samples in the Thermal and Evolved Gas Analyzer (TEGA) science instrument. The robot arm will be directed by ground operators to desired science sites around the lander via a lander-mounted stereo imaging system. The robot arm will utilize an impedance-based force feedback technique for sensing ground interactions by the arm's end-effector and for protecting the mechanical structure and actuator systems from damage as a results of interactions with soil of unknown composition. As with the Pathfinder mission, the engineers who developed this robot arm faced considerable challenges associated with mass and volume constraints as well as with operating within the harsh Martian environment.

In 2001, NASA will launch a landed payload that will contain elements of the Pathfinder and the Mars Polar Lander payloads. Specifically, Sojourner's flight spare, named Marie Curie, will be utilized to explore the terrain surrounding the lander. In addition, the 2001 lander will contain the MVACS robot arm that will perform digging and trenching experiments. Currently, NASA is in the planning stages for the so-called Mars Sample Return (MSR) missions in 2003 and 2005. The aim of these missions is the collection and storage of samples collected from the Martian surface and the return of these samples to the Earth for detailed analysis. In support of the MSR missions, NASA and JPL have developed a technology prototype of the rover that will be used for the collection of Mars rock and soil samples. This vehicle is called the FIDO (Field Integrated Design and Operations) rover and is pictured in Figure 2.8. This vehicle carries as payload a series of scientific instruments that are used to classify science targets including a high



**Figure 2.8:** FIDO rover during field operations.

resolution multi-spectral stereo imaging system, a near-IR point spectrometer, a close-up micro-imager, a Mössbauer spectrometer, and a prototype of a coring device used to drill and collect rock samples. The rover also carries other stereo camera systems used primarily for rover navigation purposes. During recent field trials of this rover in a relevant desert terrain, the robotic system was operated by ground controllers using a combination of autonomous and semi-autonomous on-board rover software to remotely identify scientific targets, approach the targets, and drill core samples from the target rock.

## 2.1.5 REFERENCES

Baumgartner, E. T. and S. B. Skaar, "An Autonomous Vision-Based Mobile Robot," *IEEE Transactions on Automatic Control*, 39(3):493-502, 1994.

Baumgartner, E. T. and P. S. Schenker, "Autonomous Image-Plane Robot Control for Martian Lander Operations," *Proceedings of the IEEE International Conference on Robotics and Automation*, 1:726-731, Minneapolis, Minnesota, April 1996.

Bickler, D., "Roving over Mars," *Mechanical Engineering*, 120(4):74-77, 1998.

Cox, I. J., "Blanche - An Experiment in Guidance and Navigation of an Autonomous Robot Vehicle," *IEEE Transactions on Robotics and Automation*, 7:193-204, 1991.

Craig, J. J., "Introduction to Robotics: Mechanics and Control," Chapter 3, 2<sup>nd</sup> edition, Addison-Wesley, Reading, Massachusetts, 1989.

Gelb, A., *Applied Optimal Estimation*. Cambridge: MIT Press, 1974.

Gennery, D., "Camera Calibration Including Lens Distortion," Internal Report D-8550, Jet Propulsion Laboratory, California Institute of Technology, 1991.

Helpmate Robotics, Inc., <http://www.ntplx.net/~helpmate/>, 1997.

Hoffman, B. D., E. T. Baumgartner, T. Huntsberger, and P. S. Schenker, "Improved Rover State Estimation in Challenging Terrain," *Autonomous Robots*, in press, June 1999.

Hutchinson, S., G. Hager, P. Corke, "A Tutorial on Visual Servo Control," *IEEE Transactions on Robotics and Automation*, 12(5):651-670, 1996.

Leonard, J. J. and H. F. Durrant-Whyte, "Mobile Robot Localization by Tracking Geometric Beacons," *IEEE Transactions on Robotics and Automation*, 7:376-382, 1991.

Paige, D., W. V. Boynton, D. Crisp, A. M. Harri, C. J. Hansen, H. U. Keller, L. A. Leshin, R. D. May, P. H. Smith, and R. W. Zurek, "Mars Volatiles and Climate Surveyor Integrated Payload," LPI Workshop on Evolution of Martian Volatiles, Houston, Texas, February 1996.

Robotic Industries Association, "Robotics Industry Has Best Year Ever in 1997," <http://www.robotics.org>, 1998.

Schenker, P. S., E. T. Baumgartner, S. Lee, H. Aghazarian, M. S. Garrett, R. A. Lindemann, D. K. Brown, Y. Bar-Cohen, S. S. Lih, B. Joffe, and S. S. Kim, B. H. Hoffman, T. Huntsberger. 1997a. Dexterous Robotic Sampling for Mars In-Situ Science. Intelligent Robotics and Computer Vision XVI, SPIE Volume 3208:170-183 Pittsburgh, Pennsylvania, October 1997.

Skaar, S. B., W. H. Brockman, and W. S. Jang, "Three Dimensional Camera Space Manipulation," *International Journal of Robotics Research*, 9(4):22-39, 1990

Shirley, D. and J. Matijevic, "Mars Pathfinder Microrover," *Autonomous Robots*, 2:283-289, 1995.

Tsi, R. Y., "A Versatile Camera Calibration Technique for High-Accuracy 3D Machine Vision Metrology using Off-the-Shelf TV Cameras and Lenses," *IEEE Transactions on Robotics and Automation*, 3(5):404-471, 1987.

Wettergreen, D., "Robotic Walking on Natural Terrain: Gait Planning and Behavior-Based Control for Statically-Stable Walking Robots," PhD Dissertation, Technical Report No. CMU-RI-TR-95-42, Carnegie Mellon University, December 1995.

Yoder, J.-D., E. T. Baumgartner, and S. B. Skaar, "Initial Results in the Development of a Guidance System for a Powered Wheelchair," *IEEE Transactions on Rehabilitation Engineering*, 4(3):143-151, 1996.

# CHAPTER 3 - Crawlers and Portable Scanners

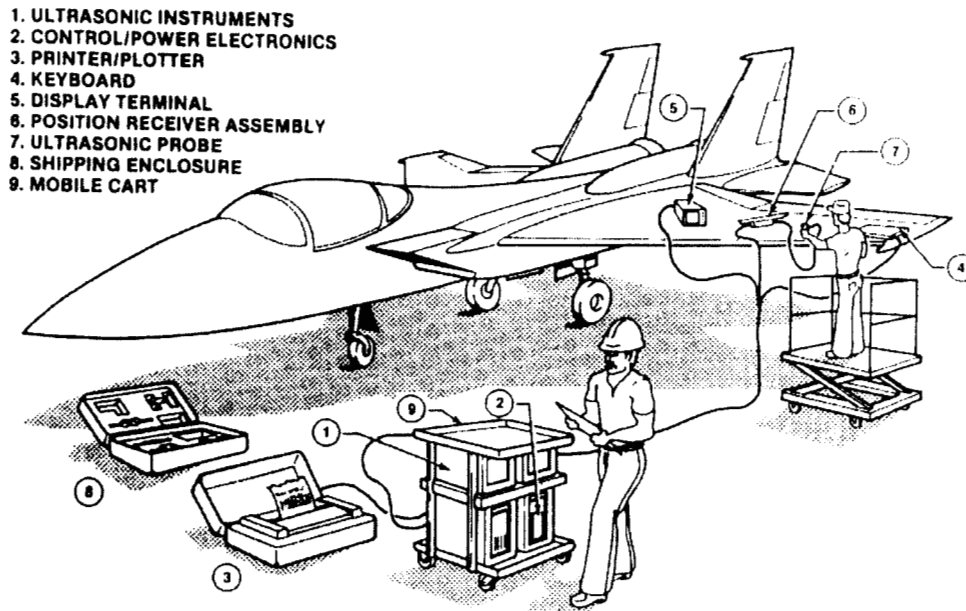
Yoseph Bar-Cohen,  
JPL, Caltech, 4800 Oak Grove Dr., Pasadena, CA 90740  
818-354-2610, fax 818-393-4057, [yosi@jpl.nasa.gov](mailto:yosi@jpl.nasa.gov)

CHAPTER 3 - CRAWLERS AND PORTABLE SCANNERS .....	1
3.1 BACKGROUND .....	1
3.1.1 REFERENCES .....	4

## 3.1 BACKGROUND

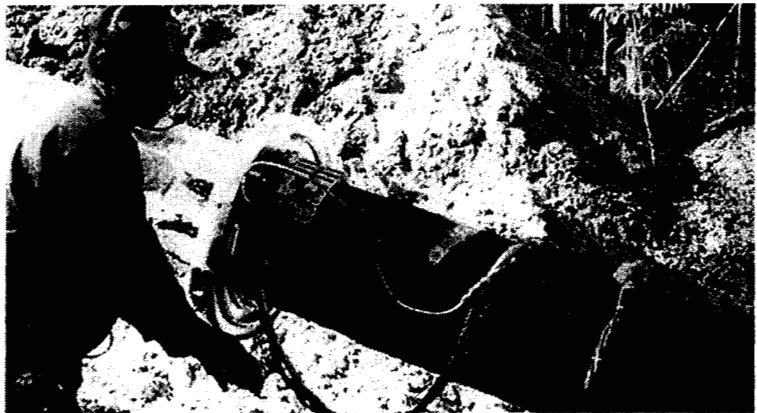
Large ultrasonic scanners have been in use by industry for over four decades. With the evolution of personal computers and microelectronics, it became possible to produce portable C-scanners that can operate in depot and field conditions [Backes & Bar-Cohen, 1996, and Bar-Cohen & Backes, 1999]. The early generations of portable scanners were relatively heavy and consisted of a simple bridge that can be carried to the field in a mobile set of boxes to perform scanning, data acquisition, imaging and storage. To support the formation of the C-scan images, encoding methods were developed to identify the probe location while operating on aircraft structures. Such position encoding methods included the use of acoustic waves, optical scales and others. The acoustic encoding technique was one of the earliest to be used as on the ISIS, which was developed by General Dynamics in the early 80<sup>th</sup> under an Air Force contract (see Figure 3-1). Since the position determination relied on sound wave velocity in air, which is critically dependent on temperature, humidity, wind speed and direction, this encoding method was found to be highly inaccurate. This deficiency led to the phasing out of the acoustic encoding and most of the current portable scanners rely on optical encoders. To secure the portable C-scan bridge to the inspected structure, particularly when inspecting vertical or upside down surfaces, strapping techniques and suction cups are widely used. An example of a scanner with straps is shown in Figure 3-2, whereas a scanner that is attached using suction cups is shown in Figure 3-3.

The introduction of portable C-scan bridges enabled to semi-automate the ultrasonic field inspection and to significantly improve the reliability of such field tests. Since aircraft structures have a complex geometry, flat rigid C-scan bridge are involved with data acquisition difficulty due to a gap between the flat surface of the bridge and the curved surface of the aircraft. To minimize this gap and make the bridge conform to the inspected structure, flexible bridges were introduced in recent years. Examples of such flexible a scanner include the PANDA (made by Tektrend, Quebec, Canada), MAUS (Boeing, St. Louis, MO) and ISCAN (made by Fraunhofer Institute, Germany) as shown in Figure 3-4. Being a contact-scanning device, the spring-loaded transducer holder has the flexibility to conform the contour of the bridge to the tested aircraft structure. The scanner arm can be flexed to adapt the bridge curvature to the surface contour of the aircraft and thus ensuring the transducer contact to test surface during scanning.

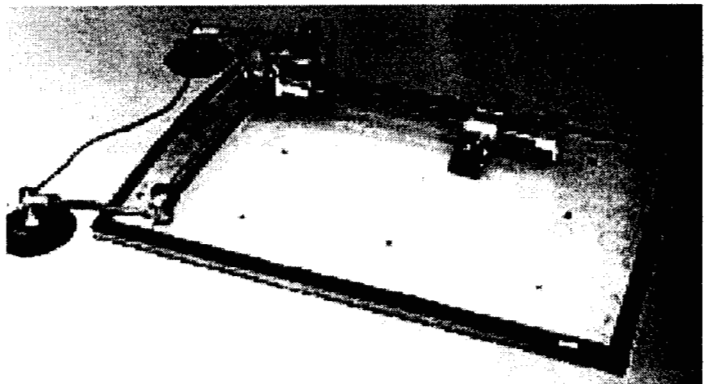


**Figure 3-1:** The In-Service Inspection System (ISIS) is one of the early generations of the portable C-scan for field operation (General Dynamics).

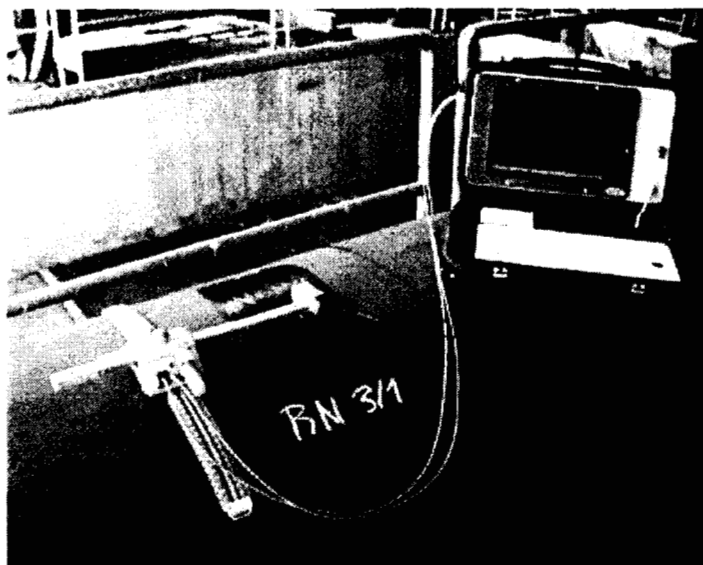
**Figure 3-2:** C-scan bridge strapping firmly attaches the scanner to the test object allowing automatic field inspection. (AEA Technology Energy, UK).



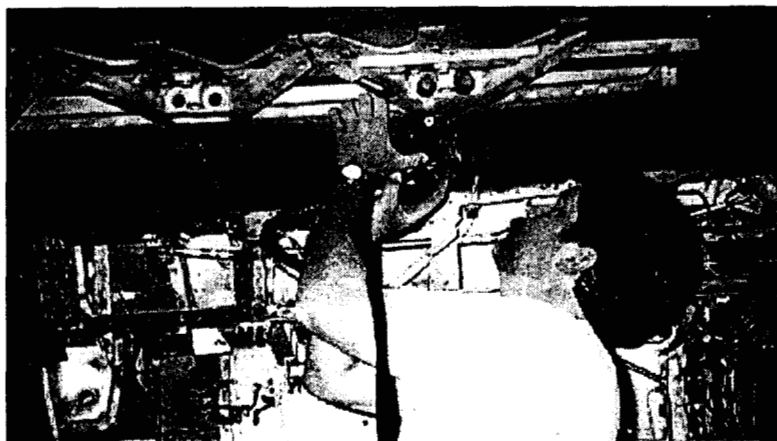
**Figure 3-3:** A scanner using a portable bridge and two suction cups to secure the bridge position during scan (QMI, Costa Mesa, CA).



**Figure 3-4:** A view of the ISCAN's flexible bridge (Fraunhofer Institute) conforming to a pipe surface.



Considering the limitation of stationary scanners, the McDonnell Douglas Corp. developed at the end of the 1980's a scanner called MAUS that allows semi-mobile scanning. MAUS uses a hand-held scanner that translates a series of probes sideways while an operator is responsible for moving the scanner head forward and backward. A photographic view of the MAUS for testing an aircraft structure at a depot setting is shown in Figure 3-5. Unfortunately, inspecting vertical or upside-down surfaces require manual positioning of the scanner head and for the operators this is a very tiring task.



**Figure 3-5:** A view of the application of MAUS and the hand-held probe in a field test.

In recognition of similarity in scanning requirements for multiple NDE methods, efforts made in recent years to produce scanners with interchangeable modules. Such modules include mostly ultrasonic and eddy-current pulser/receiver and sensor components. Such a capability is available on such systems as the MAUS, PANDA and other scanners.

Generally, in a single scanning session, current scanners can cover a limited area defined by the scanner-bridge dimensions. To cover a large area of an aircraft multiple scans need to be performed either of the following two alternatives:

- (a) An operator can move the scanner-bridge from one location to another while forming scan-tiles, which eventually cover the full structure.
- (b) Using multiple rail segments, where the probe mount is made to ride similar to a train and as the scan reaches the end of a rail segment, a rear segment is moved to the front allowing efficient use of the rail segments. Recent models of the MAUS were equipped with this capability.

Viewing the progression of the field inspection technology as an evolutionary process, the next phase in development has been the complete mobility of the scanner, namely the development of crawlers. The first crawlers that effectively "walk" on structures, while controlling their adherence with suction cups, were reported in the early 90's. The developed crawlers are described in great details in the following sections of this Chapter.

### **ACKNOWLEDGEMENT**

The chapter was written at the Jet Propulsion Laboratory, California Institute of Technology, under a contract with the National Aeronautics and Space Administration.

### **3.1.1 REFERENCES**

- Backes P., and Y. Bar-Cohen, "Miniaturization Technologies for Aircraft Inspection," JPL, Pasadena, CA, *Internal JPL Report* No. D-13876, (July 1996).
- Bar-Cohen Y., and P. Backes, " Open-architecture robotic crawlers for NDE of aircraft structures," Materials Evaluation, Vol. 57, No. 3 (1999) pp.361-366.

## 3.2 ROBOTIC CRAWLER WITH OPEN ARCHITECTURE

Yoseph Bar-Cohen and Paul Backes,  
JPL, Caltech, 4800 Oak Grove Dr., Pasadena, CA 90740  
818-354-2610, fax 818-393-4057, [yosi@jpl.nasa.gov](mailto:yosi@jpl.nasa.gov)

3.2	ROBOTIC CRAWLER WITH OPEN ARCHITECTURE .....	1
3.2.1	<i>CRAWLERS</i> .....	1
3.2.2	<i>MULTIFUNCTION AUTOMATED CRAWLING SYSTEM</i> .....	3
3.2.3	<i>AUTONOMOUS CRAWLERS USING INTELLIGENT NNDE</i> .....	4
3.2.4	<i>PLATFORM FOR MINIATURE NDE INSTRUMENTS</i> .....	6
3.2.5	<i>REFERENCES</i> .....	7

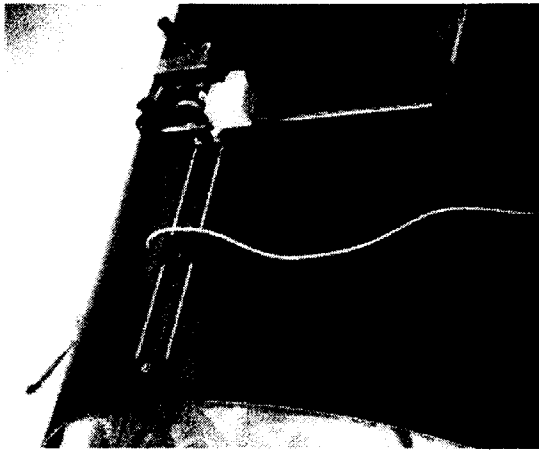
### 3.2.1 CRAWLERS

Performing NDE using such methods as ultrasonics and eddy current, which require a probe to obtain data and scanning to cover large areas, is time consuming and involved with difficulties when applied in field conditions. Rapid inspection of large structures is an ongoing challenge to the NDE community. The need for such a capability grew significantly in recent years as a result of the increase in the numbers of aircraft with composite primary structures and of aging aircraft still in service. Generally, metallic structures are susceptible to corrosion and fatigue cracking whereas composites are sensitive to impact damage that can appear anywhere on the structure. Using manual scanning, field inspection is labor intensive, time consuming and susceptible to human error, whereas removal of parts from an aircraft for a lab test is costly and may not be practical. Effective field inspection requires a portable, user friendly system that can rapidly scan large areas of complex structures. The development of such scanners requires multidisciplinary expertise including NDE, telerobotics, neural networks, automated control, imbedded computing and materials science.

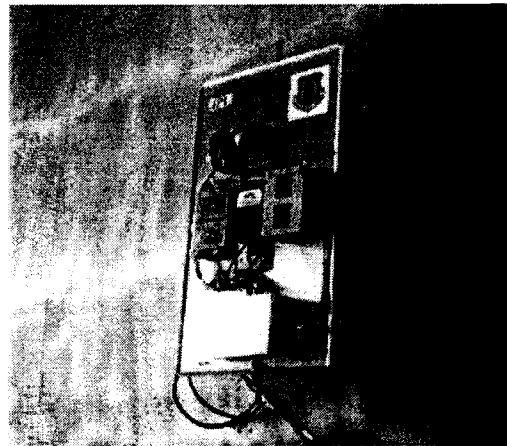
In recent years, various portable inspection systems have emerged including scanners that are placed at selected locations and sequentially repositioned to fully cover the desired areas [Bar-Cohen & Backes, 1999a]. An example of such scanner is shown in Figure 3-6, where the C-scan bridge (QMI, Costa Mesa, CA) is secured to the test structure using vacuum suction-cups. The capability of the developed systems followed the technology evolution and the overall trend is towards full automation with a desire to have a completely autonomous inspection capability. Increasingly, crawling devices are reported as a solution to the need for rapid inspection and the use of suction cups has become a leading form of controlled adherence. In the last several years, several successful mobile portable scanners have emerged including the Automated Non Destructive Inspector (ANDI) [Siegel, 1998] and the Autocrawler [Bahr, 1992]. Recently, JPL developed the Multifunction Automated Crawling System (MACS) offering an open architecture robotic platform for NDE boards and sensors [Bar-Cohen & Backes, 1999a and Bar-Cohen, et al, 1999b]. MACS is a small, highly dexterous crawler designed to perform complex scanning tasks. It uses suction cups for controlled attachment and ultrasonic flexural traveling wave motors for mobility. MACS (shown in Figure 3-7) was designed to inspect large structures particularly in field and depot conditions and it established the foundations for the development of a "walking" computer platform with standard plug-in NDE boards. This concept offers the opportunity to larger pool of companies and individuals to become potential producers of NDE

instruments. Thus, a significant cost reduction can be enabled with a fast transition of novel concepts to practical use. The potential formation of large base of users and developers would lead to rapidly improving, affordable and tailorable systems with potential success similar to the personal computers. In Figure 3-8 a schematic diagram is showing the various components that are needed to operate an open architecture crawler. The crawler consists of a mobile platform with a suite of sensors that can include visual, eddy current, ultrasonic and other sensors. An intelligence algorithm allows performing effective signal processing and data interpretation.

Remote monitoring is one of the avenues of future development where centrally located experts can be responsible for the inspection. Such experts can be equipped with know-how, database, analytical tools, CAD drawing, and accept/reject criteria. These experts will need to deal only with questionable information where the redundant non-defective areas will be screened by the crawler system. Remotely controlling the crawler via Internet using password will allow authorized users to simultaneously operate and view the performance as well as evaluate the test results. Inspection needs can be addressed rapidly, particularly in cases of crisis where it is necessary to examine a full flight of a particular aircraft model all over the world.

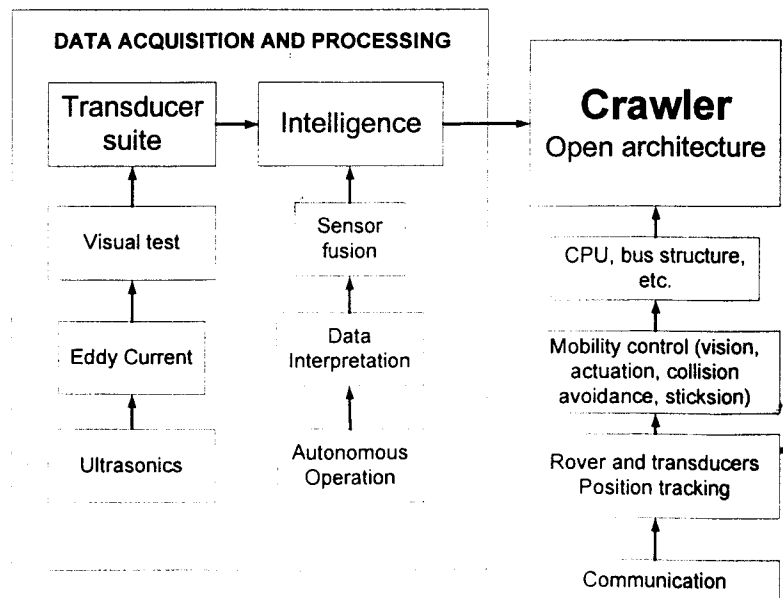


**Figure 3-6:** A scanner is secured to a test structure using suction cups (QMI, Costa Mesa, CA).



**Figure 3-7:** The JPL developed MACS crawling on the C-5 aircraft (Bar-Cohen, et al 1999b).

**Figure 3-8:** Schematic diagram of the components of an open architecture crawler.



A combination of visual, tap testing, eddy current, and ultrasonics are expected to be the leading NDE capabilities that would be integrated into a MACS platform. The potential sensors and NDE methods will be described in Chapter 4. The evaluation of flaws using multiple NDE methods requires data fusion [Gros, 1996] and neural network data interpretation as discussed in Chapter 7. Programming the crawler travel on complex structures can employ telerobotic capabilities similar to the one developed for the exploration of Mars, including the rover of the Mars Pathfinder mission (see Chapter 2). MACS is currently using an umbilical cord for power, control, and communication as well as pressure tubing for ejection and activation of the vacuum suction cups. Further enhancement would lead to the development of an autonomous crawler that can be operated on aircraft structures during idle time and thus reduce the need to ground aircraft for inspection. Making an autonomous crawler would require the integration of miniature vacuum pump, as well as on-board power and computing capabilities. To protect aircraft elements that rise above the surface from accidental damage, a vision system and collision avoidance software need to be used. Employing local Global Positioning Systems (GPS) can provide absolute coordinates without the need for complex, costly and heavy encoders. The information regarding the location of the crawler on the aircraft in relation to the detailed drawings can help assessing flaws criticality.

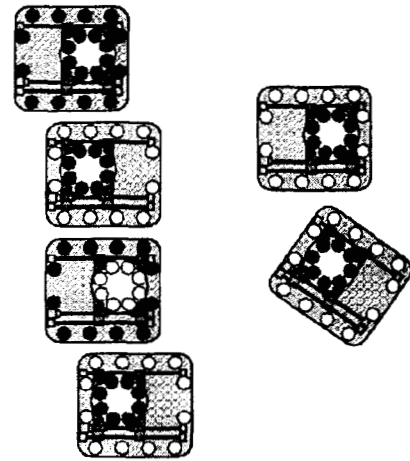
### **3.2.2 MULTIFUNCTION AUTOMATED CRAWLING SYSTEM**

Scanning an aircraft using a portable bridge has been an effective step in addressing the need for field testing capability. However, the limited area that is covered by the scanner-bridge in a single scan is constraining the speed of scanning large area. Further, the rigidity of the bridge prohibits its use for inspection of complex areas particularly near joint with a wing. Reaching beyond the readily accessible areas requires scaffolding, which can damage the aircraft during windy conditions and are time consuming to install. Mobile scanners can greatly increase the rate of inspection, minimize human errors and offer flexibility of reaching various areas of the aircraft. These scanners need to have a controlled adherence capability to maintain attachment to the structure surface while inspecting it. Generally, crawlers are increasing emerging as the solution for the need for unconstrained mobility and dexterity while conducting automatic scanning. The use of suction cups has become a leading form of controlled adherence to aircraft surfaces and several successful scanners were developed in the last several years.

In recognition of the need to have a compact, more maneuverable robotic platform, JPL recently developed a small, highly dexterous crawler so-called Multifunction Automated Crawling System (MACS). This crawler was designed to perform complex scanning tasks [Bar-Cohen & Backes, 1999a and Bar-Cohen, et al, 1999b] taking advantage of its ability to easily turn or move forward and backward while being attached to a curved surface (see Figure 3-9). A schematic view of MACS traveling and rotating while activating its legs and suction cups is shown in Figure 3-10 and from different angle views are shown in Figure 3-11. MACS employs ultrasonic motors for mobility and suction cups for surface adherence. It has two legs for linear motion, with one leg serving as the rotation element for turning. This mobility configuration allows performing any simultaneous combination of motion, including linear travel as well as rotation around the central axis. MACS can be applied to inspecting composite and metallic structures for detection of cracks, corrosion, impact damage, unbonds, delaminations, fire damage, porosity and other flaws, as well as paint thickness measurement. Also, this crawler can be designed to identify dents and individual fasteners.

The development of MACS was benefited from the ongoing JPL development of miniature planetary rovers, as demonstrated by the Mars Pathfinder Mission, as well as telerobotic and NDE techniques. MACS was developed to serve as a generic robotic platform that can be used for many applications, including inspection, paint removal and painting of ships as well as testing/maintaining aircraft. Having many users is expected to lead to lower cost systems that will be improved by a large pool of users and developers. The monitoring of MACS activities can be designed for local control or control via the Internet with password access. A standard PC architecture will enable rapid implementation of new sensors, which can be easily integrated into the setup. To define the crawler functions, plug-and-ply boards will need to be developed and thus enable a new NDE industry that can rapidly introduce novel products as well as transfer technology to commercial use. The JPL's telerobotic program and extensive planetary exploration experience with rover technology provided a valuable resource to this emerging and enabling technology.

**Figure 3-9:** MACS crawler mobility control. Solid circles represent activated suction cups and hollow circles represent resting cups. Forward travel is shown on the left and a simultaneous travel/rotation is shown on the right.

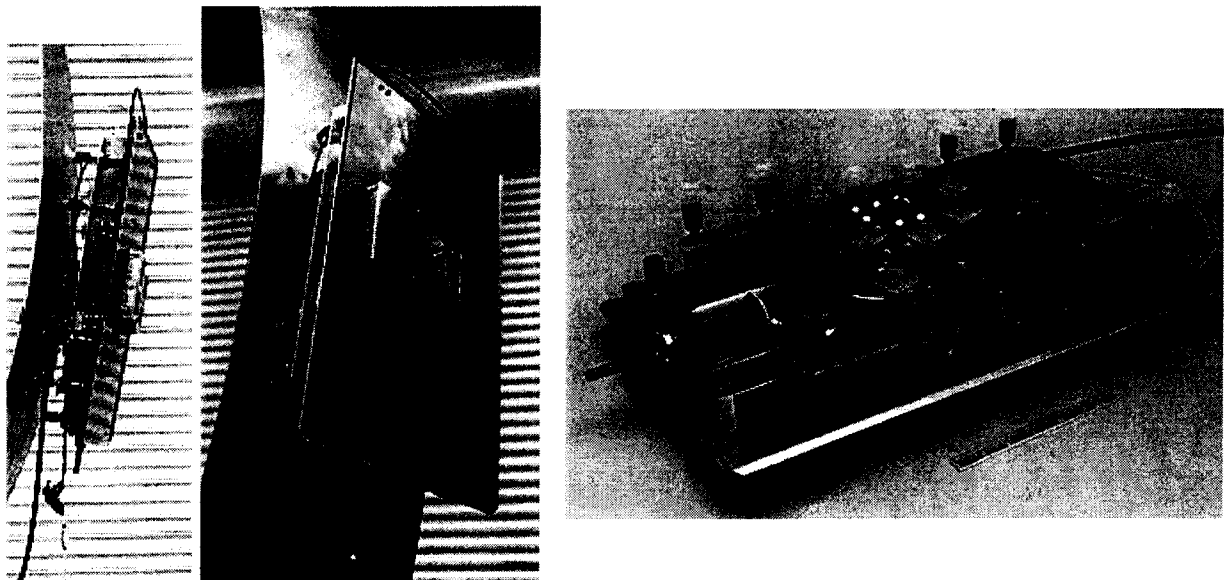


The ability to crawl on surfaces has been enabled by use of suction cup elements that are extended at the stage of attachment. An air pressure in the range of 80 to 120-psi, as can be obtained from conventional pressure lines, is used to eject the suction cups onto the test surface at the moment that the specific leg is made to adhere to the surface. Individual venturi pumps provide each suction cup with sufficient vacuum to assure effective attachment. The ability to adjust the ejection distance of the individual rods allows the crawler to travel on curved surfaces as shown in Figure 3-10. The smallest diameter of the curved surface, which can be inspected by MACS, depends on the suction cups total ejection length and the size of the crawler platform.

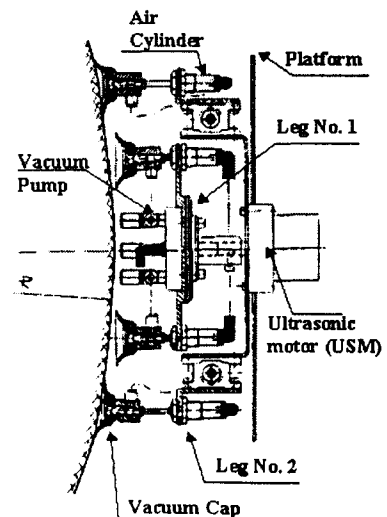
### 3.2.3 AUTONOMOUS CRAWLERS USING INTELLIGENT NNDE

Autonomous operation of NDE crawlers can make a significant impact on the future of field inspection of complex structures, such as aircraft. An autonomous crawler can be monitored remotely by centrally located experts that are equipped with know-how, database, analytical tools, CAD drawing, and accept/reject criteria. Such a capability will allow rapid response to inspection needs, particularly in cases of crisis where it is necessary to examine a full flight of a particular aircraft model worldwide. An autonomous crawler can be operated during aircraft idle time, including night shift, reducing the need to remove an aircraft from service for inspection. Sensors that are based on visual, eddy current and ultrasonic NDE methods are expected to serve as key inspection tools on future autonomous crawlers. Autonomous robotic technology is

currently being studied in numerous areas and at JPL it is being considered for planetary exploration, where the Mars Pathfinder already enjoyed some of its benefits. Miniature robotic technologies with on-board intelligence are being developed for future missions allowing a rover to examine, select and collect planetary samples while avoiding obstacles during operation in an unknown terrain. Since communication between Earth and various planets takes several minutes or more each way, the need for autonomous operation rather than a direct remote control is critical to the success of such NASA missions. The JPL's crawler MACS is currently using umbilical cord for power, communication/control and to provide air pressure for the ejection and activation of the vacuum suction cups. Future efforts are expected to minimize the content of the cord to a safety cable, power and communication. Potential development will reduce the umbilical cord content further to the level of only safety cable with a miniature on-board pressure pump, power, wireless communication, and computing capability. Progress in the field of miniature electro mechanical system (MEMS) is expected to greatly benefit the inspection crawler technology (see Chapter 6 for more information).



**Figure 3-10:** A photographic view of MACS from different angles, where the two legs and the crawler ability to be attached to a curved surface are shown.



**Figure 3-110:** Cross section view of MACS is illustrating its capability to crawl on curved surfaces.

Crawlers can employ local Global Positioning Systems (GPS) and laser localization to determine the absolute coordinates. Further, such GPS systems allow relating the location of the crawler on the aircraft to the detailed drawing and thus assist in the data interpretation for the determination of the acceptability or rejection of flaws as well as the necessary corrective action. To protect aircraft elements that rise above the surface from accidental damage, a vision system can be used in conjunction with collision avoidance software. Data fusion and neural network interpretation can be used to perform intelligent signal acquisition as well as flaw detection and characterization [Vazquez & Bar-Cohen, 1990 and Gros, 1996]. Further discussion of the topic of data analysis and evaluation is given in Chapter 7.

### **3.2.4 PLATFORM FOR MINIATURE NDE INSTRUMENTS**

The personal computer (PC) technology offers a model for smart mobile platforms, namely the establishment of the equivalent to the motherboard. Various companies are making boards and components for PC allowing them to concentrate on their strength and innovation, rather than having to produce a complete new system each time they launch a new product. As an example, manufacturers of a modem are concentrating on improving their product or introducing new boards without having to make a complete personal computer. The key issue is that these companies can dedicate their capability and resources to well defined product area and it is possible due to the motherboard architecture standard to which they maintain compliance.

Crawlers can be developed as "walking computer", i.e. mobile platform with on board motherboard. NDE boards need to be developed while commercially available control software, power, intelligence and communication capabilities can be used. The crawlers can be produced by telerobotic companies, which will have standard bus architecture offering a plug-in capability for miniature NDE instruments. Such crawlers will allow the NDE industry to concentrate on making unique miniature instruments modules for plug-in onto the crawler platform and making driver software for the control of the modules. This field is multidisciplinary and just as in the case of the PC technology it is very difficult for a single company to possess all the necessary expertise. This approach offers opportunity for a larger pool of potential companies to produce components and the ability to use commercially available components, thus significantly reduce cost. The engineering side of the crawler technology involves the development of power supply, mainframe, bus and wireless communication, position tracking (local GPS, encoders, etc.), controlled attachment, actuators and motion control. In the area of NDE instruments miniaturization, the field is starting to see some progress but there is much work that needs to be done and more companies need to be involved. The JPL's MACS crawler can serve as a baseline technology for an industry standard. The micro-electronic mechanical systems (MEMS) technology will enable future generations of extremely small scanning NDE instrumentation.

The field is still relatively new and more development is needed before an autonomous crawler can become available for robotic inspection of aircraft structures. To accelerate the development, the principal author of this section has taken an initiative through ASNT to have Sessions on Robotics Miniaturized NDT Instruments in each of the ASNT conferences since the '96 Fall Conference, which was held at Seattle, WA. Efforts are being made to nurture the growth of the pool of companies that are producing miniature instruments and modular plug-ins.

### ACKNOWLEDGEMENT

The chapter was written at the Jet Propulsion Laboratory, California Institute of Technology, under a contract with the National Aeronautics and Space Administration.

### 3.2.5 REFERENCES

- Backes P., and Y. Bar-Cohen, "Miniaturization Technologies for Aircraft Inspection," JPL, Pasadena, CA, *Internal JPL Report* No. D-13876, (July 1996).
- Bahr V., "Wall-Climbing Robot in Non-Structural Environment," *Transaction Robotics Research, Robotics International, Society of Manufacturing Engineering*, Vol. 2 (1992), pp. 1-24.
- Bar-Cohen Y., and P. Backes, "Open-architecture robotic crawlers for NDE of aircraft structures," *Materials Evaluation*, Vol. 57, No. 3 (1999a) pp.361-366.
- Bar-Cohen Y., B. Joffe and P. Backes "Multifunction Automated Crawling System (MACS)", U.S. Patent No. 5,890,553, April 6, 1999b
- Gros X.E., *NDT Data Fusion*, <http://www.riam.kyushu-u.ac.jp/fracture/xav16.htm> ISBN: 0340676485 Arnold, London, UK (1996)
- Siegel M., P. Gunatilake and G. Podnar, "Robotic Assistants for Aircraft Inspectors," *IEEE Instrumentation & Measurement Magazine* (March 1998) pp. 16-30.
- Vazquez C. A., and Y. Bar-Cohen, "Application of Artificial Intelligence to NDE," *McDonnell Douglas Corp. Report* No. K4870, Long Beach, CA. (April 1990) pp. 1-32.

# CHAPTER 4: NDE SENSORS

## 4.1 OVERVIEW ON SENSORS

Yoseph Bar-Cohen,  
JPL, Caltech, 4800 Oak Grove Dr., Pasadena, CA 90740  
818-354-2610, fax 818-393-4057, [yosi@jpl.nasa.gov](mailto:yosi@jpl.nasa.gov)

<b>CHAPTER 4: NDE SENSORS .....</b>	<b>1</b>
4.1 OVERVIEW ON SENSORS .....	1
4.1.1 VISUAL .....	1
4.1.1.1 Dual-Pass Light Reflection (D-Sight™) .....	2
4.1.1.2 Edge Of Light™ (EOL) .....	2
4.1.2 EDDY CURRENT .....	3
4.1.2.1 Magneto-Optics Imager (MOI) .....	3
4.1.2.2 Pulsed Eddy Current (PEC) .....	4
4.1.2.3 Superconducting Quantum Interference Device (SQUID) .....	4
4.1.3 RADIOGRAPHY .....	6
4.1.3.1 Compute Tomography Scan .....	7
4.1.3.2 Reverse Geometry X-Ray (RGX) Imaging .....	8
4.1.3.3 Microfocus X-ray Microscopy .....	9
4.1.4 ULTRASONICS .....	9
4.1.4.1 Dry Coupling Techniques .....	10
4.1.4.1.1 Air-Coupled transducers .....	10
4.1.4.1.2 Electromagnetic acoustic transducer (EMAT) .....	11
4.1.4.1.3 Laser induced ultrasound .....	11
4.1.4.2 NDE of Composites using Oblique Insonification .....	12
4.1.4.3 Portable Real-Time Imager Using CCD .....	13
4.1.5 SHEAROGRAPHY .....	14
4.1.6 THERMOGRAPHY .....	15
4.1.6.1 Thermal Wave Imaging .....	15
4.1.7 REFERENCE .....	16

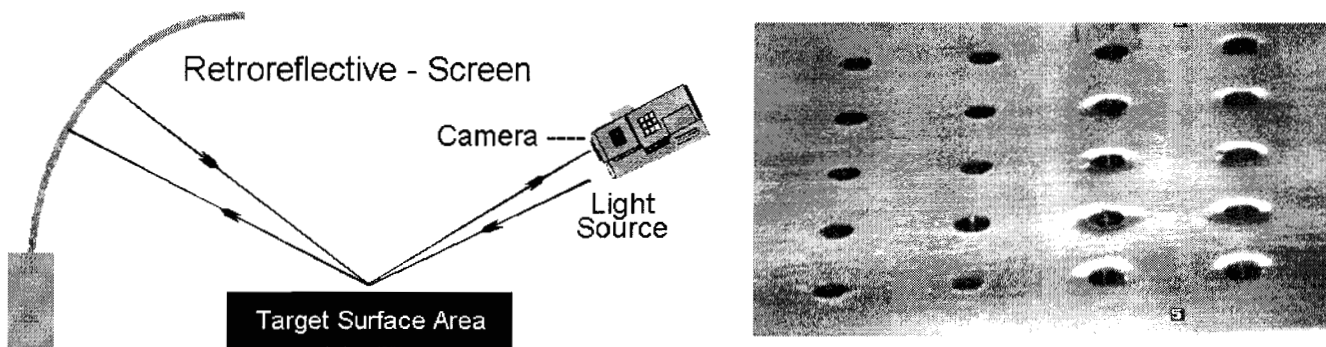
A key element to automation of nondestructive inspection is the use of sensors that are electro-mechanically manipulated to perform the test. Ultrasonics has been one the first methods to be automatically operated in C-scan system and it was followed gradually with the application of automation to all other NDE methods. The sensors and the form of application of the various methods are reviewed in this chapter.

### 4.1.1 VISUAL

Visual inspection is continuing to be the leading NDE method and it represents the highest percentage of the inspection procedures that are applied to aircraft structures in service. To enhance the capability of inspectors to perform visual inspection, new tools were developed including improved illumination techniques, miniature video and dexterous small-diameter boroscopes. Two visual inspection techniques, that worth noting for their automation potential, include the D-Sight and the Edge of Light (EOL). While D-Sight already found its way to practical use, the EOL technique is relatively new and it is still in development stages.

#### 4.1.1.1 Dual-Pass Light Reflection (D-Sight™)

Surface and near-surface flaws, such as corrosion in metals and impact damage in composites, are causing local surface deformation. The visual inspection technique called D-Sight (Diffrauto Limited) enhances the appearance of this deformation and increases its visibility [Forsyth, et al, 1998]. A D-Sight inspection system consists of a CCD camera, a white light source mounted slightly above the camera lens [<http://www.diffrauto.com/products/dsight/dsight.htm>], and a retro-reflective screen. In Figure 4-1, a schematic view is showing the principle operation of D-Sight and on the right an example of test result for cold worked holes can be seen. The system's screen is made of a reflective micro-bead layer and is the most important element of the D-Sight system. While the screen returns most of the light in the same direction of the incidence, a slight amount of light is dispersed. When a surface is illuminated by a light source, local surface curvatures are focusing or dispersing the light onto the retro-reflective screen. A light pattern is formed on the screen and is reflected back to the source with a slight dispersion. This path of the light is backlighting the part surface and enhances the scattering effect of surface deformations. By viewing the surface slightly off-axis from the light source a unique pattern appears near local surface deformations. This pattern consists of bright and dark gray scale variations, where higher curvatures appear more intense due to the effect of focusing and diffusing the light. To obtain a sufficient level of diffused light the surface must be reflective, otherwise a thin layer of liquid needs to cover the surface to increase its reflectivity.



**Figure 4-1:** D-Sight principle of operation (left) and an example of the test result for cold worked holes (Diffrauto).

#### 4.1.1.2 Edge Of Light™ (EOL)

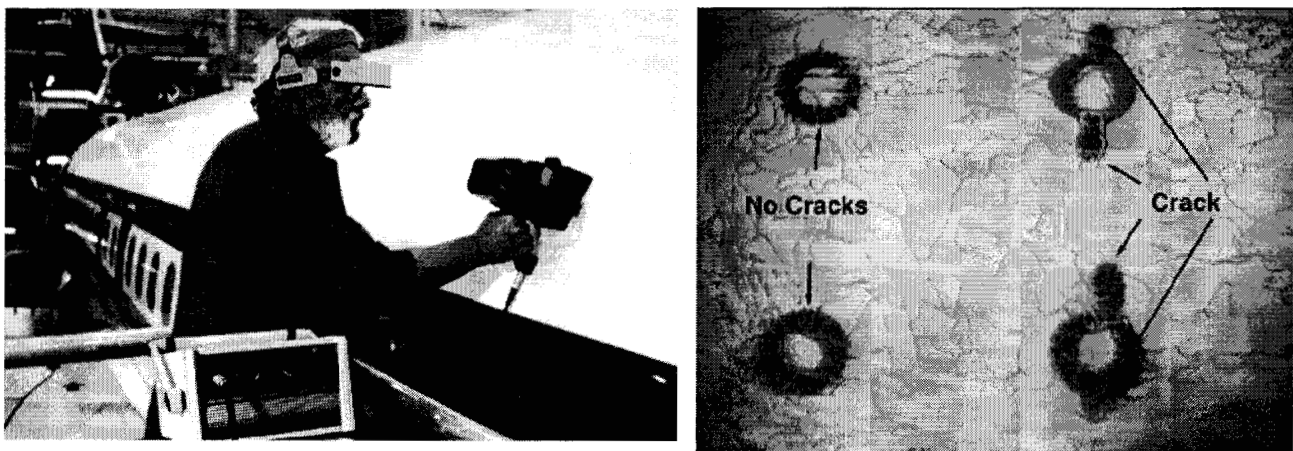
Another technique of enhancing the surface deformation that is caused by flaws is the Edge of Light™ (EOL) [Forsyth, et al, 1998]. It employs elements commonly used in optical scanners and it uses the scattered light from surface deformation and variations in the surface slope to produce an image that consists of light intensity variations. The technique is relatively quick having scanning speeds on the order of 2 to 20-linear cm/sec using line scan widths of 10-cm or more. EOL inspection results are easily interpreted, as they closely resemble the actual subject. The technique has been demonstrated to be applicable to detection of corrosion in surfaces and joints, as well as flaws in gas turbine components and turbine disks. For some applications, EOL was shown to have better detection capability than liquid penetrant, magnetic particle, ultrasonic inspections, or optical microscopy.

### 4.1.2 EDDY CURRENT

For over three decades, eddy current has been one of the leading in-service inspection methods for crack detection around and inside fastener holes. Significant improvements were made to enhance the method capability, reliability and user friendliness. Modeling the interaction of eddy currents and flaws contributed significantly to the understanding of the key parameters as well as the reduction in the effect of noise and liftoff. Improved probes and instrumentation were developed and low frequencies were effectively used to enable inspection of metallic layered structures for detection of flaws in the second and third layers. The Magneto-Optics Imager (MOI) has been one of the spin-offs of the eddy current method and it is being practically implemented by the aircraft industry. Another eddy current technique that emerged in recent years is the pulse eddy current. The early phases of the development of this technique were made at Iowa State University and South West Research Institute and currently it is being transitioned to a practical hardware at the Canadian National Research Council. Further, To detect cracks in thick or multilayered metallic structures, the technique called SQUID was developed. These three techniques are briefly described herein.

#### 4.1.2.1 Magneto-Optics Imager (MOI)

In order to simplify the detection of flaws, the Magneto-Optics Imager (MOI) was developed as a means of visualizing the eddy current response [Fitzpatrick, et al, 1996; and Thome, 1997]. The Magneto-Optic Imager (MOI) combines planar eddy current and magneto optic imaging and it is applicable to inspection of metallic structures for detection of surface and subsurface flaws. MOI can be used to visualize flaws in real time through paint and other surface coverings and to project the results on a heads up display and/or a monitor. MOI is employed in a hand-held (see Figure 4-2) portable instrument that requires minimal training and its capability greatly increases the speed and reliability of inspection. This technique is currently being used extensively for aircraft inspection by airlines, maintenance facilities and the military. The MOI probe head, which is shown in Figure 4-2, can be easily carried by a mobile robot to perform an automatic inspection. This possibility will be described in more details later in this Chapter.



**Figure 4-2:** A photographic view of an MOI inspection (left) and an image of indication of cracks around fasteners (right) (PRI, Torrance, CA).

#### **4.1.2.2 Pulsed Eddy Current (PEC)**

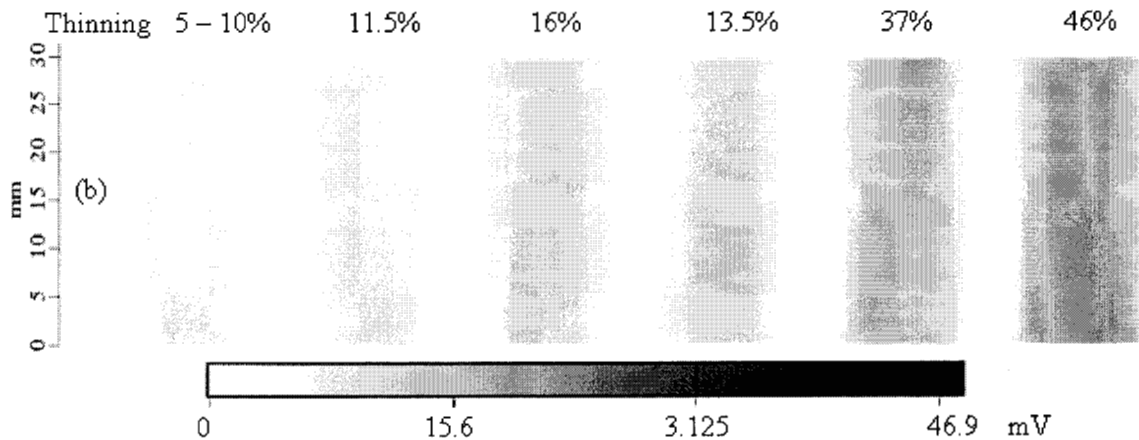
Conventional eddy current techniques use single frequency sinusoidal excitation and measure flaw responses as impedance or voltage changes on an impedance plane display. To detect flaws, inspectors interpret the magnitude and phase changes, however these parameters are sensitive to many variables that hamper the flaw characterisation. Multiple frequency measurements can be combined to more accurately assess the integrity of a structure by reducing signal anomalies that may otherwise mask the flaws. Initial development led to the use of dual frequency eddy-current where frequency mixing functions allowing quick application of the technique. This approach has been shown to be useful in reducing the effects of variations in plate spacing when inspecting for second layer corrosion in lap splices [Thompson, 1993]. The dual frequency technique offers advantageous when performing large area inspections by means of eddy current C-scans of specimens with corrosion under fasteners [Lepine, 1997]. Unfortunately, conventional multiple frequency techniques can provide limited quantitative data and are difficult to use for flaw visualisation in an intuitive manner.

Swept frequency measurements using impedance analysers perform well in quantitative corrosion characterisation studies, especially when they are interpreted in conjunction with theoretical models [Mitra, et al, 1993]. However, the application of these techniques is too laborious. In contrast to the conventional eddy current method, pulsed eddy current (PEC) excites the probe's driving coil with a repetitive broadband pulse, such as a square wave. The resulting transient current through the coil induces transient eddy currents in the test piece, associated with highly attenuated magnetic pulses propagating through the material. At each probe location, analogous to ultrasonic inspection data, a series of voltage-time data pairs are produced as the induced field decays. Since a broad frequency spectrum is produced in one pulse, the reflected signal contains flaw depth information. Physically, the pulse is broadened and delayed as it travels deeper into the highly dispersive material. Therefore, flaws or other anomalies close to the surface affect the eddy current response earlier in time than deep flaws. Similar to ultrasonic techniques, the modes of presentation of PEC data can include A-, B- and C-scans [Bieber, et al, 1998]. Interpretation, therefore, may be considered more intuitive than conventional eddy current data. The excitation pulse, signal gain and sensor configurations can be modified to suit particular applications. Examples of C-scan results of testing two plat layers with various degrees of thickness loss on the top of the second layer are shown in Figure 4-3. Obviously, the similarities to ultrasonics make the application of automation to the PEC technique a relatively easier task

#### **4.1.2.3 Superconducting Quantum Interference Device (SQUID)**

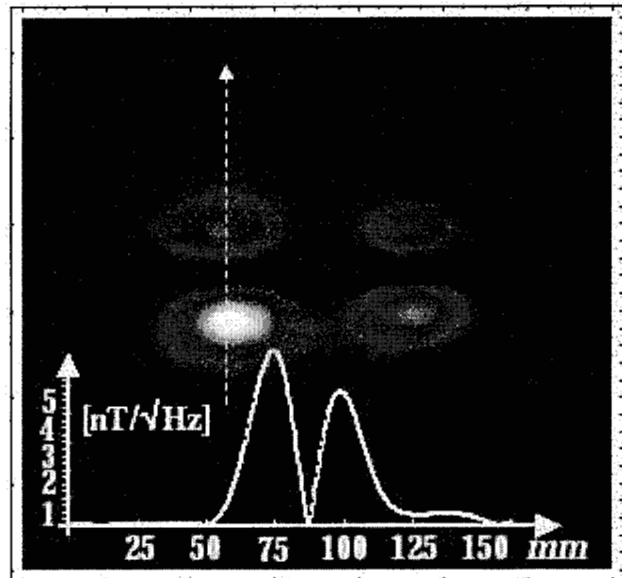
SQUID is a magnetic field sensor for eddy current measurements that are highly sensitive even at low frequencies and this sensitivity is nearly independent of frequency. This property offers an advantage for magnetic field sensor in applications where a low excitation frequency is needed for large depth of penetration. The technique requires cooling to cryogenic levels and it has been demonstrated to be highly effective for flaw detection applications. Recent research in SQUID-based NDE systems [e.g., Kreutzbruck, 1998] has proven their superiority over conventional systems when searching for cracks in depth of 10 mm or more [Ma and Wiksw, 1994]. Further, it was shown to have an improved signal to noise ratio of up to 3 orders of magnitude for cracks deeper than 13mm. Additionally, the high bandwidth available with certain SQUID systems makes measurements over a wide frequency range possible without

having to change the sensor. The high dynamic range (the ratio between the highest field change which can be measured before the system goes into saturation and the lowest detectable field) allows one to detect small field changes in the presence of large background fields, as produced by edge effects or inhomogeneities in conductivity. The technique is effective mostly in low frequency applications for the detection of deep lying defects, in multilayer structures, rivet plates and aircraft wheels. One concern that needs to be taken into account is that for deep structures the eddy currents are spread over a larger area and the spatial resolution might be too low for practical purposes. The large dynamic range of SQUID allows shorter integration time and therefore faster scanning is possible. Figure 4-4 shows the eddy current field distribution above a sample with 40-mm long and 0.6-mm high crack tested through a 13-mm thick aluminium plate. Depending on the variation of the conductivity of the covering plate, a substantial background occurs, which limits the reliable detection of deep lying and small cracks. Integrating a SQUID probe into a manipulation system that allows scanning of complex shape structures makes this technique more practical and enhances the inspection speed.



**Figure 4-3:** PEC amplitude c-scan of 2-layer plate specimen with metal loss located at the top of the second layer [Lepine, 1997].

**Figure 4-4:** The field distribution above a sample with 40 mm long and 0.6 mm high crack covered by a 13 mm thickness aluminium plate. [Kreutzbruck, 1998]



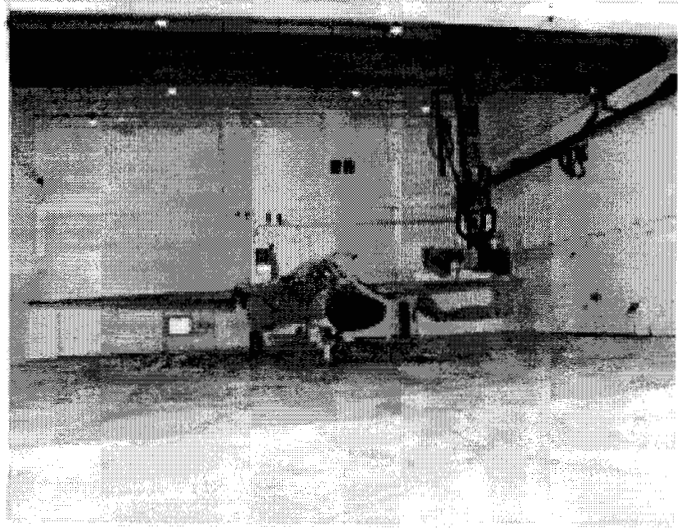
### 4.1.3 RADIOGRAPHY

The capability of radiography to provide an image that is relatively easy to interpret made it an attractive NDE technique for both industrial and medical applications. The health hazard associated with the exposure to this ionizing radiation and the use of films to record the images constrained the application of radiography. The development of real time imaging techniques for radiographic visualization helped overcoming the time consuming process that was involved with film recording and enabled the automation of the inspection process. Moreover, computer processing of digitized images offered image enhancement capabilities as well as the quantification of the inspection criteria.

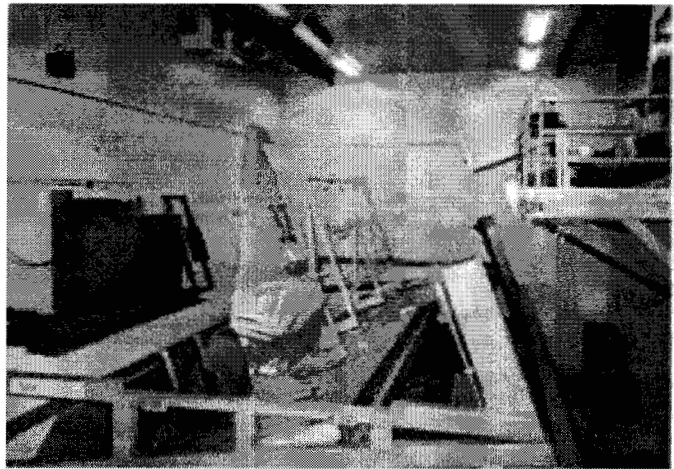
The need to inspect large structures as big as a full aircraft wing was effectively address at McClellan Air Force Base inspection facility. A robotic setup that carries the source of radiation and the detector has been in used since 1988. A photographic view of the system in relation to an inspected F111 aircraft is shown in Figure 4-5. Generally, X-ray radiography is a widely used technique, whereas the complexity of the Neutron radiographic (also known as N-ray) limited its application to well defined critical problems. One of the most significance applications of N-ray radiography is the inspection of aging aircraft. The N-ray method is particularly effective in detecting hydrogen-based substances such as moisture and corrosion in extremely small quantities. In spite of the complexity that is associated with the application of this technique, efforts were made to adapt it to inspection at aircraft maintenance facilities. The most notable success is the McClellan AFB depot application, which was introduced to service in 1989 for detection of fluids and inspection of pyrotechnic device. For this purpose, 1-megawatt TRIGA nuclear reactor was developed in four separate inspection bays. The large number of neutrons produced by this reactor makes high-resolution imaging that is significantly higher than practical with isotope or generator types of sources. Both film radiography and image enhanced real-time neutron radiography are options of the system using six axis, component positioning robots that manipulate items as large as 30 feet by 12 feet. Later, the capability was modified to allow performing Neutron tomography for special applications where conventional imaging techniques fall short. This technology was adapted to detecting excessive hydration levels that cause hydrogen embrittlement in titanium jet engine fan blades. Further, McClellan AFB has adapted a Maneuverable Neutron Radiography System that is a hanger based robotic system using a Californium 252 thermal neutron source to perform N-ray inspections of aircraft without component removal from the airframe. The Programmable Overhead Positioner is a 6-axis overhead gantry robot that features the ability to enhance images at near real-time N-ray inspections on structures such as wings and stabilizers. Also, this system is applicable for inspection of fuselage structures using film type N-ray radiography. Further, a Programmable Underside Positioner is employed using a rail mounted 4-axis robot that is designed to inspect engine bays or structural panels which require underside access. Bay access clearances of 83 feet width, 9 feet depth, and 25 feet height allow access of large fighter size aircraft and various helicopter models. In Figure 4-6, a photographic view is showing one of the N-Ray inspection systems testing an aircraft stabilizer at the McClellan AFB.

Other radiographic techniques that deserve attention include the CT scan, Reverse Geometry X-ray and Microfocus X-ray microscopy. These techniques will be reviewed briefly in the following sub-sections.

**Figure 4-5:** Robotic X-ray scanner testing an F111 aircraft at McClellan AFB [Courtesy of Thomas Ducharme, 1999].

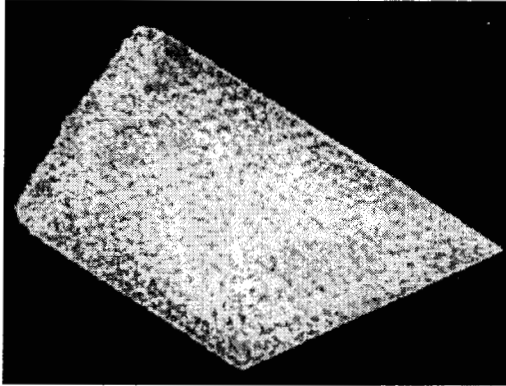


**Figure 4-6:** Automated Neutron Radiography Scanner testing a wing of an aircraft at McClellan AFB [Courtesy of Thomas Ducharme, 1999].

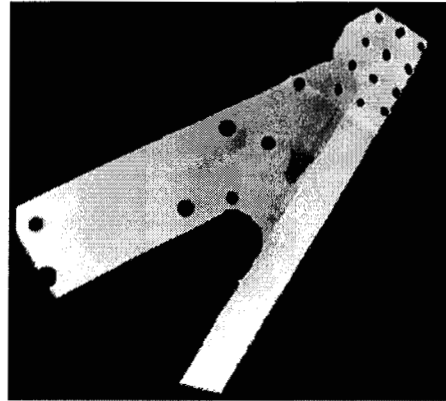


#### 4.1.3.1 Compute Tomography Scan

Computer processing of the X-ray transmission coefficient distribution in a structure obtained from a series of viewing angles is used to produce computed tomography (CT) scan [Kak & Slaney, 1988]. For over three decades, this radiographic technique has been widely in use as an important medical tool. At the early 80's, the technique was transferred to industrial use by researchers at the Air Force Materials Laboratory. The technique is highly effective in testing composite structures and it provides a quantitative information about the distribution of the material density. Images can be produced and manipulated in real-time and allow recognition, localization and classification of material defects (e.g. pores, blowholes, foreign bodies). The inspection can be done automatically in arbitrary test samples (e.g. in metal, ceramic, glass or synthetic material castings). Three-dimensional position and extension of a defect can be determined by evaluating pairs of stereoscopic transmission images [Chen, et al, 1990]. Depending on the object geometry, the acquisition of stereoscopic images can alternatively be done by translation or rotation of the sample. The defect extension in direction of transmission is calculated by using the absorption law adapted for polychromatic radiation. An example of CT scan of a graphite/epoxy sample is shown in Figure 4-7.



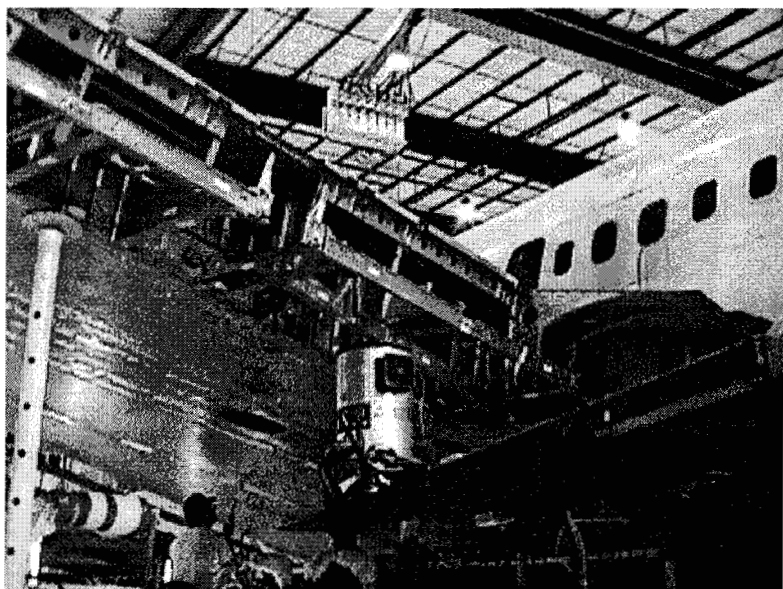
**Figure 4-7:** CT image of the density distribution in a reference graphite/epoxy sample.



**Figure 4-8:** RGX image of corrosion in an F-111 Horizontal Stabilizer Tip Cap (Digiray).

#### 4.1.3.2 Reverse Geometry X-Ray (RGX) Imaging

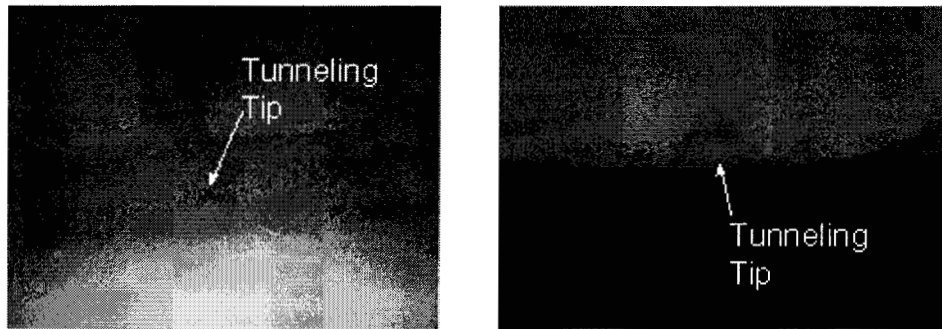
In contrast to conventional radiography, RGX reverses the relative sizes of source and detector as well as the location of the object [Dolan, et al, 1993]. The object is placed adjacent to the large, computer-controlled raster-scanning source, whereas the point detector is placed at a distance. This arrangement allows scattered radiation to bypass the detector, thereby increasing the contrast sensitivity (signal-to-noise ratio). The technique has been demonstrated to detect such flaws as corrosion, impact damage, and water entrapment in aluminum and composites. In the case of corrosion on aircraft, it was possible to detect the loss of material down to as little as 1.0%, even when the material loss is disguised by the presence of corrosion products. An example of a Reverse Geometry image of corrosion in an F-111 Horizontal Stabilizer Tip Cap is shown in Figure 4-8. A view of an RGX system inspecting a Boeing 707 wing area is shown in Figure 4-9 where an array of 8 detectors is placed above the wing and the X-ray tube source is below the wing. Generally, the distance between object and detector can be easily increased to reduce parallax effects and increase throughput for large area honeycomb and/or thick honeycomb inspection.



**Figure 4-9:** A view of a Reverse Geometry X-ray system inspecting a Boeing 707 wing area.

#### 4.1.3.3 Microfocus X-ray Microscopy

Using a small source to provide a great magnification of the inspected object, Microfocus X-ray Microscopy operates similarly to conventional radiographic techniques [Olivas, et al, 1997]. Conventional radiographic techniques generate X-rays from a thick target, typically tungsten, oriented at 30° or 45° angles to the electron beam source. X-ray images are produced with limited magnification. Through the use of a thin film target oriented normal to the electron beam source, samples are positioned opposite to the beryllium window thereby minimizing working distance and maximizing magnification. The microfocused beam (~3  $\mu\text{m}$ ) further enhances resolution by increasing sharpness of the image as compared to the one obtained using larger focal spot sizes. Geometric magnification for typical fine-focus applications are ranging from ~3X to 1000X with capabilities of extending beyond 2000X. For conventional transmission microfocus X-ray, the tube voltage ranges from 10 - 225kV with focal dimensions from 3 to 200  $\mu\text{m}$ . By manipulating the sample and viewing a real-time image, defects normally obscured in conventional 2-D background noise can be readily imaged. The technique is widely used for NDE of microelectronics and aerospace applications for parts with miniature internal components. An example of images obtained using Microfocus X-ray from two different viewing angles are shown in Figure 4-10, where a hydrophone with a microns size tunneling tip was examined. Since the image is produced electronically in real-time this technique can be automated for microelectronics production line inspection and other quality assurance applications.



**Figure 4-10:** Microfocus X-ray image of a hydrophone tunneling tip as viewed from isometric (left) and profile (right) views.

#### 4.1.4 ULTRASONICS

Ultrasonics is one of the most versatile and informative NDE methods and was the first method to be automated. The various modes, that these waves can support, allow the extractions of detailed information about flaws as well as determining various material properties. Techniques were developed employing the various wave modes as well as the scattering and mode-conversion that are associate with the wave interaction. Such techniques include the Acousto-Ultrasonics, which is practically used for flaw screening, and the ultrasonic angular insonification to induce the polar backscattering and leaky Lamb waves. As discussed in Chapter 3, portable scanners were developed to perform rapid inspection. For applications where mechanical scanners are not applicable, transducer array and CCD technology were used to simplify the imaging process. The difficulties associated with the need for liquid couplant, which affected mostly field applications, led to the development of various fixtures including water filled boots and wheels, bubblers and squirters. Recently, a dripless bubbler was developed at Iowa State University where water is recycled using a vacuum pump [Patton &

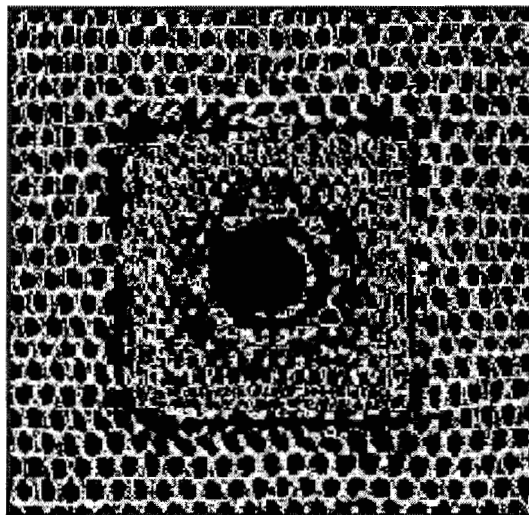
Hsu, 1998]. Even though the bubbler adds significant mass to the probe mount, it maintains most of the water and it was demonstrated as an effective technique of performing the equivalent of immersion in field conditions. Alternative dry coupling techniques were also developed including the use of air-coupled piezoelectric transducers, Electro-Magnetic Transducers (EMAT) and Laser Ultrasonics [Green, 1997]. These alternative techniques of eliminating the need for water coupling address an important issue that affect the practicality of automated ultrasonic inspection in field conditions.

#### **4.1.4.1 Dry Coupling Techniques**

The inability to transmit and receive ultrasonic waves through air or gas was a limiting factor in developing rapid field inspection as well as testing materials that are porous or water sensitive. Most ultrasonic NDE applications operate at frequencies in the range of 1- 10 MHz, where traveling through air is highly attenuative. The acoustic impedance of air differs significantly from the one for the piezoelectric transmitter and the test part causing large percentage of energy reflection. Therefore, only a very small fraction of the energy is transmitted through the part and the transducer interfaces.

##### *4.1.4.1.1 Air-Coupled transducers*

One solution to overcoming this air-coupling problem without using additional transition media can be the induction of sufficiently high sound level and using high-gain, low-noise amplification [Grandia & Fortunko, 1995; and Wykes, 1995]. To enhance the transmitted energy, the transducer needs to be used with no backing layers and thus taking advantage of the high mechanical-quality factor  $Q$  of piezoelectric disks. Also, to improve the generation and reception efficiencies of the transducer, its front protection layer is made of a thin porous material having low specific impedance. The transducer needs to be driven by tone-bursts with a center frequency that exactly matches the thickness-mode resonance. In addition, using focused transducers one can further increase the sound pressure and sensitivity. Such modifications of the transducers and hardware allowed the operation of air-coupled ultrasonic C-scans at the Megahertz frequency range. While it is still limited to materials with relatively low acoustic impedance, such as composites, it is already being used extensively at various industrial applications where water can not be used as a coupling medium. In Figure 4-11, an example of a C-scan is shown where a solar honeycomb panel with a 5x5-cm stiffener insert was tested using a 400 KHz air-coupled through-transmission. The bonded honeycomb core, the area of the insert and the missing core can be seen easily.



**Figure 4-11:** A 400 KHz air-coupled through-transmission C-scan of solar honeycomb panel with a 5x5-cm stiffener insert [Grandia & Fortunko, 1995].

#### *4.1.4.1.2 Electromagnetic acoustic transducer (EMAT)*

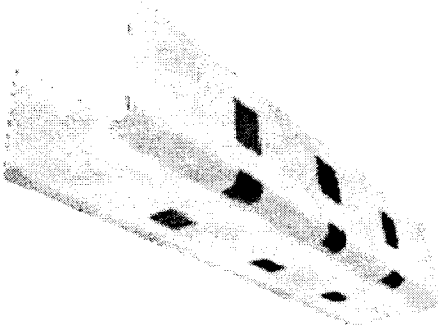
EMAT is a type of transducer that uses eddy current to generate and receive acoustic signals and it offers the capability to perform dry coupling [Oursler & Wagner, 1995]. The technique allows the induction of specific ultrasonic modes including normal beam and angle-beam shear wave, Shear Horizontal (SH) plate wave, Rayleigh wave and Lamb wave [Hübschen, 1998; and Hutchins, et al, 1987]. The ability to induce horizontally polarized shear waves has a great significance for the inspection of austenitic welds. Another advantage of this type transducer is their ability to operate at high temperatures. However, the main disadvantage of EMAT arises from its relatively low transmitted ultrasonic energy constraining the transducer dynamic range by electronic noise. As a result, such transducers are limited to the lower frequency range. Another effect that is associate with the low transmitted energy is the critical dependence of the induced energy on the probe proximity to the test object. For practical applications, this distance is commonly maintained below 1-mm.

#### *4.1.4.1.3 Laser induced ultrasound*

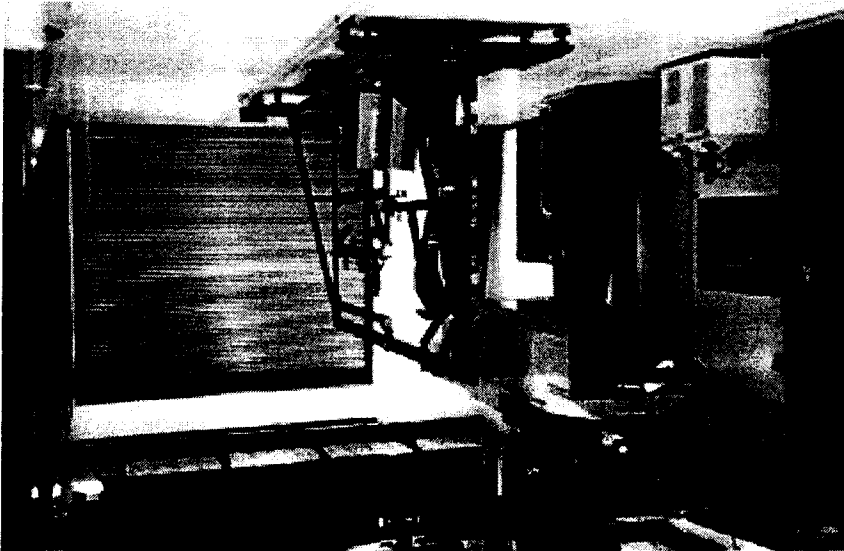
Laser ultrasonics is one of the effective techniques of inducing and receiving ultrasonic waves without the need for a couplant. The need for beam steering to perform the inspection makes this technique an ideal one for automatic inspection. The received signals are evaluated very similar to the pulse-echo technique and parts can easily be scanned from a distance of about 3-4 meters. The technique induces short pulses in the range of 10- $\mu$ sec causing a rapid heating and expansion of the surface forming elastic pulses. The reflected signals are examined by an interferometric setup and such systems were developed by several universities including the Center for NDE at John Hopkins University as well as the Canadian National Research Council [e.g., Scruby & Drain, 1990; and Monchalín, et al, 1998]. Also, a commercial system was developed by UltraOptec (Québec, Canada), which was delivered for operation at the Air Force maintenance facility at McClellan AFB (See Figure 4-12) for inspection of composite and bonded structures [Fiedler, et al, 1997]. The technique is effective for inspection of structures with complex geometry allowing examination of surfaces with a slop of up to about  $\pm 45^\circ$ . This capability was applied to mapping defects in parts that are contoured and presenting the results in 3-D (see Figure 4-13) with no critical orientations requirement for the incident beam. The limiting factor in the scanning speed is the inability to induce pulses at high rate, where an average of 100 pulses/sec is commonly used. Overall, the cost and the sensitivity of the laser ultrasonic technique are limiting the wide usage of laser ultrasonics. New techniques are continuously being introduced in an effort to reduce the cost of the hardware. However, the sensitivity is fundamentally bounded to about 45dB because there is a lower limit to the detection sensitivity as defined by the detection of a single phonon, whereas the upper limit is set by the desire to avoid thermal damage to the surface of the test structure. The commercially available systems offer user friendly imaging software which displays A-scans, B-scans and C-scans as well as 3-D ultrasonic images that are easy to manipulate for various angles of view.

Composite materials are now making a significant percentage of aircraft and spacecraft flaw critical structures. These materials susceptibility to flaws during production and assembly as well as the cost associated with their inspection presented issues of concern to the NDE community. Moreover, these materials are reaching service duration for which flaws due to aging are requiring a greater attention. Standard NDE techniques, which were developed to inspect metallic structures, were adapted by the industry for inspection of composites partially accounting for the multi-layered anisotropic nature of these materials. The adapted NDE techniques provide limited and mostly qualitative information about the material properties and defects. The author discovery of the ultrasonic Polar Back-Scattering (PBS) [Bar-Cohen & Crane, 1982] and the leaky Lamb wave (LLW) [Bar-Cohen & Chimenti, 1994] phenomena (1979 and 1982, respectively) in composites added a powerful arsenal of quantitative NDE techniques. These phenomena are based on obliquely inscattered ultrasonic waves and the numerous analytical and experimental studies of these phenomena helped paving the path for the application of these techniques. Using PBS, the fiber orientations can be determined whereas porosity clusters and fatigue cracks can be mapped. Further, using inversion of LLW data, the elastic properties of composite panels can be determined. Flaws can be characterized uniquely, and the quality of adhesive bonded-joints can be determined [Bar-Cohen, et al, 1993; and 1999; and Bar-Cohen, 1990]. The LLW data is acquired in the form of dispersion curves that show the phase velocity as a function of frequency along various polar angles

#### 4.1.4.2 NDE of Composites using Oblique Insonification



**Figure 4-13:** A 3-D C-scan image of a curved part with flaws at various depth (identified in colors) using laser ultrasonic time-of-flight. [Monchalin, et al, 1998]

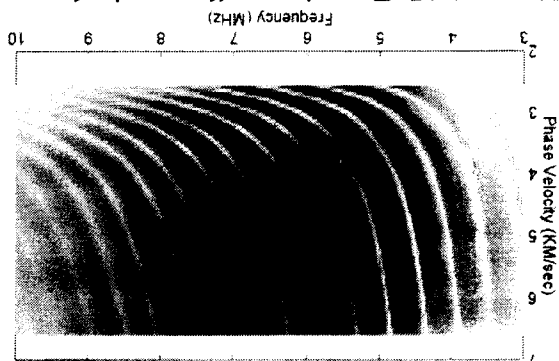


**Figure 4-12:** The laser ultrasonic scanner, LUIS system, at McClellan AFB [Courtesy of Thomas Ducharme, 1999].

with the fibers. To harness the capabilities that are offered by LLW and PBS, a computer-controlled scanner was developed jointly with QMI (Costa Mesa, CA) as a C-scan attachment. In Figure 4-14, the scanner is shown to consist of an transducer guiding arch. The arch plane represents the polar angle of the acquired dispersion curve, whereas the angle of incidence of the two transducers is controlled and guided by the arch. The height of the transducer pair as well as the polar and pitch-catch angles are all controlled at high precision. Recent enhancement of the data acquisition is enabling rapid acquisition of dispersion curves at such speed that a curve for 20 angles of incidence is obtained in less than a minute. Rapid acquisition of dispersion curves is very important for the practical implementation of quantitative mapping of the elastic properties in composite laminates. Using the new capability, LLW modes with very low amplitude are now possible to record as shown in Figure 4-15.



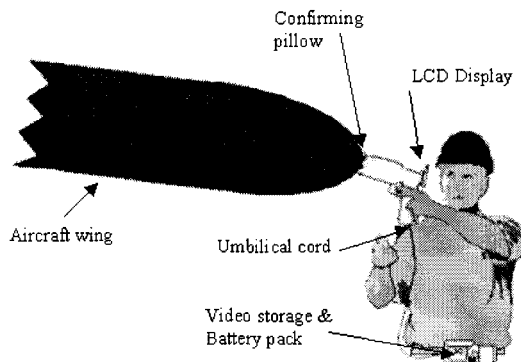
**Figure 4-14:** The LLW scanner attachment on the JPL's C-scan system.



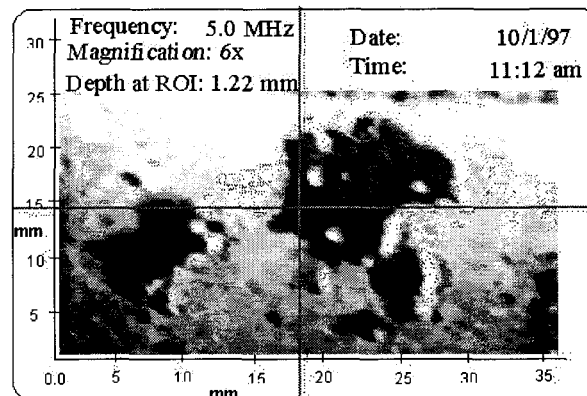
**Figure 4-15:** Experimentally acquired dispersion data with recorded very low amplitude modes.

#### 4.1.4.3 Portable Real-Time Imager Using CCD

Ultrasonic imaging system that employs two-dimensional sensing array was shown to be an effective means of field inspection [Lasser & Harrison, 1997]. An ultrasonic camera displays the images at TV frame rates and this capability contrasts the conventional C-scan, which generates the image by mechanically scanning the test area point-by-point. This real-time imager offers a portable, practical tool for rapid visualization of flaws using an integrated circuit, which converts ultrasound data into a standard TV output, enabling ultrasound imaging of an area in real time. The system operates as a pulse-echo tester (as shown schematically in Figure 4-16) and it is designed to display different viewing depths by examining various ranges of time-of-flight. The inspector applies an ultrasonic couplant over the desired test area. Then, the probe assembly is placed against the target using the pistol grip and the ultrasonic wave insomifies the target area upon squeezing a trigger. The ultrasonic pulse-echo image of the test structure appears on a small LCD screen mounted on the back of the probe. Controls are located on the handle facing the user and real-time adjustments can be made to select the desired contrast, gain, ultrasound power, pulse-echo power, etc. An example of corrosion detected in an aluminum plate is shown in Figure 4-17.



**Figure 4-16:** A schematic view of the ultrasonic video viewing system operated in field conditions (Imperium).



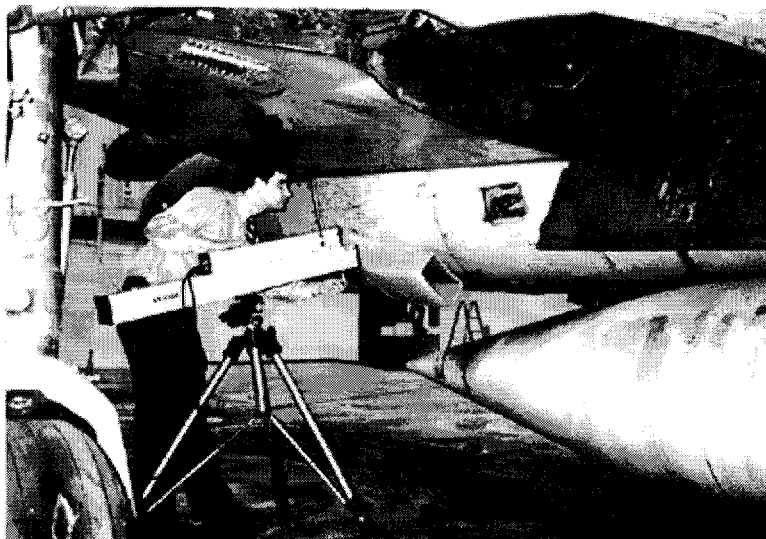
**Figure 4-17:** Pulse-echo image of corroded aluminum plate. The depth data represents the information at the crosshair cursor location.

#### 4.1.5 SHEAROGRAPHY

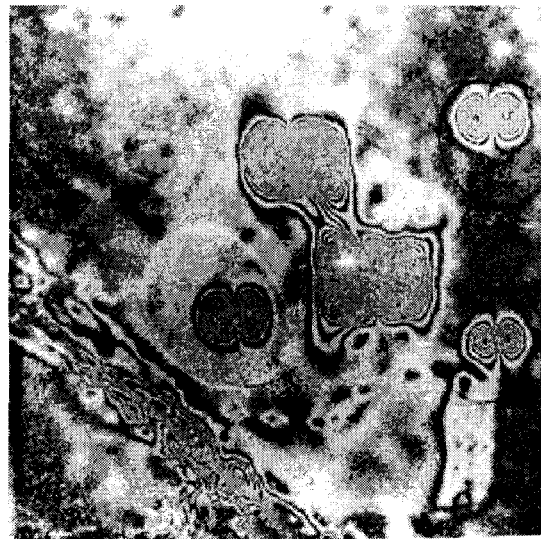
The ability of holography to produce flaw indications superpositioned onto a 3-D image of parts has been a desirable feature that was well documented since the 60's. The process involves double exposure of the structure at two different stressing levels. Unfortunately, the method has been very sensitive to vibrations or displacement of the setup and therefore was not practical for field use. The introduction of shearography as a technique of forming double exposure without concern to the system mechanical stability made it highly attractive. A digital interferometry system is used to detect areas of stress concentration caused by anomalies in the material [Maji, 1997; and Walter, 1991]. The technique senses out-of-plane surface displacements in response to an applied load. Data is presented in the form of a fringe pattern produced by comparing two states of the test sample, one before and the other after a load is applied. Electronic shearography incorporates a CCD camera and frame grabber for image acquisition at video frame rates. Fringe patterns are produced by real time digital subtraction of the deformed object-image from the reference object-image. Shearography also uses a 'common-path' optical arrangement, which provides reasonable immunity to environmental disturbances such as room vibrations and thermal air currents. As a result, shearography can be implemented without the need for sophisticated vibration isolation that is required for conventional holography. The capability of Shearography to inspect a large area in real time has significant advantages for many industrial applications and is being practically used for inspection of composite structures and pressure vessels. In 1988, Northrop Grumman Corp. introduced a shearographic system for the inspection of large structures in their production facility. This system was applied for inspection of bonded composites and metallic assemblies and their experience has shown inspection time reduction of about 75% compared to other NDE methods. Further, there are many cases where this method was found to be the only one capable of detecting the specific flaws.

To address the requirement to stress the test structure, various techniques are used, where the most effective are thermal and surface vacuum techniques. The thermal shearography is used to inspect near skin-to-core bondline, ramp areas and solid graphite laminates, whereas, vacuum

stress shearography is used to examine both near and far side bond lines in the honeycomb areas. Thermal stress shearography has been shown to be capable of inspecting large areas of composite and honeycomb materials at a rate of 60-ft.<sup>2</sup>/hour [Davis, 1996]. Example of testing an aircraft is shown in Figure 4-18 and a typical view of flaws is shown in Figure 4-19. Generally, the technique of forming shearographic images causes flaws to appear as bull's eyes.



**Figure 4-18:** Tripod mounted shearography camera/laser is shown inspecting an aircraft (Laser Technology, Inc.).



**Figure 4-19:** The bull's eyes shape of flaws in a shearographic image.

#### **4.1.6 THERMOGRAPHY**

The effect of flaws on the thermal conductivity and emissivity of test materials is analyzed by the thermographic NDE method [Jones & Berger, 1992]. Its attractive features are the capability to cover large areas in a single frame and it does not require coupling. Unfortunately, this method was found unreliable when testing bonded joints with a narrow gap between the unbonded surfaces, so-called "kissing" bond. In the early stages, liquid crystals were used to map the surface distribution of the temperature. The improvement of infrared systems made such tools highly sensitive and effective for mapping of cooling or heating profiles to rapidly indicate flaws. Examining the temporal gradient of the thermal maps, i.e., thermal flux, significantly improved the detectability of flaws.

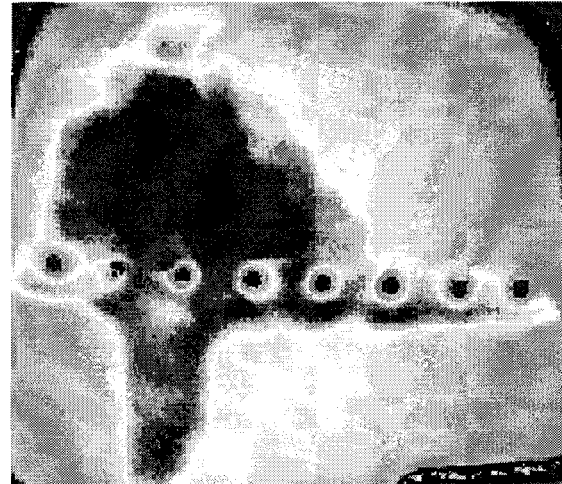
##### **4.1.6.1 Thermal Wave Imaging**

Thermal waves transmitted through test parts can be received and used to produce an image of the internal uniformity. In addition to imaging the pattern of subsurface flaws and corrosion, the technique can rapidly (a few seconds) make quantitative measurements of less than 1% material loss for various regions in the image [Favro & Thomas, 1995; and Hans, et al, 1996]. It can use as a heat source pulses from photographic flash lamps. The heat source box traps and funnels the light uniformly onto the test structure, and an infrared (IR) focal plane array camera, aimed and focused at the surface through an opening in the rear of the hand-held shroud, monitors the rapid cooling of the surface. The system operates by sending a heat pulse from the surface into the material, where it undergoes thermal wave reflection at either the rear surface or at any interior

surface at which the thermal impedance changes, e.g., at disbonds, delaminations, etc. The effect of these thermal wave reflections is to modify the local cooling rate of the surface. The cooling rate, in turn, is monitored through its effect on the IR radiation from the surface, which is detected by the camera, and processed by the controlling computer as a sequence of images. The contrast in the processed images reveals the presence of defects in the interior or variations in the thickness of the material. In Figure 4-20, Thermal Wave image example is shown for corrosion and unbond near a tear strap/stringer of a Boeing 737 aircraft.

**Figure 4-20:** Thermal Wave Image of Corrosion and Disbonding near tear strap/stringer of a Boeing 737

[<http://thermal.physics.wayne.edu/~han/han.html>].



#### ACKNOWLEDGEMENT

The chapter was written at the Jet Propulsion Laboratory, California Institute of Technology, under a contract with the National Aeronautics and Space Administration.

#### 4.1.7 REFERENCE

- Bar-Cohen Y., "Nondestructive Inspection and Quality Control," ASM International Handbook, Vol. 3, Adhesive and Sealant, Section 9, (1990), pp. 727-798.
- Bar-Cohen Y., A. K. Mal and S. -S. Lih, "NDE of Composite Materials Using Ultrasonic Oblique Insonification," Materials Evaluation, Vol. 51, No. 11, (Nov. 1993) 1285-1296.
- Bar-Cohen Y., and D. E. Chimenti, "Leaky Lamb Waves in Fiber-Reinforced Composite Plates," Review of Progress in Quantitative NDE, Vol. 3B, D. O. Thompson and D. E. Chimenti (Eds.), Plenum Press, New York and London (1984), pp. 1043-1049.
- Bar-Cohen Y., and R. L. Crane, "Acoustic-Backscattering Imaging of Subcritical Flaws in Composites," Materials Evaluation, Vol. 40, No. 9 (1982), pp. 970-975.
- Bieber J.A., C. Tai, J.C. Moulder, "Quantitative Assessment of Corrosion in Aircraft Structures Using Scanning Pulsed Eddy Current", Review of Progress in QNDE, Vol. 17A, D. O. Thompson and D. E. Chimenti (Eds.), Plenum Press, NY (1998), p 315.
- Chen C.M., S.Y. Lee, and Z.H. Cho, "A parallel implementation of 3D CT image reconstruction on hypercube multiprocessor," IEEE Transactions on Nuclear Science, Vol. 37, No. 3 (1990), pp. 1333 - 1346
- Davis C.K., "Shearographic and Thermographic NDE of the Space Shuttle Structure and Thermal Protection Systems," Proceedings of the Technology 2006, Anaheim, California, <http://www.abpi.net/T2007/papers/mr/docs/shear.htm> October 29-31, 1996.

- Dolan K.W., D.J. Schnebeck, R.D. Albert, and T.M. Albert, "Reverse Geometry X-Ray Imaging for NDT Applications," Proceedings of the JANNAF NDE Subcommittee Meeting, CPIA, (1993).
- Favro L.D., and R.L. Thomas, "Thermal Wave Hardware Evolution Using the NDI Validation Center," Materials Evaluation, 53, 840-843 (1995).
- Fiedler C. J., T. Ducharme and J. Kwan, The laser ultrasonic inspection system (LUIS) at the Sacramento Air Logistic Center," Review of Progress in Quantitative NDE, Plenum Press, NY, Vol. 16, (1997), pp. 515-522.
- Fitzpatrick G. L., D. K. Thome, R. L. Skaugset, W. C. L. Shih, "Magneto-Optic/Eddy Current Imaging of Subsurface Corrosion and Fatigue Cracks in Aging Aircraft," Review of Progress in Quantitative NDE, Vol. 15A, D. O. Thompson and D. E. Chimenti (Eds.), Plenum Press, NY, (1996), pp. 1159-1166.
- Forsyth D. S., J. P. Komorowski, R. W. Gould and A. Marincak, "Automation of Enhanced Visual NDT Techniques," The Canadian Society for NDT, Proceedings of the First Pan-American Conference for Nondestructive Testing, Toronto, Canada, Sept 14-18 1998
- Grandia W.A., and C.M. Fortunko, "NDE Applications of Air-coupled Ultrasonic Transducers," Proceedings of the 1995 IEEE Ultrasonic Symposium, ISSN 1051-0117, Vol. 1 (1995), pp. 697-709.
- Green, R. E., "Emerging Technologies for NDE of Aging Aircraft Structures," Proceedings of the Workshop on Intelligent NDE Sciences for Aging and Futuristic Aircraft, C. Ferregut, R. Osegueda and A. Nunez (Eds.), UTEP, El Paso, TX, ISBN 87404-279-8, (1997), pp.267-278.
- Hübschen G., "Generation of Horizontally Polarized Shear Waves with EMAT Transducers," NDT.net, <http://www.ndt.net/article/0398/huebsch/hueb.htm>, March, Vol.3, No.3 (1998)
- Hutchins D.A., F. Hauser, S.B. Palmer, "Experimental studies into ultrasonic mode conversion," Proceedings of the Ultrasonics International 87 Conference, Butterworth; Guildford, UK E06 ISBN 0408023481 (1987) pp. 561-565.
- Jones T., and H. Berger, "Thermographic Detection of Impact Damage in Graphite Epoxy Composites," Materials Evaluation, Vol. 50, No. 12, (1992), pp. 1446-1453.
- Kak A.C., and M. Slaney, Principles of Computerized Tomographic Imaging, IEEE, Inc., New York: IEEE Press, (1988)
- Kreutzbruck, M.V., M. Mück, U. Baby and C. Heiden, "Studies in Applied Electromagnetics and Mechanics," <http://www.ndt.net/article/ecndt98/aero/005/005.htm> (NDT.net - September 1998, Vol.3 No.9), Vol. 13, IOS Press, Amsterdam (1998).
- Lasser M., G. Harrison, "A Real time, High Resolution Imaging System for Aging Aircraft Inspection," Proceedings of the Workshop on Intelligent NDE Sciences for Aging and Futuristic Aircraft, C. Ferregut, R. Osegueda and A. Nunez (Eds.) UTEP, El Paso, TX ISBN 87404-279-8, (1997), pp.1-9.
- Lepine B.A., and R.T. Holt, "An Eddy Current Scanning Method for the Detection of Corrosion Under Fasteners in Thick Skin Aircraft Structures", Canadian Aeronautics and Space Journal, (March 1997), pp. 28-33.
- Ma, Y.P., and J.P. Wikswo Jr., "SQUID Eddy Current Techniques for Detection of Second Layer Flaws," Review of Progress in QNDE, Vol. 13A, D.O. Thompson and D.E. Chimenti (Eds.), Plenum Press, NY (1994) pp. 303-309.
- Maji A. K., "Assessment of Electronic Shearography for Structural Inspection", Experimental Mechanics J., Vol. 34, No. 2, (1997), pp. 197-204.

- Mitra S., E. Uzal, J.H. Rose, J.C. Moulder, "Eddy Current Measurements of Corrosion-Related Thinning in Aluminium Lap Splices", Review of Progress in Quantitative NDE, Vol.12, Plenum Press, NY, (1993) pp. 2003-2010.
- Monchalain, J.-P., C. Néron, M. Choquet, D. Drolet, M. Viens, "Laser-Ultrasonics Inspection And Characterization of Aeronautic Materials," Proceedings 1st Pan-American Conference for NDT, PACNDT '98, Canadian Society for NDT, Toronto, Canada, 14-18 September 1998.
- Olivas J. D., S. Bolin, Y. Bar-Cohen, E. J. Chern and J. J. Shaw, "NDE of Space Flight Hardware: Case Study - Microelectromechanical Systems," Proceedings of the 97'ASNT Spring Conference, Houston Texas, March 17-20, (1997), p. 71-73.
- Oursler D.A.; Wagner, J.W., "Narrow-band hybrid pulsed laser/EMAT system for noncontact ultrasonic inspection using angled shear waves," Materials Evaluation, Vol. 53, No. 5 (1995), pp. 593-59.
- Patton T. C., and D. K. Hsu, "Recent Developments of the Dripless Bubbler Ultrasonic Scanner," Review of Progress in QNDE, Vol. 15B, D. O. Thompson and D.E. Chimenti (Eds.), Plenum Press, New York, (1998), pp. 2045-2051.
- Scruby, C. B. and Drain, L. E., Laser-Ultrasonics: Techniques and applications, Adam Hilger, Bristol, UK (1990).
- Thome D. K., "Development of an Improved Magneto-Optic/Eddy-Current Imager," DOT/FAA /AR report No. 97-37, <http://www.tc.faa.gov/its/worldpac/techrpt/ar97-37.pdf>, Final SBIR Phase II Report, Department of Transportation, FAA Technical Center, (1997), pp. 1-54.
- Thompson J.G., "Subsurface Corrosion Detection in Aircraft Lap Splices Using a Dual Frequency Eddy Current Inspection Technique," Materials Evaluation, Vol. 51 (Dec. 1993), pp 1398-1401.
- Walter P., "The Aging Aircraft Non-destructive Inspection Development and Demonstration Centre," Proceedings of the 3rd International Conference on Aging Aircraft, Washington, November (1991).
- Wykes C., "Advances in air-coupled ultrasonic transducers," Nondestructive Testing and Evaluation, Vol.12, No.3, (1995) pp. 155-180.

## 5.2 ELECTROACTIVE CERAMIC ACTUATORS

Stewart Sherrit, Y. Bar-Cohen, and Xiaoqi Bao,  
JPL, Caltech, 4800 Oak Grove Dr., Pasadena, CA 90740  
818-354-3891, fax 818-393-4057, [Stewart.Sherrit@jpl.nasa.gov](mailto:Stewart.Sherrit@jpl.nasa.gov)

<b>5.2 ELECTROACTIVE CERAMIC ACTUATORS .....</b>	<b>1</b>
5.2.1 <i>ELECTROMECHANICAL CERAMICS</i> .....	1
5.2.1.1 Piezoelectric Materials .....	1
5.2.1.2 Electrostrictive Materials .....	3
5.2.2 <i>STRAIN AMPLIFIERS USING ELECTROCERAMICS</i> .....	4
5.2.2.1 Piezoelectric Stacks .....	5
5.2.2.2 Piezoelectric Bimorphs .....	5
5.2.2.3 Uni-layer Benders .....	6
5.2.2.4 Flextensional Amplification .....	6
5.2.2.5 Cantilevers .....	7
5.2.2.6 Resonance Amplification .....	7
5.2.3 <i>PIEZOELECTRIC MOTORS</i> .....	8
5.2.3.1 Quasi-static Designs .....	9
5.2.3.2 Standing Wave Designs .....	10
5.2.3.3 Travelling Wave Designs .....	10
5.2.4 <i>OTHER APPLICATIONS OF ELECTROACTIVE CERAMICS</i> .....	15
5.2.5 <i>REFERENCES</i> .....	15

Actuators are used to mobilize and manipulate various components of robots and automatic systems. In many applications the necessary functions require compact high-precision actuation mechanisms and such a capability is inherent to electroactive ceramic materials. In this section the principles that are responsible for the actuation mechanism of piezoelectric and electrostrictive ceramics are covered. A large number of reference books have been written about piezoelectrics including [Cady, 1964; Jaffe, et al, 1971; Uchino, 1996; Cross et al. 1986; and Levinson, 1988]. Significant information about the initial research in the field of piezoelectrics, ultrasonics and actuators can be found in a series of books called [Physical Acoustics, 1964-1980] edited originally by W.P. Mason.

The description of the principles of transduction and actuation in electroactive ceramics in this Section is followed with a review of several basic mechanisms of inducing large actuation strain including strain amplifiers and ultrasonic motors (USM). USM represents emerging motor technology that already found wide usage in drive mechanisms of cameras and other optical devices. As the efficiency of these motors is improved and the recognition of their unique capabilities widens a growing list of new applications are increasingly being reported.

### 5.2.1 ELECTROMECHANICAL CERAMICS

#### 5.2.1.1 Piezoelectric Materials

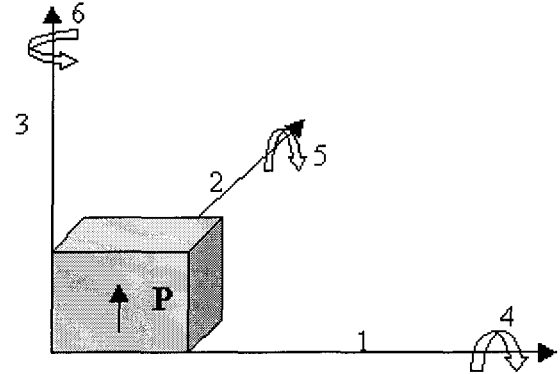
The phenomenon of piezoelectricity is responsible for the direct and converse effects, which are two distinct but related relationships. The direct effect describes the generation of charge on a crystal face as the result of an application of a stress, while the converse effect describes the generation of a mechanical strain as a result of the application of an electric field. At low values of stress and electric field the relationship between charge and stress, as well as

strain and field, is observed to be linear for piezoelectric materials. Under a change in the polarity of the electric field, the charge reverses sign going from positive to negative and the strain switches from dilation to contraction. The property of piezoelectricity in ceramics, such as Lead Zirconate Titanate (PZT), is closely related to another phenomenon of practical interest called ferroelectricity. This is described by the presence of a spontaneous polarization in a crystal that can be changed between two or more distinct directions with respect to crystal axes that are subjected to an external electric field. After sintering a random polarization is present in the ceramic. The polarization is partially aligned by poling which requires applying a large field at an elevated temperature for a set time. After poling the ceramic has a net polarization parallel to the poling field and the material has  $C_{\infty}$  symmetry. Materials with  $C_{\infty}$  symmetry are isotropic in the plane perpendicular to the poling direction. In order to describe the material completely under the application of small fields or stress there is a need for five independent elastic constants, three independent piezoelectric constants and two permittivity constants. The polarization direction is called the 3-direction (see Figure 5.2-1). A linear piezoelectric material can be described by a set of coupled linear equations that are derived from the elastic Gibbs energy function  $G_1$ .

$$\begin{aligned} S_{ij} &= -\frac{\partial G_1}{\partial T_{ij}} = s_{ijkl}^D T_{kl} + g_{nij} D_n \\ E_m &= \frac{\partial G_1}{\partial D_m} = \beta_{mn}^T D_n - g_{mij} T_{ij} \end{aligned} \quad (1)$$

where S, T, D, and E are the strain, stress, electric displacement and electric field. The subscripts take account of the directional dependencies as are shown in Figure 5.2-1.

**Figure 5.2-1:** Directional notation for poled ferroelectric ceramic. The 3-direction is the polarization direction



The superscripts correspond to the defining boundary conditions of the specific constants. Other representations of the linear equations of piezoelectricity are based on the use of other thermodynamic potentials and they are shown below. These sets of linear equations can be transformed from one to the other through equations found in the IEEE Standard on Piezoelectricity [1987]. The four common sets of equations including equation 1 in contracted notation are

$$\begin{aligned} S_p &= s_{pq}^D T_q + g_{pm} D_m & S_p &= s_{pq}^E T_q + d_{pm} E_m \\ E_m &= \beta_{mn}^T D_n - g_{pm} T_p & D_m &= \epsilon_{mn}^T E_n + d_{pm} T_p \end{aligned} \quad (2)$$

$$\begin{aligned} T_p &= c_{pq}^E S_q - e_{pm} E_m & T_p &= c_{pq}^D S_q - h_{pm} D_m \\ D_m &= \epsilon_{mn}^S E_n + e_{pm} S_p & E_m &= \beta_{mn}^S D_n - h_{pm} S_p \end{aligned} \quad (3)$$

where  $d$ ,  $e$ ,  $g$ ,  $h$  are piezoelectric constants;  $s$  and  $c$  are the elastic compliance and stiffness; and  $\epsilon$  and  $\beta$  are the permittivity and the inverse permittivity. The relationship described by each of these equations can be represented in matrix form. It should be noted that equations 1 to 3 are idealizations and that the material "constants" can vary with field, stress, temperature, frequency or time and may show a considerable hysteresis.

A wide variety of piezoelectric materials from polymers to ceramics and composites are currently being used for transducers and actuators. The most commonly used commercial material is PZT and the exact properties of this material depends on the relative concentration of Lead Zirconate or Titanate and the amount of various atoms that are used to dope it. A variety of PZT materials are available and they have a wide range of material properties. In Table 5.2-1, the piezoelectric and dielectric properties of three commercially available PZT materials are listed for three different temperatures [based on: Hooker, 1998]. It should be noted that the listed properties are based on resonance measurements made using small signal values. Typically, for actuators where larger signals are used the measure material constants are higher. The percentage increase under large stress or field for these constants depends inversely on the coercive field and the increase in the material constant is accompanied by greater hysteresis.

**TABLE 5.2-1:** Piezoelectric coefficients and permittivity at three temperatures for three typical commercial PZT materials [Based on: Hooker, 1998].

Property	PZT 4			PZT 5A			PZT 5H*		
	-150°C	25°C	250°C	-150°C	25°C	250°C	-150°C	25°C	180°C
$d_{33}$ (pC/N)	210	225	360	190	350	440	260	585	900
$d_{31}$ (pC/N)	-70	-85	-130	-100	-190	-270	-115	-265	-500
$\epsilon_{33}^T$ ( $10^{-9}$ F/m)	7.1	9.7	27	5.3	10	27	7.5	28	124
*maximum in dielectric constant is at 180°C									

### 5.2.1.2 Electrostrictive Materials

Another group of electroactive ceramics that offer actuation strain capability is the electrostrictive materials. Electrostrictive materials have a nominal quadratic dependence of the strain on electric field ( $S=\gamma E^2$ ) and some compositions have been shown to have very small hysteresis.

A wide variety of notations and constants have been used to describe electrostriction and, depending on the choice of extrinsic and intrinsic variables, several coupled-field equations can be developed to describe the macroscopic behavior of electrostrictive materials. Most of the developed models are based on the earlier derivation of Mason who used a set of non-linear equations for Barium Titanate employing thermodynamic potentials (elastic Gibbs function) in terms of the electric displacement  $D_i$  and the stress  $T_{ij}$ . The equations for the electric field  $E_i$  and strain  $S_{ij}$  are:

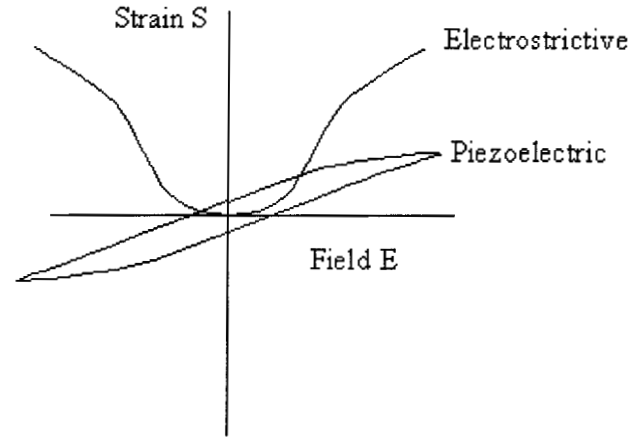
$$\begin{aligned}
 E_i &= -2Q_{klij}T_{kl}D_j + \left[ \beta_{ij}^T + R_{ijmnkl}T_{mn}T_{kl} \right] D_j + \sum_{ijkl} D_j D_k D_l + \sum_{ijklmn} D_j D_k D_l D_m D_n \\
 S_{ij} &= \left[ s_{ijkl}^D + R_{ijmnkl}D_m D_n \right] T_{kl} + Q_{ijmn}D_m D_n
 \end{aligned} \tag{4}$$

In the case where we are concerned with the strain and field for the 3-direction these equations are reduce to

$$\begin{aligned}
E_3 &= -2Q_{333}T_3D_3 + [\beta_{33}^T + R_{333}T_3^2]D_3 + \Sigma_{3333}D_3^3 + \Sigma_{333333}D_3^5 \\
S_3 &= [s_{33}^D + R_{333}D_3^2]T_3 + Q_{333}D_3^2
\end{aligned}
\tag{5}$$

where  $Q_{333}$  is the longitudinal electrostrictive coefficient,  $\beta_{33}^T$  is the inverse of the free permittivity,  $R_{333}$  is a correction which describes the change in the elastic compliance  $s_{33}^D$  as a function of the electric displacement  $D_3$  and the quadratic component of the change of  $\beta_{33}^T$  as a function of the stress. The  $\Sigma$  coefficients are corrections to the inverse permeability to describe the asymptotic behavior of the electric field as a function of the electric displacement.

In recent years, there has been considerable interest in the family of materials that is based on lead magnesium niobate - lead titanate (PMN-PT) due to their large electrostriction coefficient, high dielectric constant and low hysteresis [Cross, et al, 1980; Hom, et al, 1994; Piquette & Forsythe 1997, Sherrit and Mukherjee 1998]. In Figure 5.2-2, a schematic description is shown for the typical relationship between the strain  $S$  as a function of the electric field of a piezoelectric and an electrostrictive ceramic.



**Figure 5.2-2:** The strain field behavior of an ideal electrostrictive ceramic and a hysteretic piezoelectric material. Saturation in the strain of the electrostrictive ceramic is a result of the saturation in the electric displacement as a function of field.

Most manufactures of piezoelectric and electrostrictive materials supply nominal data that is based on small signals, however it should be kept in mind that the nominal data and the actual performance of a particular electroactive wafer may vary significantly. Such variation may be large in the case of actuators where high fields or stresses are generated.

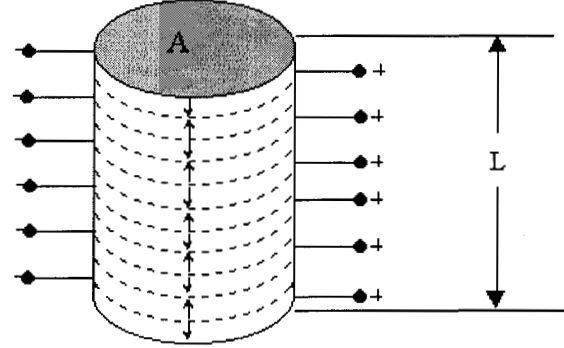
### 5.2.2 STRAIN AMPLIFIERS USING ELECTROCERAMICS

Electroactive ceramics can induce large stress levels, which are essential for many actuation tasks. Unfortunately, the accompanied strain is very small and is far below the levels that can be obtained by electromagnetic devices. To overcome this weakness, a wide variety of devices and configurations were developed to increase the strain at given levels of applied voltages. Examples of various effective mechanisms are described in this section. Further, a discussion and comparison of the cantilever, multilayer, flextensional, rainbow and bimorph configuration are given in [Near, 1996].

### 5.2.2.1 Piezoelectric Stacks

One of the most common electroceramic actuator configurations is the piezoelectric stack, which as the name implies, is a number of thin alternately poled piezoelectric layers connected mechanically in series and electrically in parallel.

**Figure 5.2-3:** Piezoelectric stack with  $n$  layers of length  $L$  and electrode area  $A$ .



For the stack configurations shown in Figure 5.2-3, assuming zero bond joint thickness, the effective piezoelectric constant and low frequency capacitance  $C$  are

$$d_{33}^{eff} = n d_{33} \quad (6)$$

$$C = \frac{n^2 \epsilon_{33}^T A}{L} \quad (7)$$

It should be noted that for a given voltage the displacement is amplified by a factor  $n$  over the displacement that would be found on a monolithic ceramic wafer having length  $L$  and area  $A$ . The displacement as a function of the voltage is then

$$\Delta x = n d_{33} V \quad (8)$$

The total displacement of a stack having a reasonable length without the use of other amplification techniques is limited at room temperature to approximately 100 microns. A recent NASA report by [Wise & Hooker 1997] provides performance data for several piezoelectric stacks that are manufactured by four different companies.

### 5.2.2.2 Piezoelectric Bimorphs

Piezoelectric bimorphs can be configured in series and parallel and examples are shown in Figure 5.2-4. Generally, bimorphs are constructed of two piezoelectric plates that are bonded with their polarity in opposite directions. Under electric field one piezoelectric layer contracts in the thickness direction while the other expands. Due to the contraction and expansion in the thickness direction one layer expands along the length and the other contracts inducing bending of the bonded layers.

For the series-configuration with a free length  $L$ , total thickness  $t$  and a transverse piezoelectric coefficient  $d_{31}$ , the tip displacement is proportional to the voltage  $V$  and is expressed as follows.

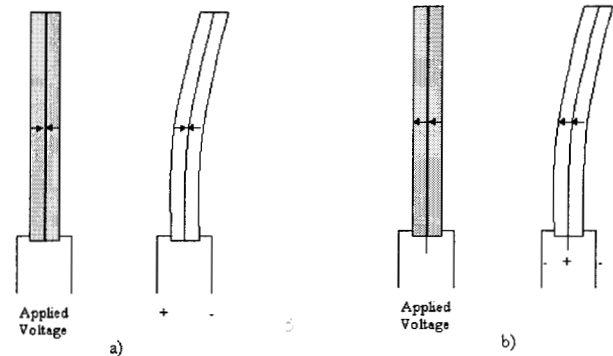
$$\Delta y = \frac{3 d_{31} V L^2}{2 t^2} \quad (10)$$

The expression for the same parameters with parallel-configuration shows a displacement that is twice the value for the series-configuration when using the same voltage level

$$\Delta y = \frac{3d_{31}VL^2}{t^2} \quad (11)$$

Tip displacements of the order of a centimeter can be induced using bimorph type actuators.

**Figure 5.2-4:** A schematic view of bimorphs in a) series; and b) parallel.

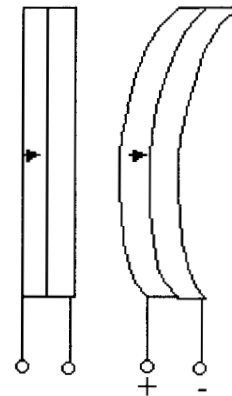


### 5.2.2.3 Uni-layer Benders

Unimorphs are similar in configuration to bimorphs with the difference that one of the layers is passive. Under expansion in the poling direction the strain in the plane perpendicular to the poling direction undergoes a contraction. As shown in Figure 5.2-5, this strain occurs only on the active layer (piezoelectric or electrostrictive material) leading to a bending of the whole device. Such devices can be used to induce relatively large deflections and the amplitude increases with the lateral dimensions. Some of the bimorph configurations that were reported in recent years include:

- RAINBOW/ CERAMBOW - This type of actuators consist of reduced and internally biased oxide wafers or differential electrode thickness. These family of actuators were developed at Clemson by [Heartling, 1997; and Barron, et al, 1996]
- THUNDER - These are thin-layer composite unimorphs that consist of ferroelectric driver and sensors and they were developed by NASA Langley [see Face International 1999].

**Figure 5.2-5:** Schematic view of a unimorph actuator

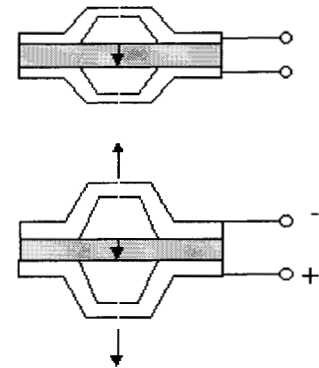


### 5.2.2.4 Flextensional Amplification

Another type of strain amplifiers is the flextensional actuator, which is also known as the Moonie and Cymbal [Dogin, et al, 1997]. Flextensional composites use endcaps to convert transverse to

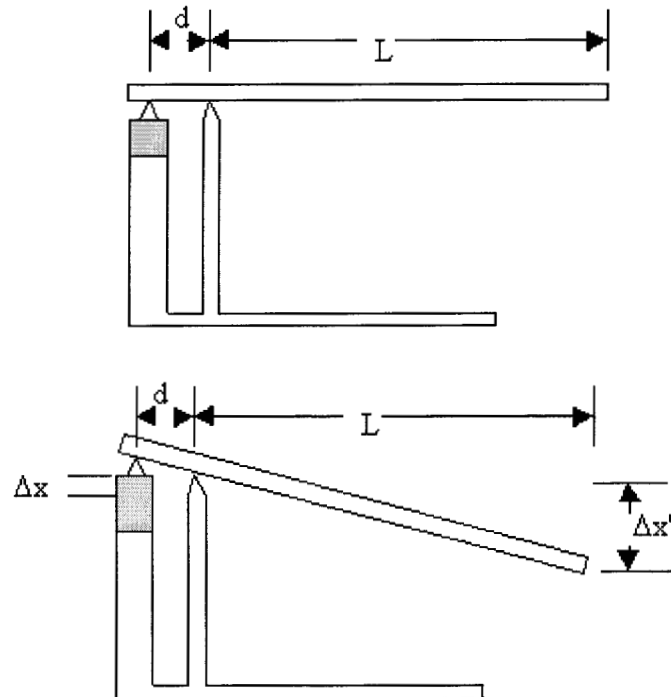
longitudinal strain. A schematic diagram of the strain amplification process for this mechanism is shown in Figure 5.2-6.

**Figure 5-2.6:** Schematic diagram of a Cymbal flextensional design



### 5.2.2.5 Cantilevers

Cantilever designs [see Burleigh Micropositioning Systems, 1991] use a lever configuration to increase the strain. An example is shown in Figure 5.2-7. A piezoelectric or electrostrictive material is connected mechanically to a lever arm and it is pivoted a distance  $d$  from the active element. From the pivot the lever arm extends out to a distance  $L$ . For a displacement  $\Delta x$  in the active element the displacement at the other end is  $\Delta x' = (L/d) \Delta x$  and thus a strain amplification of  $(L/d)$  is realized. For example if a piezoelectric stack of maximum displacement of  $100\text{-}\mu\text{m}$  is induced and a strain amplification factor  $(L/d=10)$  then displacements on the order of  $1\text{-mm}$  can be achieved.



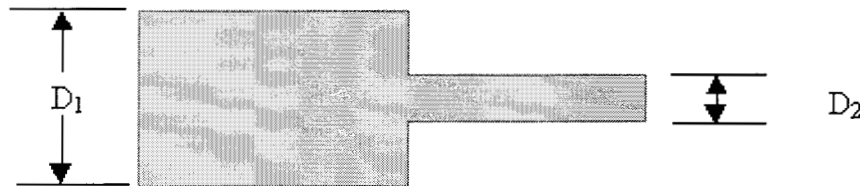
**Figure 5-2.7:** Example of cantilever design

### 5.2.2.6 Resonance Amplification

Another technique used to increase the strain that can be induced from an electroceramic material for a given field is to drive the material at its resonance frequency. In general for any mechanical system it can be shown that at resonance the strain in is amplified by a factor called the mechanical  $Q$ . The mechanical  $Q$  is a measure of the mechanical losses in the material. For

a material with high  $Q$ , the mechanical losses are small. For PZT the mechanical  $Q$  can range from 50 to 1000 and therefore for an ideal system the strain amplification can be as high as 1000 times. However, it should be noted that for materials with large  $Q$  it is very easy to drive the active element into a nonlinear regime reducing the overall amplification and/or damaging the element. Another problem with resonance amplification is that the resonance frequency for a piezoelectric material is determined from the velocity of sound and the dimension in which the material is resonating. This means that in practice for most piezoelectric materials the operating frequency is limited to the range of 100's at kHz and above.

At low frequencies, effective resonance amplification can be obtained by the configuration of ultrasonic horn. A schematic diagram of a stepped horn cross section [Belford, 1960] is shown in Figure 5.2-8. Due to the conservation of the wave momentum, at resonance, if a strain wave is induced on the large end the displacement at the small end is amplified by a factor  $M=(D_1/D_2)^2$ . This amplification is in addition to the amplification due to the material mechanical  $Q$ . Other horn configurations [Mason, 1958] include the exponential having amplification of  $M=D_1/D_2$  and the linear having amplification factor of  $M=4.61$ .



**Figure 5-2.8:** Schematic of a stepped ultrasonic horn

One advantage of ultrasonic horns is the ability to adjust the resonance frequency by changing the relative length of the two sections. The frequency can be adjusted by a factor of 2 without changing the overall length. It should be noted that the amplification is limited in practice by the critical strain of the tip material.

### 5.2.3 PIEZOELECTRIC MOTORS

Motors are an important element of automatic and robotic mechanisms. It is a common practice to drive C-scans systems, CAT scanners and other NDT mobility devices by stepping or analogue motors. Operation in hard to reach areas including field conditions or in applications where a portable systems is needed, it is essential to use compact and lightweight actuators. Most actuators are based on electromagnetic rotary motors, such as DC, AC, brush and brushless, etc. Generally, these types of motors compromise speed, which can be as high as many thousands of RPM, for torque using speed-reducing gears. The use of gear adds mass, volume and complexity as well as reduces the system reliability due the increase in number of the system components. The miniaturization of conventional electromagnetic motors is limited by manufacturing constraints and loss of performance efficiency.

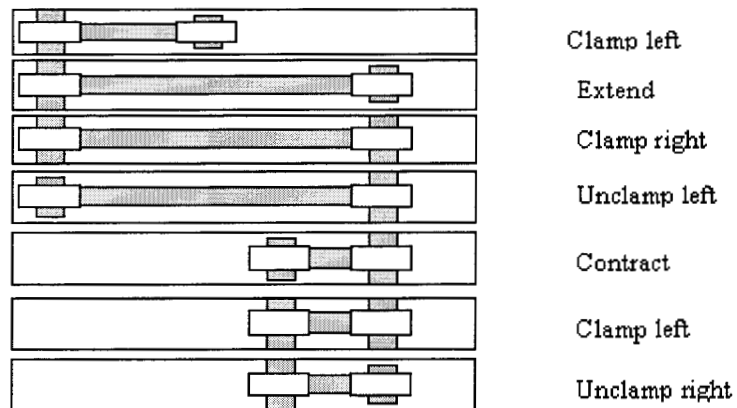
Potentially, motors that are actuated by piezoelectric ceramics offer an effective alternative to miniature actuation mechanisms [Hollerbach, et al, 1991]. These emerging motor technology can provide high torque density at low speed, high holding torque [Flynn, 1992], zero-backlash, simple construction, quiet operation and have a fast response time. These motors which are also known as ultrasonic motors (USM) can be made in annular shapes for optical applications, where

the electronics and wiring can be packaged in the center. Generally, USM are classified by their mode of operation (quasistatic or resonant, travelling), type of motion (rotary or linear) and the shape of actuation element (beam, rod, disk, etc.). Despite these distinctions, the fundamental principle is common to all of these devices. Each of these motor designs uses microscopic material deformations (usually associated with piezoelectric materials) that are amplified through either quasi-static or dynamic/resonant means. Various USM designs will be discussed herein.

### 5.2.3.1 Quasi-static Designs

Generally, most quasi-static designed ultrasonic motors are used for micro-positioning applications. One of the first ultrasonic motors was reported by N-Nagy [N-Nagy & Calderwood, 1969; and N-Nagy & Joyce, 1972] using two phase-bridge of PZT bimorph to generate rotary motion. Another quasi-static design is based on an inchworm motor as shown in Figure 5.2-9 [Shimizu, et al, 1990; Wallace & Espinoza-Faller, 1995]. This inchworm motor is fabricated with a minimum of 3 piezoelectric or electrostrictive actuators. The actuators are excited to mimic the motion of an inchworm and a timed excitation of each of the actuators is required. The actuation cycle is shown in Figure 5.2-9.

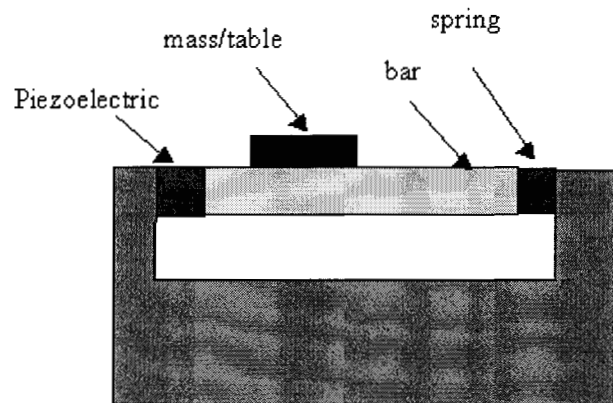
**Figure 5-2.9:** Schematic diagram of the movement of an inchworm motor/translator.



The response time of the actuator  $t$  and the stroke of the extension actuation  $\Delta x$  limit the speed of the inchworm and the maximum speed is  $v = \Delta x/t$ . For a  $20 \mu\text{m}$  stroke and 6 ms actuation time for the actuation cycle the maximum speed is on the order of 3 mm/s [Galante, et al, 1998; and Chen, et al, 1998]. One of the disadvantages of these motors is that an electrical power is required to maintain the holding force. Another quasi-static design is based on work by [Pohl, 1987] and it is known as the slider and is shown in Figure 5.2-10. A piezoelectric stack is used to displace a rod, which is supporting the mass/table to be moved. The stack is excited with a saw-tooth voltage.

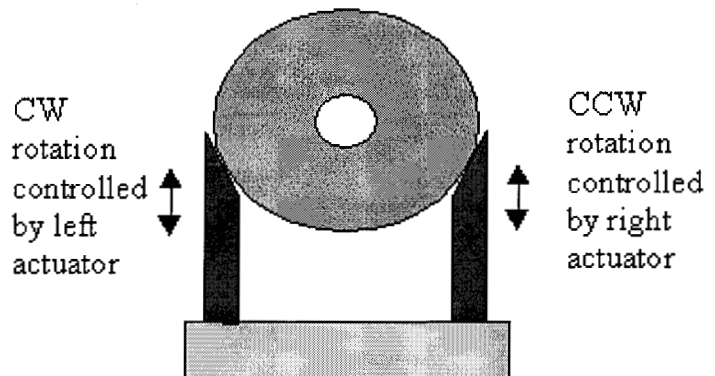
The initial displacement is gradual and the frictional force between the mass and the rod is sufficient to drag the mass/table along during the displacement. At the point of maximum displacement the stack contracts quickly breaking the friction between the two surfaces and leaving the mass/table in the maximum extension position. This is repeated at a frequency  $f$  to give a speed  $v = f\Delta x$  which is of the order of 5 mm/s. The performance of these types of motors is found to be very dependent on the surface roughness and the friction between the bar and the mass

**Figure 5-2.10:** Slider type linear motor. Motion of mass is achieved by activating the stack with a saw-tooth waveform.



One of the first piezoelectric motor designs with significant rotational speeds was outlined by Barth [Barth, 1973]. This device used extensional piezoelectric elements to produce a time varying force at a distance  $r$  from the center of a centrally supported disk as is shown in Figure 5.2-11. Microsteps are formed at a high frequency and the end result is a macroscopic rotation of the disk. The rotation direction is controlled by the choice of the actuators.

**Figure 5-3.11:** Schematic diagram of the Barth [Barth, 1973] motor



### 5.2.3.2 Standing Wave Designs

Another group of motors that use standing waves or resonances in the motor elements was developed by Vasiliev and colleagues [Vasiliev, et al, 1979]. They used resonances in an ultrasonic horn to increase the stroke of the actuator and lower the frequency. Sashida [Sashida & Kenjo, 1993; and Sashida, 1982] used a wedge type motor based on the Langevin transducer (elliptical motion at contact surface) and improved on the design showing rotational speeds up to 3000 RPM with torques of the order of 0.25 Nm. The efficiency of the motor was found to be in the range of 50-87 percent depending on the diligence of the precision machining and adjustment. The major disadvantage of these types of motors is the high wear rate.

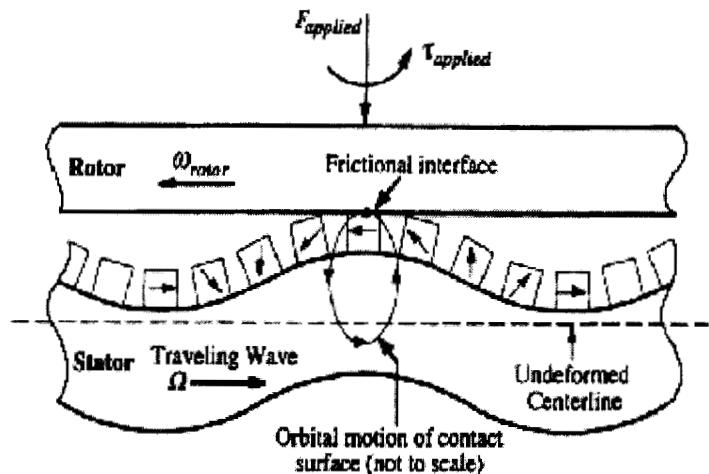
### 5.2.3.3 Travelling Wave Designs

Piezoelectric motors that operate at frequencies above 20 kHz are usually referred to as ultrasonic motors [Burleigh, et al, 1991; Uchino, et al, 1988; Inoue, et al, 1989; Zemella, 1990; Kumada, 1985; Minoru, 1983; Inaba, 1981; and Ueha & Tomikawa, 1993]. Several USM classes have seen commercial application in areas needing compact, efficient, intermittent motion [Panasonic, 1987; and Masaki, 1991]. Such applications include camera auto focus lenses [Hosoe, 1989; Cannon, 1992], watch motors [Seiko, 1992] and compact paper handling [Inoue, et al, 1989].

Ultrasonic motors are driven by high frequency micro-deformations of active materials. The gross motion is accomplished through the amplification and repetition of the micro-deformations of material. Active materials (mostly piezoelectric) are employed to induce elliptical motion on the surface of a stator at the contact points with a rotor. A frictional interface between the rotor and stator rectifies the micro-motion to produce macro-motion of the rotor. The rotor essentially rides the traveling flexural wave excited within the stator (see Figure 5.2-12). Useful work can be done by mechanically connecting a drive shaft to the rotor. Teeth, which amplify the displacements, are used to enhance the speed. The operation of USM depends on friction at the interface between the moving rotor and stator and it is a key design issue, which affects the motor extended lifetime. The torque imparted to the rotor via the stator is obtained by creating a frictional force between the teeth of the stator and the rotor. The frictional force is dependent on the normal forces applied on the rotor/stator interface. This motion transfer operates as a gear and leads to a much lower rotation speed than the wave frequency. The rotation speed can be reduced by a factor of several thousand.

To generate a traveling wave within the stator two orthogonal modes are activated simultaneously. A stator that is constructed with piezoelectric actuators induces these modes. The actuator is bonded to the stator and the flexural waves are induced by poling different sections of the actuator with the opposite polarity and driving with the appropriate voltage excitation. An example of the actuator configuration is shown in Figure 5-2.13. Geometrical examination of this pattern shows that driving the two sections using  $\cos(\omega t)$  and  $\sin(\omega t)$  signals, respectively, will produce a traveling wave with a frequency of  $\omega/2\pi$ . Also, by changing the sign on one of the drive signals, the traveling wave would reverse its direction.

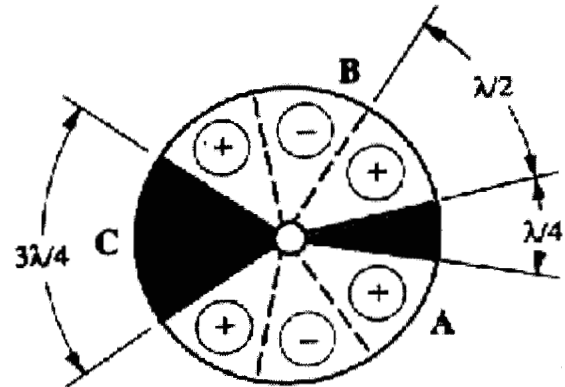
**Figure 5-2.12:** Principle of Operation of a Rotary Traveling Wave Motor (Ring type) wafers [Hagood & McFarland, 1995].



A generic description of the stator is shown in Figure 5.2-13. The stator can be driven by a piezoelectric wafer that is placed either on one surface [Cannon, 1992] or sandwiched between two wafers [Hagood & McFarland 1995]. To generate traveling wave, the piezoelectric ceramic materials internal poling is structured such that quarter wavelength out-of-phase is formed. This poling pattern is also intended to eliminate extension in the stator and maximize bending. The teeth on the stator are arranged in a ring at the radial position. In Figure 5.2-13, the solid lines indicate permanent etching on the electrode in two groups (A & B). Dashed lines indicate segments that are etched for poling purposes and then reconnected with silver paint to reduce the number of leads required. The dark areas are regions on the piezoelectric wafer that are not

activated and can be used as sensors to gauge the condition of resonance frequency. In operation A and B electrodes are driven  $90^\circ$  out of phase and produce orthogonal disk modes.

**Figure 5-2.13:** Generic stator design describing the poling sequence on the piezoelectric wafer wafers [Hagood & McFarland, 1995].



Two factors dominate the optimization of the motor performance: the tooth height and the applied axial loading. Analysis of the motor performance has shown that an increase of the teeth height increases the speed of the motor with relatively small effect on the stall torque. Further, the effect of the teeth height on the motor efficiency requires optimization since there is an increase at small values reaching a maximum at certain ratios of the teeth height to the stator thickness. The two most important characteristics of the motor are speed-torque and efficiency-torque. Typical graphs for low axial loading of a travelling wave USM yields a low stall torque and a relatively fast no-load speed. As the axial loading increases, a steady state progression is observed from high no-load speeds and low stall-torque to lower no-load speeds and high torque. This rotor speed decrease is due to the normal forcing on the stator, as the axial load increases, more energy is taken out of the stator vibration and thus the stator surface velocity decreases which in turn affects the rotor velocity. Examination of the efficiency-torque curves is showing that maximizing the output power does not maximize the efficiency. The cause of this behavior is the clamping effect that is associated with the increased load and reduced capability of the stator to resonate.

A comparison of the performance characteristics of rotary electric motors and USM is shown in Table 5.2-2. The characteristics listed in this table are given for motors without gear reduction and the data highlights the inherently higher torque density of USM. To obtain similar levels of torque-speed characteristics with conventional motors, a gear system is added to reduce the speed, thus increasing the size, mass and complexity of the drive mechanism. The general characteristics of USM make them attractive for robotic applications where small, intermittent motions are required. Since these motor designs are solid state the overall design is amenable to miniaturization [Flynn, 1992].

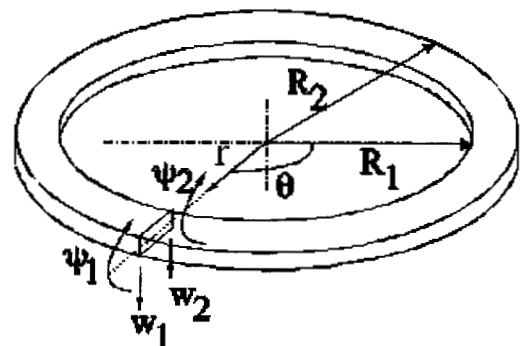
The analysis of the nonlinear, coupled rotor-stator dynamic model discussed above has demonstrated the potential to predicting motor steady state and transient performance as a function of critical design parameters such as interface normal force, tooth height, and stator radial cross section. Finite element algorithms were incorporated into the analysis and a MATLAB code was developed to determine the modal characteristics of the stator. The model accounts for the shape of the stator, the piezoelectric poling pattern, and the teeth parameters. Once the details of the stators are selected the modal response is determined and is presented on the computer monitor, as shown for example in Figure 5.2-14, where the mode  $(m, n) = (4, 0)$  is

presented. An electronic speckle pattern interferometry [Lih, et al, 1997] was used to corroborate the predicted modal response and the agreement seems to be very good as can be seen in Figure 5.2-15.

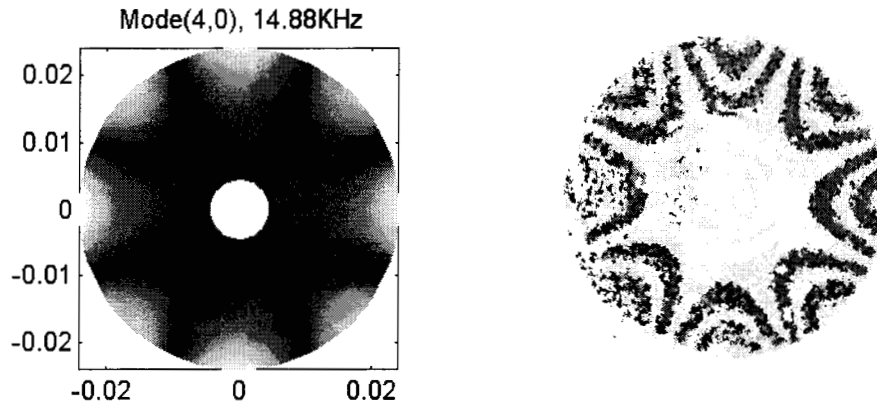
**Table 5-2.2:** Comparison of existing electromagnetic motors (EMM) and ultrasonic motors (USM) [from MIT 1999].

Type	Description	Manufacturer	Stall Torque (Ncm)	No-load Speed (rpm)	Power Density (W/kg)	Torque Density (Nm/kg)	Peak Eff.
EM	DC, brushless	Aeroflex	0.33	13,500	106	0.29	71%
EM	DC, brush	Micro Mo	0.99	4,000	-	0.04	~20%
EM	DC, brush	Maxon	1.27	5,200	-	1.13	70%
EM	DC, brush	Mabuchi	1.60	14,500	-	0.42	53%
US	Standing wave, extension /twist	Kumada	133	120	80	8.8	80%
US	Traveling wave, disk-type	Shinsei	60	100	18	2.6	27%
US	Traveling wave, disk-type	MIT	170	40	12	5.2	15%
US	Traveling wave, 8-mm ring-type	MIT	0.054	1750	108	2.1	-

The predicted resonance and measured resonance frequency for a 4.34-cm diameter steel stator are represented in Table 5-2.3. The results in Table 5-2.3 show excellent agreement between the calculated and measured data. Another advantage of USMs is their ability to handle extreme environments. In Figure 5.2-16 the effect of low temperatures and vacuum, on a 2.8-cm USM is shown, where the speed and the torque were measured down to  $-150^{\circ}\text{C}$  and at a vacuum level of  $1.6 \times 10^{-2}$  Torr. The motor showed a remarkably stable performance under these harsh conditions. Other work has shown that these motors work for up to 300 hrs at  $-150^{\circ}\text{C}$  in vacuum [Bar-Cohen, et al, 1998]. These results are very encouraging for potential application of these motors to space mechanisms



**Figure 5-2.14:** An annular finite element.

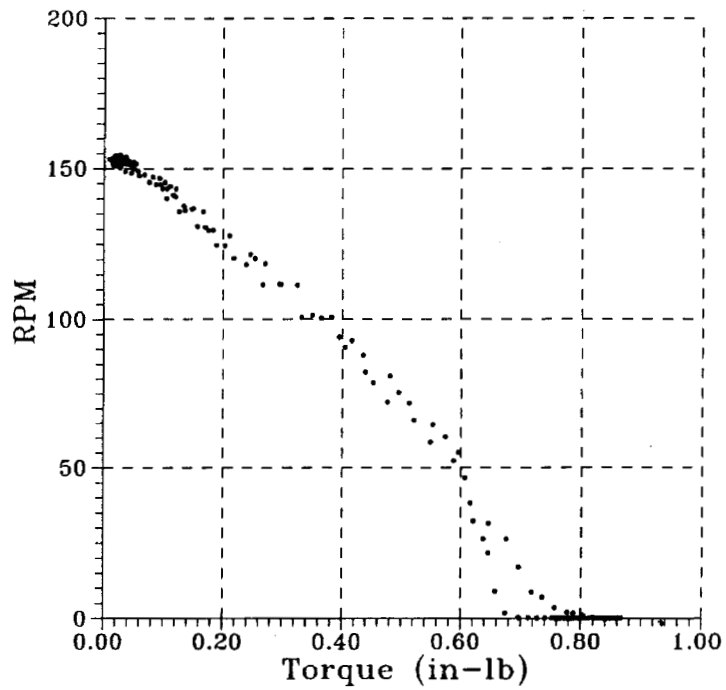


**Figure 5-2.15:** Modal response and resonance frequency (left) and experimental verification (right).

**Table 5-2.3:** The measured and calculated resonance frequencies of a USM's stator.

Mode (m,n)	Calculated Frequency (KHz)	Measured Frequency
(4,0)	14.88	14.55
(5,0)	22.48	22.37
(6,0)	31.45	31.34

**Figure 5-2.16:** Torque-speed performance of a JPL/QMI USM subjected to -150°C and 16 mTorr



## 5.2.4 OTHER APPLICATIONS OF ELECTROACTIVE CERAMICS

For many years, piezoelectric materials have been well recognized by the NDE community as the leading source for making transducers for ultrasonic probes. Overall, electroactive ceramics are applied to a large number of functions and a brief list with reference examples are as follows: valves [Marescaux, 1994; and Hogi, 1992] Pumps & Compressors [Spencer, et al, 1978; and Wang & Carter, 1986], Positioners [Jiang, et al, 1991; Choi, et al, 1996], Switches/Relays [Ota, et al, 1989; and Uchino, 1996], Agitation/Mixing, Separation/Filtration, Atomizers, Ultrasonic Transducers [Sayer & Screenivas, 1990], Ultrasonic Cleaning/Cutting/Drilling, Noise Cancellation [Kim & Jones, 1991; and Spencer & Chopra, 1996], Electro-Optical Scanning [Lee, 1979] stepping motors [Heil, et al, 1993; and Yakimov, 1996], built-in structural diagnostic sensors and other smart structures and systems [SPIE Smart Structures Proceedings].

## ACKNOWLEDGEMENT

The chapter was written at the Jet Propulsion Laboratory, California Institute of Technology, under a contract with the National Aeronautics and Space Administration.

## 5.2.5 REFERENCES

- Bar-Cohen Y., Bao X., Grandia W, (1998): "Rotary Ultrasonic Motors Actuated by Traveling Flexural Wave", Proceedings of the SPIE International Smart Materials and Structures Conference, SPIE paper 3329-82, San Diego, CA
- Barron B.W., Li G., Haertling G.H. (1996): "Temperature Dependent Characteristics of CERAM-BOW Actuators, Proceedings of the 10<sup>th</sup> IEEE International Symposium on the Application of Ferroelectrics, East Brunswick, N.J., vol. 1, pp. 305-308, August
- Barth H.V. (1973): Ultrasonic Driven Motor, IBM Technical Disclosure Bulletin, **16**, pp. 2263
- Belford J.F. (1960): "The Stepped Horn", Proceedings of the National Electronics Conference, pp. 814-822, Chicago
- Burleigh Instruments Product Catalogue, Burleigh Instruments, Inc. Fishers, New York.
- Burleigh Instruments Micropositioning Systems (1991):, Burleigh Instruments, Inc. Fishers, New York.
- Cady W.G, (1964): Piezoelectricity, McGraw-Hill, New York, 1946, republished by Dover
- Cannon (1992): "Cannon Develops an 11x25-mm Miniature Ultrasonic Motor," Cannon, Nikkei Mechanical, June
- Chen, Q. Yao, D., Kim, C.J. , Carman, G.P., (1998):, "Frequency Response of an inchworm motor fabricated with micro machined interlocking surface Mesoscale Actuator Device (MAD)", Proceeding of the SPIE Smart Structures and Materials Conference, Vol.3329, pp. 768-776, San Diego, CA
- Choi S.B., Cheong C.C., Lee C.H. (1996): "Position Tracking Control of a Smart Flexible Structure Featuring a Piezofilm Actuator", J. Guid. Control and Dyn., **19**, pp 1364-1369
- Cross L.E., Jang S.J., Newnham R.E., Nomura S., Uchino K., (1980) "Large Electrostrictive Effects in Relaxor Ferroelectrics", Ferroelectrics, **23**, pp. 187-192
- Cross L.E., Thomann H., Smolensky G.A., Uchino K.(1986): Ferroelectrics and Related Materials : Multilayer and Other Ferroelectric Ceramic Composites, Nos. 1/2/3/4 Gordon & Breach Science Pub; ISBN: 2881241506

- Dogin A., Uchino K., Newnham R.E, (1997): "Composite Piezoelectric Transducer with Truncated Conical Endcaps 'Cymbals'", IEEE Transactions on Ultrasonics, Ferroelectrics and Frequency Control, **44**, pp.597-605
- Face International (1999): THUNDER Technical Specifications, Face International Corp. 427 35<sup>th</sup> St. Norfolk, VA, 23508
- Flynn, A. (1992): "The Scoop on Ultrasonic Motors in Japan," Office of Naval Research Asian Office Scientific Information Bulletin, NAVSO P-3580, Vol. 17, No. 2, April-June, pp. 99-102.
- Flynn, A. M., Tavrow L.S., Bart S.F., Brooks R.F., Ehrlich D.J., Udayakumar K.R., Cross L.E. (1992): "Piezoelectric Micromotors for Microrobots" J. of MEMS, **1**, No. 1, pp. 44-51
- Galante, T., Frank, J., Bernard, J., Chen, W., Lesieutre, G., Koopman, G.H., (1998): "Design Modeling and Performance of a High Force Piezoelectric Inchworm Motor", Proceeding of the SPIE Smart Structures and Materials Conference, Vol.3329, pp. 756-767, San Diego, CA
- Haertling G. (1997): "Rainbow Actuators and Sensors: A New Smart Technology, Proceeding of the SPIE conference on Smart Materials, In Smart Material Technologies, vol. 3040, pp. 81-92
- Hagood N. W., McFarland A. (1995): "Modeling of a Piezoelectric Rotary Ultrasonic Motor," IEEE Transactions on Ultrasonics, Ferroelectrics and Frequency Control, **42**, No. 2, pp. 210-224
- Heil J., Dewilde Y., Jansen A.G.M., Wyder P. (1993): "Bimorph Stepping Motor for Point Contact Experiments", Rev. Sci. Instrum., **64**, pp.1347-1350
- Hogi T (1992): "A Flow Rate Control Valve using a Piezoelectric Element", JSME Int. J. II, **35**, pp. 376-379
- Hollerbach J.M., Hunter I.W. Ballantyne J. (1991): "A Comparative Analysis of Actuator Technologies for Robotics." In Robotics Review 2, MIT Press, Edited by Khatib, Craig and Lozano-Perez
- Hom Craig L., Pilgrim Steven P., Shankar Natarajan, Bridger Keith, Massuda Mona, And Winzer Stephen R. (1994): "Calculation of Quasi-Static Electromechanical Coupling Coefficients for Electrostrictive Ceramic Materials", IEEE. Trans. UFFC, **41**, pp. 542-551
- Hooker M.W. (1998): "Properties of PZT Based Piezoelectric Ceramics Between -150 and 250 °C", NASA Technical Report, NASA/CR-1998-208708
- Hosoe J (1989): "An Ultrasonic Motor for Use in Autofocus Lens Assemblies," Techno. pp. 36-41, , in Japanese.
- IEEE Piezoelectric Standard (1987): Standard on Piezoelectricity, IEEE/ANSI Std 176-1987
- Inaba R., Tokushima A., Kawasaki O., Ise Y., And Yoneno H., (1981): "Piezoelectric Ultrasonic Motor," Proceedings of the IEEE Ultrasonics Symposium, pp. 747-756
- Inoue T., Takahashi S. Suga M., (1989): "Application of Ultrasonics to Paper Transport Mechanisms," Techno, pp. 4749, in Japanese
- Jaffe B., Cook W.R., Jaffe H. (1971): Piezoelectric Ceramics, Academic Press, London,
- Jiang Z.W., Chonan S., Abe H., Tani J, (1991): "Position Control of a Flexible Arm Using Piezoelectric Bimorph Cells", Trans. ASME J. Dyn. Syst. Meas. Control, **113**, pp. 327-329
- Kim S.K., Jones J.D. (1991) "Optimal Design of Piezoactuators for Active Noise and Vibration Control", AIAA J., **29**, pp. 2047-2053
- Kugel V.D, Chandran S., Cross L.E. (1997): "A Comparative Analysis of Piezoelectric Bending Mode Actuators", Proceedings of the SPIE Smart Structures, Vol 3040, pp. 70-80
- Kumada, A. (1985): "A Piezoelectric Ultrasonic Motor," Japanese Journal of Applied Physics,

- Vol. 24, Supplement 24-2, pp. 739-741
- Lee J.K., (1979): "Piezoelectric Bimorph Optical Beam Scanners: Analysis and Construction", *Appl. Opt.*, **18**, pp.454-459
- Levinson L M. (Editor) (1988): Electronic Ceramics, Marcel Dekker ; ISBN: 082477761
- Lih S.-S., Bar-Cohen Y. , Grandia W. (1997 ): "Rotary Piezoelectric Motors Actuated By Traveling Waves," *Proceedings of SPIE*, Vol. SPIE 3041, Smart Structures And Materials Symposium, Enabling Technologies: Smart Structures and Integrated Systems, Marc E. Regelbrugge (Ed.), ISBN 0-8194-2454-4, SPIE, Bellingham, WA (June 1997), p. 912-917
- Marescaux D. (1994): "All Metal Bakeable Piezoelectric Valve", *Rev. Sci. Instrum.*, **65**, pp. 2412-2413
- Masaki Y., (1991): "Vibrator and Ultrasonic Motor Employing the Same," U.S. Patent 4,983,874, January 8
- Mason W.P.(1958): Physical Acoustics and the Properties of Solids, D. Van Nostrand Co Inc., Princeton, NJ
- Mason W.P., Thurston R., Peirce A. (Editors) (1964): Physical Acoustics - Vol 1-24, Academic Press,
- Minoru K., Ueha S., Moru E., (1983): "Excitation Conditions of Flexural Traveling Waves for a Reversible Ultrasonic Linear Motor," *Journal of the Acoustic Society of Japan*, Vol, 77, No.4
- MIT (1999):, (Hagood N) Massachusetts Institute of Technology Smart Structures Laboratory Webpage at <http://web.mit.edu/dept/amsl/amsl/labtour/slides/motor2.html>
- Near, C. , (1996): "Piezoelectric Actuator Technology", *Proceeding of the SPIE Smart Structures and Materials Conference*, Vol.2717, pp. 246-258, San Diego, CA
- N-Nagy F.L., Calderwood J.H., (1969): Abstract in *IEEE Trans. Electron Devices*, **16**, 6, pp.603
- N-Nagy F.L., Joyce G.C (1972): *Solid State Control Elements Operating of Piezoelectric Principals*, *Physical Acoustics*, **9**, pp. 129-165
- Ota T., Uchikawa T., Aihara Y, (1989): "Piezoelectric Latching Relay", *Ferroelectrics*, **93**, pp. 225-232
- Panasonic (1987): "Ultrasonic Motor", *Panasonic Technical Reference*. Panasonic Industrial Co., Division of Matsushita Electric Corp. of America, 1 Panasonic Way, Secaucus, NJ,).
- Piquette, J.C. , Forsythe, S.E., (1997): *J. Acoust. Soc. Am.*, **101**, pp.289-296
- Pohl D.W. (1987): "Dynamic Piezoelectric Translation Device", *Rev. Sci. Instrum.*, **58**, pp.54-57
- Sashida T. (1982): *Oyo Butsuri*, **51**, pp.713-720
- Sashida T., Kenjo T (1993): An Introduction to Ultrasonic Motors, Claredon Press , Oxford
- Sayer M., Screenivas K.( 1990): "Ceramic Thin Films: Fabrication and Applications, *Science*, **247**, pp1056-1060
- Seiko (1992): "Ultrasonic Micromotor Data Sheets", Seiko Instruments Inc., Precision Instruments Department, Consumer Products Div., 1-9-1 Miyakubo, Ichikawa-shi, Chiba 272, Japan
- Sherrit S., Mukherjee B.K (1998): *Proceedings of the SPIE Medical Imaging Conference*, vol 3341, San Diego
- Shimizu N., Kimura T., Nakamura T., Umebu I, (1990): "An Ultrahigh Vacuum Scanning Tunneling Microscope with a new Inchworm Mechanism, *J. Vac. Sci. Technol.* , **A8**, pp. 333-335

- Shinsei (1989): "Operation Manual for The Ultrasonic Motor," Shinsei Corporation, 18. Kasuya 2-chome. Setagaya-ku, Tokyo, 157 Japan. ( in Japanese).
- Spencer B.T., Chopra I. (1996): "Design and Testing of a Helicopter Trailing Edge Flap with Piezoelectric Stack Actuator", Proceeding of the Smart Materials and Structures Conference, Vol. 2717, pp. 120-131
- Spencer W.J., Corbet W.T., Dominguez L.R., Schafer B.D., (1978): IEEE Trans on Sonics and Ultrasonics, **SU-25**, pp. 153-156
- SPIE Smart Materials Proceedings (All Years)
- Uchino K. (1996): Piezoelectric Actuators and Ultrasonic Motors (Electronic Materials--Science & Technology, 1), Kluwer Academic Pub; ISBN: 0792398114
- Uchino K., (1996): "New Applications of Photostriction", Innovations in Materials Research **1**, pp.11-22
- Uchino K., Kato K. Tohda M. (1988): "Ultrasonic Linear Motors Using a Multilayered Piezoelectric Actuator," Ferroelectrics, Vol. 87, pp. 331-334
- Ueha S., Tomikawa Y. (1993): Ultrasonic Motors, Clarendon Press, Oxford
- Vasiliev P.E. et al. (1979):, UK Patent Application GB 2020857 A
- Vranish J. M., Naik D. P., Restorff J.S., Toter J.P (1991): "Magnetostrictive Direct Drive Rotary Motor," IEEE Trans, on Mag., Vol. 27, No, 6, p 5335, Nov.
- Wallace J.L., Espinoza-Faller F.J (1995):, "A Vibrating Reed Magnetometer Based on an Inchworm Motor and a Tunneling Tip Sensor", Meas. Sci. Technol., 6, pp. 1221-1224
- Wang W., Carter R., (1986): "PZT Ultrasonic Pump", Ultrasonics, **24**, pp. 105-106
- Wise S.A., Hooker M.W. (1997): "Characterization of Multilayer Piezoelectric Actuators for Use in Active Isolation Mounts", NASA Technical Memorandum 4742
- Yakimov V.N., (1996): "Scanning Tunneling Microscope with a Rotary Piezoelectric Stepping Motor", Rev. Sci. Instrum, **67**, pp. 384-386.
- Zemella R. J., (1990): "Design and Development of a Linear Traveling Wave Motor," MIT Master's Thesis in Aeronautics and Astronautics.

## 5.3 ELECTROACTIVE POLYMER (EAP) ACTUATORS

Yoseph Bar-Cohen and Sean Leary  
JPL, Caltech, 4800 Oak Grove Dr., Pasadena, CA 90740  
818-354-2610, fax 818-393-4057, [yosi@jpl.nasa.gov](mailto:yosi@jpl.nasa.gov)

5.3	ELECTROACTIVE POLYMER (EAP) ACTUATORS .....	1
5.3.1	INTRODUCTION .....	1
5.3.2	BIOLOGICAL AND ARTIFICIAL MUSCLES .....	2
5.3.3	IONICALLY CONDUCTING POLYMERS (ICP) .....	3
5.3.4	IONIC POLYMER METALLIC COMPOSITE (IPMC) AS BENDING ACTUATOR .....	3
5.3.5	IONIC GEL EAPS .....	5
5.3.6	ELECTRO-STATICALLY STRICTED POLYMER (ESSP) ACTUATORS .....	5
5.3.6.1	ESSP actuation force .....	5
5.3.7	FERROELECTRIC POLYMERS .....	7
5.3.8	ELECTRO-VISCOELEASTIC ELASTOMERS .....	8
5.3.9	SENSING .....	8
5.3.10	REFERENCES .....	8

### 5.3.1 INTRODUCTION

For many years, electroactive ceramics (EAC, e.g., piezoelectric and electrostrictive) have been widely used to actuate variety of mechanisms including ultrasonic motors, inchworms, switches, translators and manipulators. In contrast to EAC, EAP are relatively new actuation materials [Furukawa and Wen, 1984] with displacement capabilities that cannot be matched by the striction-limited, rigid and fragile ceramics. These materials are lighter and their displacement actuation capability can be as high as two orders of magnitude greater than EAC materials. Further, their response speed is significantly higher than shape memory alloys (SMA) with fatigue life that is many orders of magnitude longer. EAPs can be easily formed in various shapes, their properties can be engineered and they may be useful to developing unique micro-electro-mechanical systems (MEMS). Their most attractive feature is their ability to emulate the operation of biological muscles [Hunter and Lafontaine, 1992] with high toughness, large actuation strain and inherent vibration damping. A comparison between EAP, EAC and SMA is given in Table 1 and it is easy to see the superior displacement actuation capability of EAP. EAPs are typically electrically hard and mechanically soft. Namely, ferroelectric polymers have a coercive field in the range of 100 MV/m, which is of the order of 100 times the coercive fields of ceramic ferroelectrics making polymers quite stable electrically. On the other hand, these materials reach their elastic limit at lower stress levels compared to the piezoelectric ceramics. Also, the actuation stress falls far shorter than EAC and SMA actuators.

The field of electroactive polymers was established with the discovery of an electret when carnauba wax, rosin and beeswax is solidified by cooling while subjected to DC bias field [Eguchi 1925]. Following the 1969 observation of a substantial piezoelectric activity in PVF2, investigators started to examine other polymer systems and a series of applications have emerged. The list of new EAP materials has grown considerably. The number of commercially applied ones is still limited to PVF2/TRFE materials and ceramic/polymer composites.

**TABLE 1:** Comparison of the properties of some actuation materials

Property	Electro-static silicone elastomer [Kornbluh]	Polymer Electrostrictor [Zhang]	SMA	Single Crystal Electrostrictor [Shrout]	Single Crystal Magnetostrictor [Clark]
Actuation strain	32 %	4 %	8 %	1.7 %	2 %
Blocking Force/Area *	0.2 MPa	0.8 MPa	700 MPa	65 MPa	100 MPa
Reaction speed	$\mu$ sec	$\mu$ sec	sec to min	$\mu$ sec	$\mu$ sec
Density	1.5 g/cc	3 g/cc	6 g/cc	7.5 g/cc	9.2 g/cc
Drive field	144 V/ $\mu$ m	150 V/ $\mu$ m	--	12 V/ $\mu$ m	2500 Oe
Fracture toughness	large	large	large	low	large

\*Note: Values were calculated assuming the elastic properties were independent of applied field and are therefore approximate.

### 5.3.2 BIOLOGICAL AND ARTIFICIAL MUSCLES

Development of intelligent robots requires the combination of strong muscles (actuators) and acute sensors. Producing effective artificial muscle requires understanding the biological ones. Natural muscles are driven by a complex mechanism and are capable of lifting large loads at short (millisecond) response times. The performance characteristics of muscles are difficult to measure and most measurements were made on large shell-closing muscles of scallops. Peak stress of 150-300-KPa is developed at a strain of about 25%. Maximum power output is 150 – 225-W/kg; average power is about 50-W/kg with an energy density of 20-70-J/kg, which decreases with the increase in speed. Since muscle is fundamental to animal life and changes little between species, we can regard it as a highly optimized system. It is also a surprisingly complex system depending on chemically driven reversible hydrogen bonding between two polymers, actin and myosin. Muscle cells are roughly cylindrical, with diameters between 10 and 100- $\mu$ m and up to few centimeters long. Although muscles produce linear forces, motions at joints are all rotary. Therefore the strength of an animal is not just muscle force, but muscle force as modified by the mechanical advantage of the joint [Alexander, 1988], which usually varies with joint rotation (as does the muscle force). The mechanical energy is provided by a chemical free energy of a reaction involving adenosine triphosphate (ATP) hydrolysis. The release of  $\text{Ca}^{+2}$  ions seems turning on and off the conformational changes associated with muscle striction.

Actuators that are based on polymers, so called artificial muscles, cover a wide range of mechanisms including chemical [Kuhn, et al, 1950; and Steinberg, et al, 1966], thermal [Tobushi, et al, 1992; and Li, et al, 1999], electrical [Perline, et al, 1998, and Zhang, et al, 1998], magnetic [Zrinyi, et al, 1997, and Bednarek, 1998], and optical [van der Veen & Prins, 1971]. In many cases a combination of forces (e.g. electrochemical [Otero, et al, 1995]) is required to induce mechanical actuation. Half a century ago, [Kuhn et al, 1950] demonstrated that collagen filaments reversibly contracted or expanded when dipped in acid or alkali aqueous solutions, respectively. Although very little has since been done in exploiting such ‘chemomechanical’ actuators [Kuhn, et al, 1960, and Sussman, 1975], this early work pioneered the growth of a wide variety of bio-mimicking synthetic polymers.

The emphasis of this Section is on electro-active polymers (EAP). These materials are identified by the required external voltage/current to cause actuation deformation. Various materials are included in this category and they consist of electrically or ionically conducting polymers (ICP), ferroelectrics, and electrostatic actuators.

### **5.3.3 IONICALLY CONDUCTING POLYMERS (ICP)**

Ionically conducting polymers [Otero, et al, 1995, Tanaka, et al, 1982, and Abe, et al, 1998] are materials containing solvated ions that swell in response to applied voltages. The conformational changes are due to electrophoresis or electro-osmotic drag. Swelling of the polymer can occur even in the absence of applied fields as a result of sorption of solvents (usually water). Electrochemical reactions (oxidation/reduction) occur at electrodes that either promote or hinder actuation. Most reported actuators that were formed using ICP material exploited the voltage controlled swelling were formed as benders. The required voltage may vary from 1-mV to 50-V and the response time depends on thickness, diffusivity, kinetics of electrochemical reactions etc. and it can vary from milliseconds to minutes. Protective skins must be developed in order for these materials to be active in dry environments. The use of polar low vapor pressure solvents (such as propylene carbonate) helps to extend the ICP ability to perform in harsh conditions. Actuators that are based on ICP have limited driving force capability and they are typically less than 1-g.

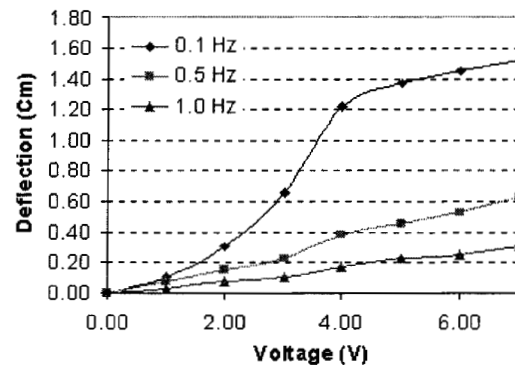
### **5.3.4 IONIC POLYMER METALLIC COMPOSITE (IPMC) AS BENDING ACTUATOR**

IPMC are films that bend under stimulation by electric currents induced by relatively low voltages. IPMC as an EAP material was realized in the early 1990's by [Oguro, et al, 1992] in Japan, and by [Sadeghipour, *et al*, 1992] and [Shahinpoor, 1992] in the United States. This material consists of chemically treated Nafion and it induces large bending deformation in the presence of low voltage. In order to chemically electrode IPMC's, metal ions (Platinum, gold or others) are dispersed throughout the hydrophilic regions of the polymer, and are subsequently reduced to the corresponding zero valent metal atoms. Its ionic polyelectrolyte is for the most part a 3-D network of macromolecules cross-linked with ionic charge groups nonuniformly distributed within the polymer matrix [Shahinpoor, 1994; and Heitner-Wirguin, 1996]. The mechanism of bending is partially related to migration of mobile ions within the networks caused by an applied electric field. The structure and properties of IPMCs have been the subject of numerous investigations (e.g., [Heitner-Wirguin, 1996]). Recent investigation by [Firoozbakhsh & Shahinpoor, 1998], suggests a strong interaction effect of surface charges. Since the actuation capability of IPMC is attributed to its ionic content, it is necessary to continuously maintain its moisture. A process developed at NASA-LaRC allowed the formation of a protective coating which serve as the equivalence of a biological skin, and was demonstrated to effectively maintained the moisture for several months [Bar-Cohen, et al, 1998].

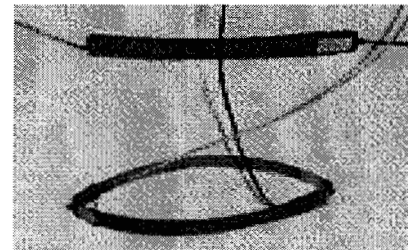
The ionic content of the IPMC is an important factor in the electromechanical response. Results using sodium cations and platinum metallization are shown in Figures 1-3 [Shahinpoor, et al, Dec. 1998]. Enhanced capabilities were reported by [Yoshiko, et al, 1998 and Oguro, et al, 1999] using Li<sup>+</sup>/gold and other types of cations. Under a relatively low voltage a large bending displacement is observed reaching saturation at values of ~4-volt, and a force to weight ratio of 40 was measured. As can be see in Figure 1, the displacement depends on the voltage and the frequency, where lower frequencies (~0.1 Hz) lead to higher displacements (approaching 25-mm

for a 25x6x0.1mm strip). The displacement reaches maximum amplitude at the resonant frequency, beyond which the response starts diminishing (>50Hz for 25mm long strip). Figure 2 were showing a pair of films that were connected to behave as a muscle, where under 4-Volts contracted by >11%, while consuming <.2-W. Since IPMC films are made of a relatively strong material with a large bending capability, they were used to emulate fingers and 4-gripper was developed (Figure 3). Such a gripper can serve as an end-effector of a miniature low-mass robotic arm. The fingers bend either inward or outward, similar to the operation of a hand, and hooks at the end of the fingers acting as nails securing gripped objects held by the fingers. The large bending capability of IPMC also enabled the fabrication of a surface wiper, operating similar to windshield wiper but with no mechanism (i.e., gear, motor, etc.). Example of the surface wiper is shown in Figure 4. This wiper is currently being considered for use to support the Jet Propulsion Laboratory Nanorover on the MUSES-CN mission to an asteroid and is expected to be launch in 2002. Recent performance tests at low temperatures showed that while the response decreases with temperature, a sizeable displacement was still observed at -140°C at vacuum of 1-torr. The decrease in actuation displacement can be compensated by increasing the voltage and it is interesting to point out that at low temperatures the response reaches saturation at a higher voltage level (~7-V at -100°C).

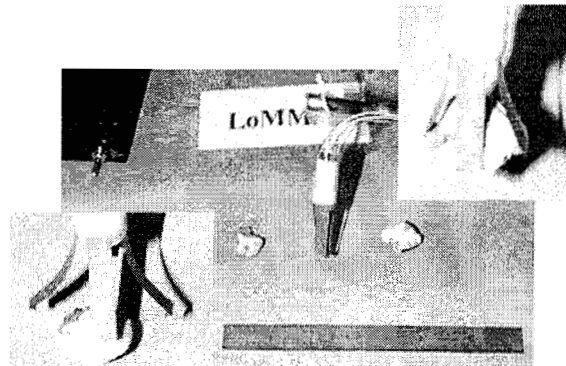
**Figure 1:** Typical response of Na+/Pt IPMC at various voltage levels and 3 frequencies.



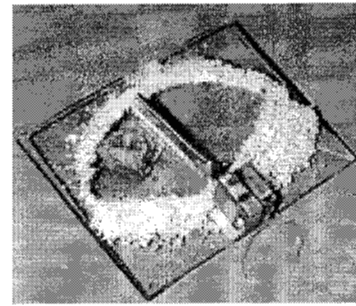
**Figure 2:** Na+/Pt IPMC film-pair. Top: reference, Bottom: activated



**Figure 3:** Four-finger gripper lifting >10-g rock using 0.1-g fingers.

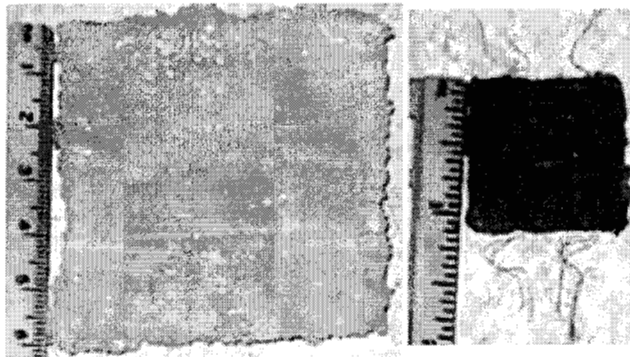


**Figure 4:** A dust wiper consisting of a Li<sup>+</sup>/Gold bending electroactive polymer and with a miniature blade (made by ESLI, San Diego, CA).



### 5.3.5 IONIC GEL EAPS

Synthetic ionic gel actuators have the potential of matching the force and energy density of biological muscles when driven chemically, usually by changing from an acid to base environment the gel becomes dense or swollen, respectively. However, the response is slow because of the need to diffuse ions into the gel and it takes with the current capability about 20-min to complete the displacement actuation.. Recent studies at the University of Arizona have shown that this response can be activated electrically (see Figure 6). When driven by embedded electrodes, these gels bend as the cathode side becomes more basic and the anode side more acidic.



**Figure 6:** Gel containing 4-pairs of electrodes swollen (left, 6-cm) and contracted (right, 3-cm).

### 5.3.6 ELECTRO-STATICALLY STRICTED POLYMER (ESSP) ACTUATORS

Polymers with low elastic stiffness and high dielectric constant can be used to induce large actuation strain by subjecting them to an electrostatic field. This characteristic allows producing longitudinal actuators that operate similarly to biological muscles using Coulomb forces between electrodes to squeeze or stretch the material. Following efforts by [Kornbluh, et al, 1995; and Perline, et al, 1998] longitudinal electrostatic actuators are made of a dielectric elastomer films and flexible electrodes. To produce a longitudinal actuator with large actuation force, two silicone layers was used with carbon electrodes on both sides of one of the layers. Wrapping the film to the shape of a rope allows making an actuator that can lift objects as shown in Figure 5. Besides using ESSP in the form of ropes that are bundled to further mimic human muscle, bending actuators can be constructed by adding a passive backing layer on one side of the electroactive film. To enhance the capability of this type of actuator, while making it contractile, studies are underway to produce EAP fibers that would be bundled to emulate muscles.

#### 5.3.6.1 ESSP actuation force

A schematic diagram of an ESSP actuator is show in Figure 5-left, and it can be represented by a parallel plate capacitor. The strain  $S$  and stress  $T$  developed when an electric field  $E$  is applied is given by:

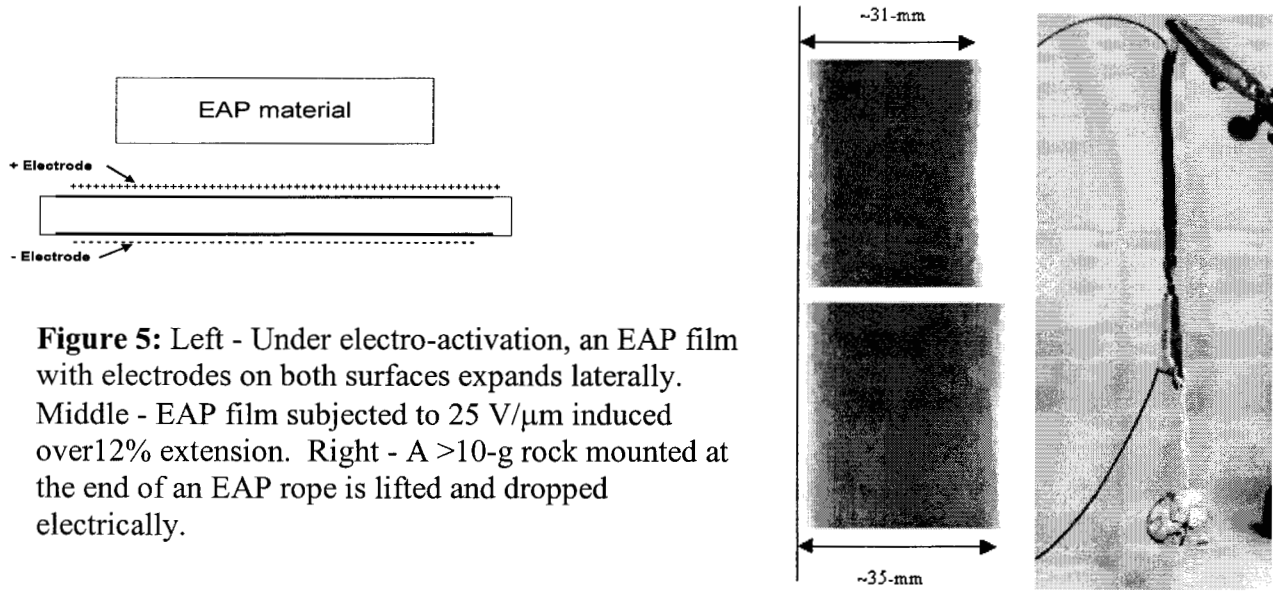
$$S = -\frac{1}{2Y} \epsilon_0 \epsilon E^2 \quad (1)$$

$$T = -\frac{1}{2} \epsilon_0 \epsilon E^2 = YS \quad (2)$$

where:  $Y$  is the Young's modulus of the dielectric between the plates with relative permittivity  $\epsilon$  (dielectric constant);  $\epsilon_0$  is the permittivity of vacuum and  $\epsilon$  is the relative permittivity; and  $E$  is the electric field across the thickness of the film. It can be seen that the effect of adding elastic dielectric material between the plates of the capacitor is to both increase the charge density and prevent the plates from shorting. The factor of  $1/2$  arises because the charge is contained only at the surface of the charged plates and the average electric field acting on this charged layer is  $E/2$ . It is important to note that the induced strain varies quadratically (nonlinear) with applied field. In 1880 Roentgen provided an early example of this effect by charging and discharging rubber bands with one end fixed and a mass attached to the free end. The force (stress) that is exerted on such a film with compliant electrodes is:

$$P = \epsilon \epsilon_0 E^2 = \epsilon \epsilon_0 (V/t)^2 \quad (3)$$

Where:  $P$  is the normal stress,  $V$  is the voltage applied across the film and  $t$  is the thickness of the film. The Poisson's ratio is assumed as 0.5.



**Figure 5:** Left - Under electro-activation, an EAP film with electrodes on both surfaces expands laterally. Middle - EAP film subjected to 25 V/μm induced over 12% extension. Right - A >10-g rock mounted at the end of an EAP rope is lifted and dropped electrically.

Use of polymers with high dielectric constants and application of high electric field leads to large forces and strains. To reach the required electric field levels one needs to either use high voltage and/or employ thin films. Under an electric field the film is squeezed in the thickness direction causing expansion in the transverse direction (See Figure 5-left). For a pair of electrodes with circular shape, the diameter and thickness changes can be determined using the following relation, where the second order components are neglected.

$$\Delta D / D_0 = (1/2) \Delta t / t_0 \quad (4)$$

Where:  $D_0$  is the original diameter of the electrodes and  $\Delta D$  is the resultant diameter change;  $t_0$  is the original thickness; and  $\Delta t$  is its change under electric activation.

ESSP actuators are subject to a major concern associated with the required large electric fields ( $\sim 100$  V/ $\mu\text{m}$ ) necessary to induce significant strains ( $\sim 10\%$ ). The actuator has to be thin ( $< 50\mu\text{m}$ ) to assure the use of achieve reasonable voltages. Overall, the associated voltage levels are close to the breakdown strength of the material and, since the dielectric breakdown may be difficult to predict, a safety factor needs to be used when designing such actuators. Moreover, the relatively small breakdown strength of air (2-3 V/ $\mu\text{m}$ ) presents additional challenge. Longitudinal actuators are produced using ESSP materials and they employ the Poisson effect that results from the film contraction. To obtain significant actuation displacements requires the use of large film material. Elastomers with Young's moduli on the order of  $< 20$  MPa and relative permittivities of 3 can induce large strain at the level of 30%. The Young's modulus is fairly temperature independent until the glass transition temperature is reached, at which point a sharp increase occurs making them too stiff to be used as electrostatic actuators.

In the above case of the ideal parallel-plate capacitor, the Maxwell stress was due to the *uniform* electric field between the plates. Another type of Maxwell force exists when the dielectric particles are placed in *nonuniform* electric fields. Uncharged particles will always be attracted to the region of stronger field regardless if it is positive or negative polarity. This force is proportional to the gradient of square of the field as well as the permittivity of the object. A familiar example of this effect is the attraction between a comb, charged by brushing ones hair, and bits of paper. An analogous effect also exist for magnetic fields, where paramagnetic and ferromagnetic materials experience a force directed to stronger magnetic field (diamagnetic materials are actually repelled by the region of stronger field). Composite materials can be made of fine ( $\sim 10$  nm) ferri/ferromagnetic particles dispersed in silicone elastomers. With such elastomers strains as high as 40% can be achieved with force level of 0.1 N and maximum field intensity of 80 mT [Zrinyi, 1996]. The disadvantage of this type of actuators is the need to for either movable permanent magnets or an electromagnet with high currents.

### 5.3.7 FERROELECTRIC POLYMERS

Poly(vinylidene fluoride) (PVDF or PVF2) and its copolymers are the most widely exploited ferroelectric polymers. These polymers are partly crystalline, with the amorphous phase being inactive. They possess Young's moduli near 1-10 GPa. A large amplitude ( $\sim 200$  MV/m) applied AC field can induce electrostrictive (nonlinear) strains of nearly 2%. However this level of field is dangerously close to dielectric breakdown, and the dielectric hysteresis (loss, heating) is very large, thus limiting it's use in practical devices. Scheinbeim [Sen, 1984] has investigated the effect of heavily plasticizing ( $\sim 65$  wt. %) ferroelectric polymers hoping to achieve large strains at reasonable applied fields. However, the plasticizer is also amorphous and inactive, resulting in decreased Young's modulus, permittivity and electrostrictive strains. Recently, Zhang [1998] has introduced defects using electron radiation to reduce the dielectric loss dramatically in P(VDF-TrFE) copolymer. This permits AC switching with a lot less heat generated. As large as 4% electrostrictive strains can be achieved at low frequency drive fields of amplitudes  $\sim 150$  V/ $\mu\text{m}$ . The elastic modulus of this material is 0.4 GPa, and therefore the mechanical energy density is quite large.

As with ceramic ferroelectrics, electrostriction can be considered as the origin of piezoelectricity in ferroelectric polymers [Furukawa, 1990]. A DC bias polarization can either be present via a *poling* process before use in a device, in which case a remnant polarization persists, or large DC electric field is applied during operation of the material in a device. In the latter case, no remnant polarization is observed when the bias is removed, and corresponds to a ferroelectric possessing a very small hysteresis in the polarization-electric field loop. Unlike electrostriction, piezoelectricity is a linear effect. Not only will the material strain when voltage is applied, but a voltage signal will be induced when a stress is applied. This enables them to be used as sensors. Care must be given to not apply too large of applied voltage, mechanical stress, or high temperature for fear of de-poling the material.

### **5.3.8 ELECTRO-VISCOELEASTIC ELASTOMERS**

Electro-viscoelastic elastomers represent another family of electroactive polymers. These EAP materials are composites of silicone elastomer and a polar phase. Before crosslinking, in the uncured state, they behave as electro-rheological fluids. An electric field is applied during curing to orient and fix in position the polar phase in the elastomeric matrix. These materials then remain in the “solid” state but have a shear modulus (both real and imaginary parts) that changes with applied electric field ( $< 6 \text{ V}/\mu\text{m}$ ) [Shiga, 1993; and 1997]. A stronger magneto-rheological effect can also be introduced in an analogous manner and as much as a 50% change in the shear modulus can be induced [Jolly, 1996; and Davis, 1999]. These materials may be used as alternatives to electrorheological fluids for active damping applications. To obtain precision control of robotic arms, with a closed-loop system, active damping is necessary.

### **5.3.9 SENSING**

Sensors are necessary for feedback control of robotic applications. Polymer base sensors offer resilience, fracture tolerance and low mass. Piezoelectric polymers have advantage over piezoelectric ceramics because of broadband response, and their ease of being able to be formed in complex shapes. They are widely used to emit and detect ultrasonic waves and ranging sensors are used for robotics to avoid obstacles and retrieve objects [Dario, 1988]. The pyroelectric effect (i.e. a change in temperature results in a voltage signal) is also present in these materials and enables them to be used as heat sensors. In the case of electrostatic actuators one can use feedback from the capacitive response of the actuator to sense its actuation behavior.

Future development of miniature systems will involve integration of actuators, sensors and their drive electronics. The size of such systems is reaching micron levels in the form of micro-electro-mechanical systems (MEMS) and this technology will be reviewed in Chapter 6.

### **ACKNOWLEDGEMENT**

The chapter was written at the Jet Propulsion Laboratory, California Institute of Technology, under a contract with the National Aeronautics and Space Administration.

### **5.3.10 REFERENCES**

Abe Y., A. Mochizuki, T. Kawashima, S. Yamashita, K. Asaka, and K. Oguro, “Effect of bending behavior of counter cation species in perfluorinated sulfonate membrane-platinum composite,” *Polym. Adv. Technol.*, Vol. 9 (1998), pp. 520-526.

- Alexander R. M., Elastic Mechanisms in Animal Movement, The Cambridge University Press: Cambridge, 1988.
- Bar-Cohen Y., T. Xue, M. Shahinpoor, J. O. Simpson, and J. Smith, "Flexible, low-mass robotic arm actuated by electroactive polymers (EAP)," *Proceedings of the SPIE International Smart Materials and Structures Conference*, SPIE Paper No. 3329-07, San Diego, CA, 1-6 (March 1998).
- Dario, P., "Transducers for advanced robotics," pp. 221-236 in Application of Ferroelectric Polymers. T.T. Wang, J.M. Herbert, and A. M. Glass (Eds.) New York: Chapman and Hall (1988).
- Davis, L.C., "Model of magnetorheological elastomers," *J. Appl. Phys*, Vol.85, No.6 (1999), pp.3348-3351.
- Eguchi M., *Phil. Mag.*, Vol. 49, (1925)
- F. K. Li, W. Zhu, X. Zhang, C. T. Zhao, and M. Xu, "Shape memory effect of ethylene-vinyl acetate copolymers," *J. Appl. Polym. Sci.*, Vol. 71, No. 7 (1999), pp. 1063-1070.
- Firoozbakhsh, K., and M. Shahinpoor, "Mathematical Modeling of Ionic Interactions and Deformation," *Proc. SPIE Smart Materials and Structures Conf.*, March 3-5, 1998, San Diego, CA, Publication No. SPIE 3323-66, (1998)
- Furukawa and J. X. Wen, "Electrostriction and Piezoelectricity in Ferroelectric Polymers," *Japanese Journal of Applied Physics*, Vol. 23, No. 9, 1984, pp. 677-679.
- Furukawa, T. and Seo, N., "Electrostriction as the origin of piezoelectricity in ferroelectric polymers," *Jpn. J. Appl. Phys*, Vol. 29, No. 4 (1990), pp. 675-680.
- G. van der Veen and W. Prins, *Phys. Sci.*, Vol. 230 (1971) , pp. 70.
- H. Tobushi, S. Hayashi, S. Kojima, "Mechanical properties of shape memory polymer of polyurethane series," *JSME Int. J.*, Ser. I. Vol. 35, No 3 (1992), pp.296-302.
- Heitner-Wirguin, C. "Recent advances in perfluorinated ionomer membranes: Structure, properties and applications," *Journal of Membrane Science*, V 120, No. 1, pp. 1-33, 1996.
- Hunter I. W., and S. Lafontaine, "A comparison of muscle with artificial actuators," *IEEE Solid-State Sensor and Actuator Workshop*, 1992, pp. 178-165.
- Jolly, M.R., Carlson, J.D., Munoz, B.C., Bullions, T.A., "The magnetoviscoelastic response of elastomer composites of ferrous particles embedded in a polymer matrix," *J. Intel. Mat. Syst.*, vol. 7. No. 6 (1996), pp. 613-622.
- Kornbluh, R. Pelrine R. and Joseph, J. "Elastomeric dielectric artificial muscle actuators for small robots," *Proceeding of the 3<sup>rd</sup> IASTED International Conference*, Concur, Mexico, June, 14-16, 1995.
- Kuhn W., A. Ramel, D. H. Walters, G. Ebner, and H.J. Kuhn, "The production of mechanical energy from different forms of chemical energy with homogeneous and cross-striated high polymer systems," *Adv. Polym. Sci.*, Bd. 1 (1960), pp. 540-592.
- Kuhn W., B. Hargitay, A. Katchalsky, and H. Eisenburg, "Reversible dilatation and contraction by changing the state of ionization of high-polymer acid networks," *Nature*, Vol. 165 (1950), pp. 514-516.
- Zrinyi M., L. Barsi, D. Szabo, and H. G. Kilian, "Direct observation of abrupt shape transition in ferrogels induced by nonuniform magnetic field," *J. Chem. Phys.*, Vol. 106, No. 13 (1997), pp. 5685-5692.
- Oguro K., N. Fujiwara, K. Asaka, K. Onishi, and S. Sewa, "Polymer electrolyte actuator with gold electrodes," Proceedings of SPIE's 6<sup>th</sup> Annual International Symposium on Smart Structures and Materials, Newport Beach, CA, paper 3669-39, 1-5 March, 1999

- Oguro, K., Y. Kawami and H. Takenaka, "Bending of an Ion-Conducting Polymer Film-Electrode Composite by an Electric Stimulus at Low Voltage," *Trans. Journal of Micromachine Society*, Vol. 5, (1992) pp. 27-30.
- Otero T. F., H. Grande, J. Rodriguez, "A new model for electrochemical oxidation of polypyrrole under conformational relaxation control," *J. Electroanal. Chem.*, Vol. 394 (1995), pp. 211-216.
- Q. M. Zhang, V. Bharti, and X. Zhao, "Giant electrostriction and relaxor ferroelectric behavior in electron-irradiated poly(vinylidene fluoride-trifluoroethylene) copolymer," *Science*, Vol. 280, pp.2101-2104 (1998).
- R. E. Perline, R. D. Kornbluh, and J. P. Joseph, "Electrostriction of polymer dielectrics with compliant electrodes as a means of actuation," *Sensor Actuat. A*, Vol. 64 (1998), p.77-85.
- Roentgen, W.C., "About the changes in shape and volume of dielectrics, caused by electricity," *Ann. Phys. Chem.*, Vol. 11 (1880), pp.771-786.
- S. Bednarek, "Susceptibility of magnetodielectrics within an elastomer matrix to length changes in heterogeneous magnetic field," *Appl. Phys. A*, vol. 66, pp.643-650 (1998).
- Sadeghipour, K., R. Salomon, and S. Neogi, "Development of a Novel Electrochemically Active Membrane and 'Smart' Material Based Vibration Sensor/Damper," *Smart Materials and Structures*, (1992) 172-179.
- Sen, A., Scheinbeim, J.I., and Newman, B.A., "The effect of plasticizer on the polarization of poly(vinylidene fluoride) films," *J. Appl. Phys.*, Vol.56, No.9, pp.2433-2439 (1984).
- Shahinpoor M., Y. Bar-Cohen, J. O. Simpson and J. Smith, "Ionic Polymer-Metal Composites (IPMC) as Biomimetic Sensors, Actuators & Artificial Muscles- A Review," *Smart Materials & Structures Journal*, Vol. 7, No. 6, (December, 1998) pp. R15-R30
- Shahinpoor, M., "Conceptual Design, Kinematics and Dynamics of Swimming Robotic Structures using Ionic Polymeric Gel Muscles," *Smart Materials and Structures*, Vol. 1, No. 1 (1992) pp. 91-94.
- Shahinpoor, M., "Continuum electromechanics of ionic polymeric gels as artificial muscles for robotic applications," *Smart Materials and Structures*, Vol. 3, pp. 367-372, 1994.
- Shiga. T. Okada, A., and Kurauchi, T., "Electroviscoelastic effect of polymer blends consisting of silicone elastomer and semiconducting polymer particles," *Macromolecules*, vol. 26, pp.6958-6963 (1993).
- Shiga, T. "Deformation and viscoelastic behaviour of polymer gels in electric fields," *Adv. Polym. Sci.*, Vol. 134, pp. 131-163 (1997).
- Steinberg I. Z., A. Oplatka, and A. Katchalsky, "Mechanochemical engines," *Nature*, vol. 210, (1966) pp.568-571.
- Sussman M. V., "Mechanochemical availability," *Nature*, Vol. 256 (1975), pp. 195-198.
- Tanaka T., I. Nishio, S.T. Sun, and S. U. Nishio, "Collapse of gels in an electric field," *Science*, vol. 218, pp. 467-469 (1982).
- Yoshiko A., A. Mochizuki, T. Kawashima, S. Tamashita, K. Asaka and K. Oguro, "Effect on Bending Behavior of Counter Cation Species in Perfluorinated Sulfonate Membrane-Platinum Composite," *Polymers for Advanced Technologies*, Vol. 9 (1998), pp. 520-526.
- Zhang, Q.M. , Bharti, V., Zhao, X., "Giant electrostriction and relaxor ferroelectric behaviour in electron-irradiated poly(vinylidene fluoride-trifluoroethylene) copolymer," *Science*, Vol. 280, (1998) pp. 2101-2103.
- Zrinyi, M, Barsi, L., Buki, A., "Deformation of ferrogels induced by nonuniform magnetic fields," *J. Chem. Phys.*, Vol. 104, No. 21 (1996), pp. 8750-8756.

# CHAPTER 10: FUTURE TRENDS IN ROBOTICS AND AUTOMATED NDE

<b>CHAPTER 10: FUTURE TRENDS IN ROBOTICS AND AUTOMATED NDE .....</b>	<b>1</b>
10.1 ROBOTICS AND AUTOMATIC NDE.....	1
10.2 BIOLOGICALLY INSPIRED (BI) SYSTEMS .....	3
10.1.1 INTRODUCTION .....	3
10.2.2 MAIN AREAS OF INTEREST.....	3
10.2.3 LOW LEVEL CONTROL .....	4
10.2.3.1 Passive stability .....	4
10.2.3.2 Neural Control .....	4
10.2.3.2 Behavior and Reflex Based Control .....	5
10.2.4 HIGH LEVEL CONTROL.....	5
10.2.4.1 Subsumptive Architecture.....	5
10.2.4.2 Cooperative Robotics.....	5
10.2.5 MOBILITY .....	6
10.2.5.1 Legs .....	6
10.2.5.2 Peristaltic Motion .....	7
10.2.5.3 Other BI Mobility Systems.....	8
10.2.6 ACTUATION.....	8
10.2.7 MULTIPLE SENSOR SYSTEMS AND SENSOR FUSION .....	9
10.2.8 MULTIPLE USE STRUCTURES AND SYSTEMS.....	9
10.2.9 REFERENCES.....	10
10.2.9.1 Publications and Correspondence.....	10
10.2.9.2 Internet Sites.....	10
10.3 HAPTIC INTERFACES.....	11
10.3.1 ROBOTS AS HUMAN SURROGATES.....	12
10.3.2 HAPTIC SYSTEMS .....	13
10.3.3 REFERENCES.....	17

## 10.1 ROBOTICS AND AUTOMATIC NDE

Yoseph Bar-Cohen

Jet Propulsion Laboratory, Caltech, 4800 Oak Grove Dr., Pasadena, CA 90740

818-354-2610, fax 818-393-4057, [yosi@jpl.nasa.gov](mailto:yosi@jpl.nasa.gov)

By the end of the second Millennium, the field of NDE has reached a mature level that allows designers to account for the probability of detection in the safety factors when developing fracture critical structures. Robotics and automation greatly enhances the capability, reliability and speed of performing inspection. Crawlers and various robotic scanners are bringing the capabilities of effectively inspecting large and complex structures to field conditions. New generations of open architecture miniature crawlers are emerging with a ability to reach areas that are difficult to access by human operators. Such system are lowering the inspection cost, minimizing the requirements for trained inspectors, increasing the reliability of the inspection and offering higher probability of detection. This book covered various aspects of the robotics and support technology that are needed to mobilize such scanners and using them as platforms for multiple sensors.

The implementation of robotic inspection technology for practical NDE is hampered by economical factors and by the required rigorous tests prior to certification of the involved procedures. While various size scanners found a wide range of applications in inspection facilities and field operations, crawlers have not been adapted to standard inspection procedures. It is envisioned that further technology progress as well as increased recognition of the capability and benefits will gradually lead to emergence of such robots in depot and other inspection facilities. Technology evolution of robotics, microelectronics and computers will lead to increased capabilities, lower operation cost and higher performance speed. While it is difficult to determine what will be the type or characteristics of future inspection robots, the authors of this chapter attempted to envision possible trends based on their telerobotics experience. This chapter is intended to provide an inspiring and futuristic view of the potential directions that NDE may adapt in the third Millennium.

## 10.2 BIOLOGICALLY INSPIRED (BI) SYSTEMS

*FINAL*

Brett Kennedy

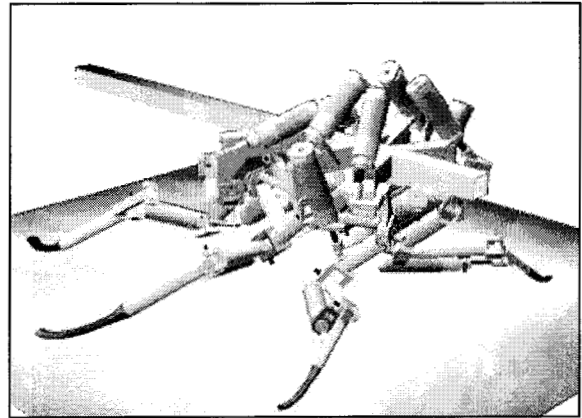
JPL, Caltech, 4800 Oak Grove Dr., Pasadena, CA 91109

818 354-6444, fax 818-393-3254, [bkennedy@telerobotics.jpl.nasa.gov](mailto:bkennedy@telerobotics.jpl.nasa.gov)

### 10.1.1 INTRODUCTION

The idea of emulating Nature in engineering design is not a new one. However, we as engineers need to be ever aware of new and different way to apply Nature's lessons. Some are readily apparent, such as the fact that mass-penalty increases nonlinearly with the characteristic dimension. Other lessons are more subtle, such as the application of ant society organization to cooperative robotic systems. The idea is to selectively apply these lessons and examples in the efforts to design robotic systems for NDE. An example of a robotic system utilizing biologically inspired design can be found in Figure 1.

**Figure 1:** A hexapedal robot shows cockroach kinematics [Case Western Reserve University, Biologically Inspired Robotics Laboratory]



A cautionary note must be made about the application of Nature and biology to engineering. We must look for inspiration from natural design rather than seek to emulate it. The heedless creation of biological analogs can lead to unnecessary design constraints and untenable solutions. Unlike Nature, we are able to consciously pick and choose aspects to incorporate into our designs. We can even, to some degree, define a cooperative environment within which our designs function. For more information on the similarities and differences in design in the natural and artificial worlds, Stephen Vogel's *Cats' Paws and Catapults* (1998) provides a detailing of concepts and examples, as well as illustrations of why Nature's answer to a problem should not always be Humankind's answer.

The following will provide an overview of some of the lessons and pointers taken from biology, as well as some possible applications of these ideas to NDE systems. Several areas key to system design will be discussed.

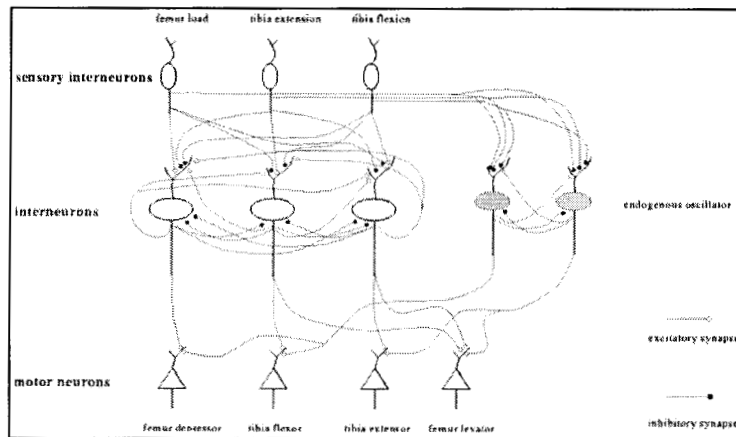
### 10.2.2 MAIN AREAS OF INTEREST

Nearly all areas of engineering design can be influenced by biology. Controls (both high and low level), computing, mobility, actuation, and general design philosophies can all find inspiration from the natural world. Each of the areas will be taken in turn and the possible application of BI robots will be fleshed out.

## 10.2.3 LOW LEVEL CONTROL

### 10.2.3.1 Passive stability

All terrestrial animals with the exception of bipeds (namely, humans) have body plans that allow for passive stability. In the static or quasi-static regimes, this fact is easy to see and understand for creatures such as insects and spiders. With six or eight sprawling legs, they will always have multiple points of contact with the work surface while standing or walking. Therefore, the center of gravity is almost guaranteed to be within the confines of the supports. The role of body plan and mechanics while in the dynamic regime is not as obvious. Robert Full of the University of California, Berkeley [1999] has been exploring an interesting aspect of some insect movement that he has termed passive dynamic stability. In essence, the mechanics of the insects he has studied (primarily cockroaches) ensure that the mechanical system (the insect) can reject disturbances without any active feedback when moving at speed. Disturbances, in this case, take the form of moderate obstacles or loose terrain. This stability makes unnecessary a brain complex enough to understand in full all aspects of the terrain, body mechanics, and kinematics in the time constraints imposed by running (cockroaches run at 50 Hz). In terms of robotic design, the creation of simple systems capable of high-speed traverse would seem to be possible.



**Figure 2:** A schematic showing the neural net associated with leg movement in insects [Nelson Lab, Neuronal Pattern Analysis (NPA) Group, Beckman Institute, University of Illinois @ Urbana Champaign]

### 10.2.3.2 Neural Control

When feedback becomes involved, Nature turns to neural controllers. Of all BI concepts, the use of neural nets in robotics have certainly seen the most work done over the last 40 years, and it will be mentioned several times in this piece. What, in fact, could be more natural than to emulate the biological structure which governs computation? In terms of control, the design of a neural feedback loop is well established. However, it is also one of the more abused concepts as well. As they are normally created through an iterative process that requires no *a priori* knowledge of the relationship between input and output or governing equations of the system, neural controllers are excellent candidates for highly non-linear systems. However, they are limited by the set of input and output conditions used in their creation. For this reason, they are

no more a magic bullet for control schemes than other paradigms such as proportional, integral, derivative (PID) control. That said, neural networks can be made adaptive given sufficient computing power, just as other schemes have been.

### 10.2.3.2 Behavior and Reflex Based Control

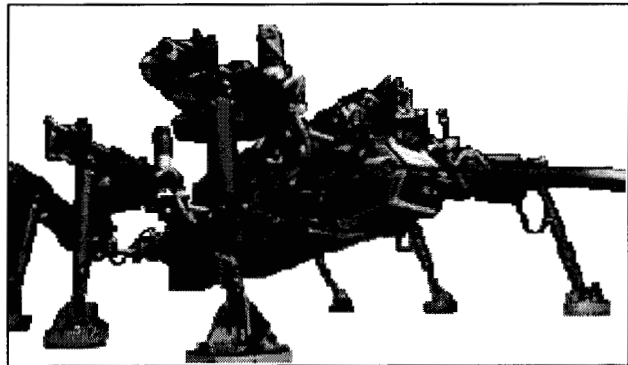
Moving up the hierarchy of control levels, behaviors and reflexes use feedback loops to perform specific functions. As reflexes are simply behaviors that are immediately activated by stimuli, they will be treated as a subset. Behaviors, as applied to robotics, are minimal chunks of code designed for a specific task. They can be instantiated in any number of ways from classic coding to neural loops. Behaviors are generally simple things such as wall following, goal acquisition, or obstacle avoidance. One good example of a BI behavior is the foothold finder created for Robot II at Case Western Reserve by Quinn and colleagues [Biologically Inspired Robotics Laboratory web page]

## 10.2.4 HIGH LEVEL CONTROL

### 10.2.4.1 Subsumptive Architecture

While what has been described may sound like simple subroutines, behaviors can become truly powerful when arranged in a subsumptive architecture. In this arrangement, several behaviors (such as wall following, goal seeking) compete to direct the actual actions of the robot. The resolution of the competition is decided by the weighting of the importance of those behaviors. In this way, the system is working as a higher level neural net. Moreover, these simple behaviors can be grouped into higher-order behaviors, which themselves have weight. In this way, relatively simple pieces of code can produce complex actions.

**Figure 3:** *Attila* is one of the most advanced platforms to be controlled through subsumptive architecture. [MIT Artificial Intelligence Laboratory].



### 10.2.4.2 Cooperative Robotics

Cooperative robotics has implications for several areas. Several classes of units can be created, each of which has a specific set of abilities. Unlike nature, a robotic network could utilize a central “mind” to coordinate efforts between units. However, a paradigm that relies more on the direct interaction between units to communicate, similar to ant or bee colonies could also be used (see example in Figure 4). In terms of control and planning, this structure is much like subsumptive control in that it uses simple subsystems to perform complex tasks. (Just look at the complexity of a child’s ant farm). In this case, a few basic behaviors are given over to each individual unit. The multiple interactions between these units creates the complexity

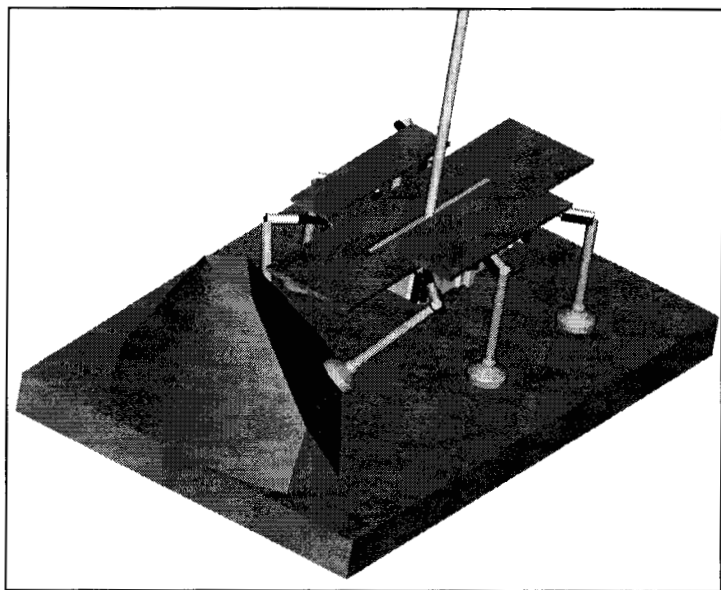
necessary to complete the task desired. Of course, a hybrid of coordinated and cooperative control could be created.

## 10.2.5 MOBILITY

### 10.2.5.1 Legs

With relatively few exceptions, terrestrial animals use legs for mobility. Therefore, there is a strong existence proof that legs are a reasonable and possibly desirable mobility method for robots as well. The question, then, is whether legs allow for more capable robots than can be otherwise designed. The answer, not surprisingly, is, yes, *for certain cases*. Traditionally, legs have been seen as the mobility system for the most difficult terrain, including steep angles of approach and complex surfaces (see example in Figure 5). However, one of the most persuasive arguments for legs is their capability of multiple use. While legs have greater design demands than other systems such as wheels, they can provide more utility as they can be used as manipulators, anchors, and test probes, as well as for mobility.

As an example of this concept, one need only look at the average insect leg. An excellent description and diagram of such a leg can be found in *Sense Organs of Insect Legs and the Selection of Sensors for Agile Walking Robots* by Fred Delcomyn et al, 1996. In general, a leg will be used as a motivator for locomotion. However, it is also festooned with various sensors: tactile, strain, and chemo-sensitive. These sensors provide the insect with information for navigation and goal acquisition (food). In addition, these legs are used, in some insects, to manipulate their environment such as the transport of pollen by bees, the capture of prey by mantids, and the construction of nests by mud daubers, and to effect maintenance on themselves, such as self-grooming of antennae. As applied to NDE robots, a legged system could apply these concepts toward inspection tasks where the robot can crawl into hard to reach areas and perform inspection tasks. For instance, cracks could be probed in search of chemical leaks by one set of legs while the other sets maintained stability or anchor the robot. An example of a multi-leg robot conducting a task of examining an object is shown in Figure 6.

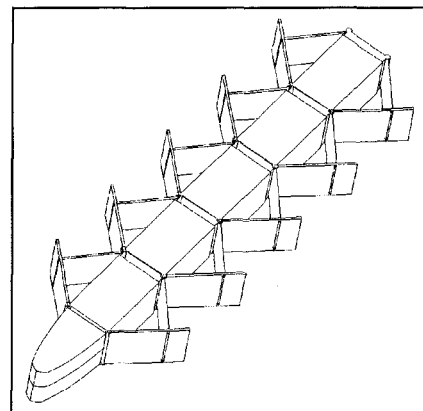


**Figure 6:** A 6-legs robot using one of the front legs to probe an object. [Kennedy, 1998]

### 10.2.5.2 Peristaltic Motion

Another successful locomotion technique from nature is peristaltic motion. Chief adherents to this are earthworms and the legless reptiles of order Amphisbaenia. Peristaltic motion relies on a body plan that is made up of multiple identical units, in those cases muscular rings. These units create two different motions. One consists of the radial expansion of the rings. This expansion provides an anchoring force against tunnel walls. The other motion is a longitudinal expansion, providing forward motion. By combining and coordinating these motions among the units, these animals are able to move within their tunnels. With some imagination, this paradigm could be applied to NDE. Although both the animals mentioned are burrowers, the basic motion could easily be applied to pipe crawlers. Basically, peristaltic motion can be used in situations in which the open path width is small compared to the length of the robot.

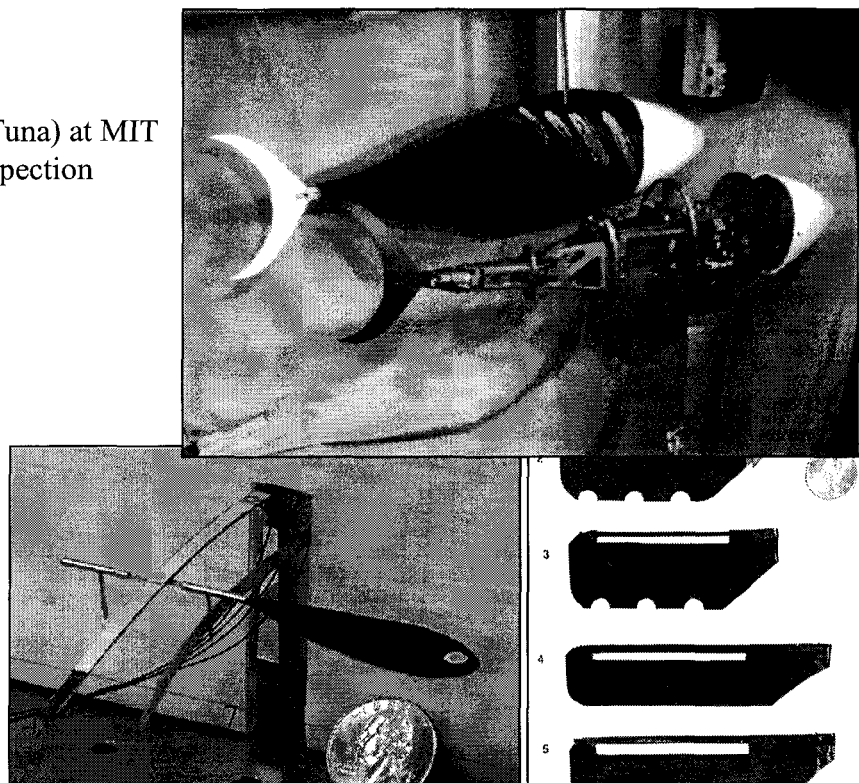
**Figure 7:** A schematic view of a simple mechanism for peristaltic locomotion. [Kennedy, 1998]



### 10.2.5.3 Other BI Mobility Systems

As we begin to expand the realms in which robots move, namely air and water, more modes of movement derived from nature suggest themselves. MIT researchers have built several robotic fish (as shown in Figure 8), which could be used for maritime inspection. As systems shrink, researchers have suggested flying robots that use insectile flying modes. The beginnings of such robots are shown in Figure 9.

**Figure 8:** Robotic fish (RoboTuna) at MIT could evolve into maritime inspection systems. [MIT Tow Tank]



**Figure 9:** Pictures of wings and a wing actuator under development at Vanderbilt. [Vanderbilt Microrobotics Laboratory]

### **10.2.6 ACTUATION**

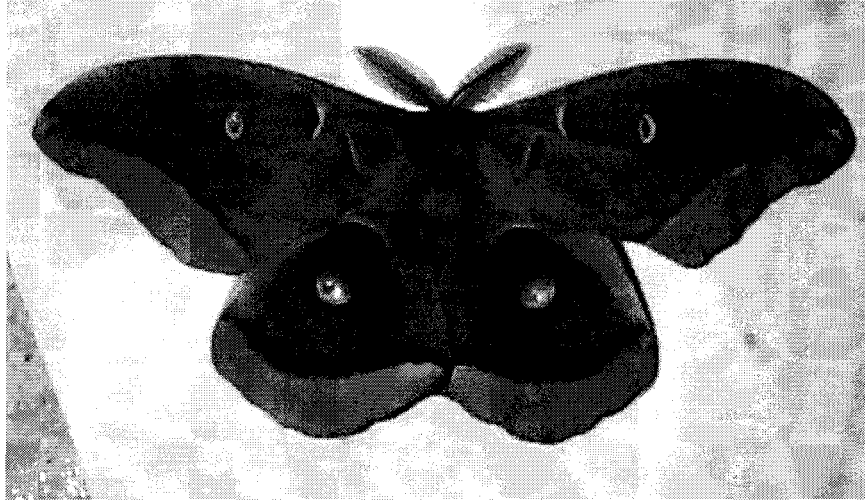
Actuators that can serve as analogs for biological muscle have long been the goal of research. Such devices could make the design of biomorphic body plans much easier. Section 5 was dedicated to this topic and as could be seen one of the most promising technologies is the electroactive polymers (EAP).

### **10.2.7 MULTIPLE SENSOR SYSTEMS AND SENSOR FUSION**

While the advisability of copying sensing techniques directly from nature is debatable, we might take heed of the fact that nature organizes its sensors in a very different way than is generally done in robotics. Instead of a few sophisticated sensors that provide all the information for particular functions (i.e., a stereo camera pair that provides all navigation information), animals tend to use a multitude of sensors of different types for feedback on their environment and goals acquisition. Again the average insect leg provides a model (Delcomyn, et al.). It carries several different sensors and multiple copies of each. Moreover, each one of those sensors can affect a function such as navigation. Clearly, even in a relatively unsophisticated animal, a great deal of sensor fusion is occurring.

As the number and type of sensors becomes larger, a special structure must be created to deal with the information. In higher animals, the cerebellum, a section of the brain, performs this task. It essentially acts as a clearing-house for information. Researchers at JPL's CISM laboratory are now at work on a silicon version of this vital brain structure.

Engineers have long had analogs of the senses of touch, sight, and temperature. However, it is only recently that a practical analog has been created for smell (and, by extension, taste). The e-nose, such as the one currently under development at Caltech (Goodman et al.) is essentially a chip with chemical receptors built in, as well as the circuitry necessary to recognize particular odors. Changes in the receptors' properties when they bond to particular molecules indicates the presence of those molecules. As these sensors can be tailored to particular molecules, leak sniffing robot becomes a real possibility.



**Figure 10:** A moth, with its chemo-sensitive antennae, provides a model for a robotic “sniffer”. (Scott Henniger)

### 10.2.8 MULTIPLE USE STRUCTURES AND SYSTEMS

As touched on in the section on legged mobility, one of the most important ideas from biology is the concept of multiple use structures and systems. While some of the applications of this idea are more obvious, such as the use of legs for both mobility and manipulation, others are more subtle. In some cases, the dual nature of a device has more to do with how it is perceived than how it is used. An instance of this is the use of certain sensors for both navigation and inspection. Vision would lend itself well to this concept, but it is certainly not limited to vision. At a more sophisticated level, one could imagine the information from several sensors, which would normally have other uses, being fused for inspection purposes. For instance, given a force-feedback control scheme with strain gauges for feedback, the extension of a limb in contact, as given by joint encoders and kinematics, the spring constant (hardness) of a material could be calculated. Again, the pattern recognition capabilities of neural nets could come into play in dealing with the wide range of input.

Multiple use structures are important the viability of biomorphic designs for economic reasons. Since using animal-like body plans and sensor arrangements requires more hardware (actuators and sensors) than more traditional designs, every part of the robot must provide a relatively larger return of functionality and information due to the greater cost of design and manufacture. By more tightly integrating systems and hardware greater efficiency of investment to functionality can be achieved.

### 10.2.9 REFERENCES

#### 10.2.9.1 Publications and Correspondence

Delcomyn, Fred et al. *Sense Organs of Insect Legs and the Selection of Sensors for Agile Walking Robots*. The International Journal of Robotics Research, Vol. 15, No. 2, April 1996

Espenschied, K. S., Quinn, R. D., Chiel, H. J., and Beer, R. D., "Biologically-Based Distributed Control and Local Reflexes Improve Rough Terrain Locomotion in a Hexapod Robot," *Robotics and Autonomous Systems*, Vol. 18, pp. 59-64, 1996.

Full, Robert. Personal communication, 1999

Goodman, Rodney et al. *The Caltech Electronic Nose Project*, web page, 1999

Ting, L.H. et al., *Dynamic and Static Stability in Hexapedal Runners*. *J. exp. Biology* 197, 251-269, 1994

Vogel, Stephen. *Cat's Paws and Catapults*, W.W. Norton & Co., New York, 1998

#### **10.2.9.2 Internet Sites**

Biologically Inspired Robotics Laboratory, Case Western Reserve University,  
<http://biorobots.cwru.edu/>

Nelson Lab, Neuronal Pattern Analysis (NPA) Group, Beckman Institute, University of Illinois  
@ Urbana Champaign, <http://soma.npa.uiuc.edu/labs/nelson/nelson.html>

Artificial Intelligence Laboratory, MIT, <http://www.ai.mit.edu/>

Vanderbilt University, Microrobotics Laboratory,  
<http://www.vuse.vanderbilt.edu/~meinfo/labs/micro/micro.htm>

Poly-PEDAL Laboratory, U.C. Berkeley, <http://polypedal.berkeley.edu/>

Towing Tank, MIT, <http://web.mit.edu/afs/athena.mit.edu/org/t/towtank/www/>

## 10.3 HAPTIC INTERFACES

Yoseph Bar-Cohen

Jet Propulsion Laboratory, Caltech, 4800 Oak Grove Dr., Pasadena, CA 90740

818-354-2610, fax 818-393-4057, [yosi@jpl.nasa.gov](mailto:yosi@jpl.nasa.gov)

Constantinos Mavroidis, and Charles Pfeiffer,

Robotics and Mechatronics Laboratory, Mechanical and Aerospace Engineering Department,  
Rutgers University, The State University of New Jersey

and

Christopher Culbert and Darby F. Magruder,

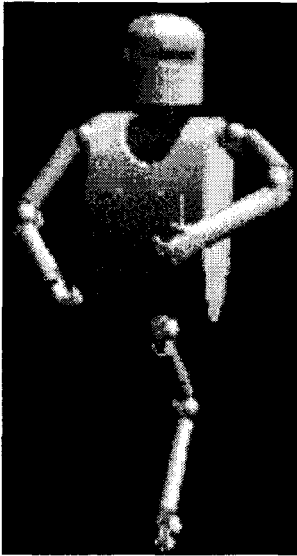
NASA, Johnson Space Center, Houston, TX

For many years, scientists and engineers sought to develop robots that can eventually operate autonomously and eliminate the need for human operators. However, there is an increasing realization that there are some tasks that humans can perform significantly better but, due to associated hazards, distance, physical limitations and other causes, only robots can be employed to perform these tasks. Performing such tasks remotely requires operating robots as human surrogates and such a capability has been the goal of many studies in recent years. Significant progress has been made, including for example the NASA Johnson Space Center development of the robotic astronaut, called Robonaut (see Figures 1 and 2). This robot is capable of performing various tasks at remote sites and was designed such that a human operator who is wearing gloves and/or suit with sensors can control it. Unfortunately, due to unavailability of force and tactile feedback capability in the control suit/glove, the operator determines the required action by visual feedback, i.e. looking at the Robonaut action at the remote site. This approach is ineffective and is limiting the potential tasks that Robonaut can perform. As human activity in space increases there is an increasing need for robots to perform dexterous Extra Vehicular Activity (EVA). Existing space robots are inadequate substitutes for an astronaut because they:

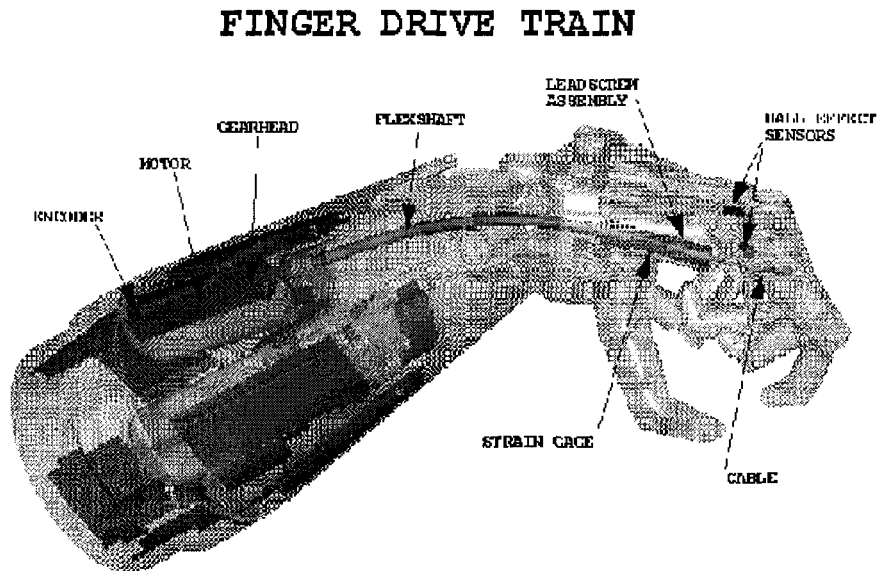
- (1) require additional special alignment targets and grapple fixtures.
- (2) are too large to fit through tight EVA access corridors.
- (3) do not possess adequate speed and dexterity to handle small and complex items, soft and flexible materials, as well as most common EVA interfaces.
- (4) are controlled by operators that have only visual feedback limiting incredibly their "perception" of the work-environment.

Therefore, there is a great need for dexterous, fast, accurate teleoperated space robots with the operator's ability to "feel" the environment as if she or he is "present" at the robot's operation field. Effective telepresence requires that human operator "feel" the stiffness, temperature, and vibration of the object that is being remotely or virtually manipulated/actuated. The mechanical and thermal characteristics of the remote object needs to be intuitively mirrored including the reaction forces and backward displacements. Such systems need to respond to data by remote sensors or from virtual reality sources at selected points or joints. Providing thermal feedback

can be easily conducted by existing technology, whereas the mechanical feedback using miniature elements is critically needed and are being under development. A wide range of remote NDE applications can employ such a technology particularly for applications where it is not safe for direct presence of human operator.



**Figure 1:** Robonaut - a robotic astronaut under development at NASA-Johnson Space Center.



**Figure 2:** The Robonaut arm and hand are controlled remotely by a human operator. Having a "feeling" of the mechanical condition at the remote site is critical to the effective use of the arm.

### 10.3.1 ROBOTS AS HUMAN SURROGATES

Telepresence requires that a human operator control the action of a remotely operated robot. In the case of the NASA Robonaut, the human operator must control nearly fifty individual degrees of freedom. The use of three axis hand controllers would present a formidable task for the operator. Because Robonaut is anthropomorphic, the logical method of control is one of a master-slave relationship whereby the operator's motions are essentially mimicked by the robot. If the user is to interact in a natural way with the robot, the interface must be intuitive, accurate, responsive and transparent. If the user is to control the robot motions in a naturally perceived way, an interface device must be provided which is capable of determining what the user is doing without interfering with their motion or encumbering their body. Furthermore, the operator must be able to extract information about the robot and its environment to effectively control the robot.

To date, there are no effective commercial alternatives to unencumbering haptic feedback devices for the human hand. As a result, intuitive teleoperated control of such robots as the Robonaut is currently being compromised. Tactile feedback devices that provide operator awareness of contact between work space objects and the robot structure is a key technology area for the effective control of dexterous robots. The use of a haptic mechanism internal to a cyber-glove offer greater usability of cyber-gloves while eliminating the bulkiness and clumsiness associated with an exoskeleton based haptic device.

### 10.3.2 HAPTIC SYSTEMS

To address the need for surrogate robots that remotely mirror human action and reaction, the engineering community has started developing haptic (tactile and force) feedback systems [Burdea, 1996]. At the present time, haptic feedback is a less developed modality of interacting with remote and virtual worlds compared to visual and auditory feedback. Thus, realism suffers especially when remote and virtual tasks involve dexterous manipulation, or interaction in visually occluded scenes. A very good description of the current state-of-the-art in haptic and force feedback systems can be found in [Burdea, 1996; Brown and Reger, 1998; US Navy, Office of Training Technology, 1999].

Tactile sensing is created by skin excitation that is usually produced by devices also called “tactile displays”, [Howe, 1999]. These skin excitations generate the sensation of contact. Tactile feedback is easier to produce than force feedback with present actuator technology, and the interface tends to be light and portable [Burdea, 1996]. Force sensitive resistors, miniature pressure transducers, ultrasonic force sensors, piezoelectric sensors, vibrotactile arrays, thermal displays and electro-rheological devices are some of the innovative technologies that have been used to generate the feeling of touch. An example is the tactile feedback suit that was developed by Begej Co. for NASA JSC [Li, 1993]. It consists of arrays of small pneumatic bellows on the arms, chest and abdomen. While tactile feedback was conveyed by the mechanical smoothness and slippage of a remote object, it could not produce rigidity of motion [Burdea and Langrana, 1993]. Thus, tactile feedback alone cannot convey the mechanical compliance, weight or inertia of the virtual object being manipulated [Burdea, 1996].


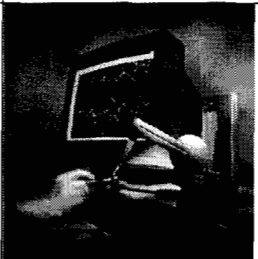


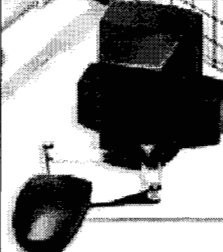


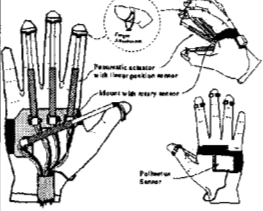
Force feedback devices are designed to apply forces or moments at specific points on the body of a human operator. The applied force or moment is equal or proportional to a force or moment generated in a remote or virtual environment. Thus, the human operator physically interacts with a computer system that emulates a virtual or remote environment. Usually, the force/moment feedback is applied at the operator’s hand or arm. Recently, several force feedback devices have been developed to transfer forces at the human operator’s knee and ankle. There are many important applications for force feedback devices. Force-feedback devices are the immediate descendants of the “master-slave” teleoperation systems that started to be developed in the 1940’s. Tele-operation is the remote control of robot manipulators that have and are being used in nuclear, underwater and space robotic tasks. In current systems, force-feedback is used in conjunction with virtual reality in several other applications such as:

1. entertainment and video games where the user realistically interacts with the virtual world using several modalities including force feedback.
2. training of specialists in difficult tasks where real prototypes can not be found easily. Examples are the training of medical doctors and surgeons and the training of pilots and astronauts,
3. rehabilitation of patients with neuromotor disabilities.

Force feedback devices are distinguished into portable and non-portable interfaces. Several examples for such devices are shown in Table 1. Force feedback joysticks, mice [Cybernet Systems Co., 1995; Immersion Corp., 1999; Haptic Technologies] and small robotic arms such

as the Phantom [Massie and Salisbury, 1994; Sensable Technologies, 1999] are non-portable devices which allow users to feel the geometry, hardness and/or weight of virtual objects. These systems are mechanically attached to the ground or to a fixed structure outside the user's body. The main advantage of non-portable force feedback system is that they do not tire the user, since the interface weight is supported by the desk to which it is attached [Burdea, 1996]. However, hand freedom of motion and dexterity are limited since these devices have a much smaller work volume and degrees of freedom than the user's hand. The simplest non-portable haptic systems are force feedback game controller joysticks and force feedback mice that usually offer a low force and inaccurate feedback at low cost. Examples are: the Microsoft Sidewinder (Table 1, System 1), the Impulse Engine (Table 1, System 2), the MouseCAT (Table 1, System 3) and the Feel-IT (Table 1, System 4)

**Table 1: Various Haptic Interface Systems**

Name	Technology	Picture	Name	Technology	Picture
<b>1) Sidewinder</b> force feedback pro [Microsoft, 1999]	DC Motors Low Bandwidth Low Resolution (Game Controller)		<b>5) The Phantom Desktop System</b> [Sensable Technologies, 1999]	DC Motors (Expanded Workspace)	
<b>2) Impulse Engine 2000</b> [Immersion Corp, 1999]	DC motors High Bandwidth Max force output 8.9N		<b>6) PenCAT</b> [Haptic Technologies, 1999]	DC Motors	
<b>3) MouseCAT</b> [Haptic Technologies, 1999]	DC Motors		<b>7) Magnetic Levitation Haptic Interface</b> [Berkelman, et al., 1996]	Magnetic Levitation	
<b>4) Feel-IT mouse</b> [Immersion Corp., 1999]	DC Motors		<b>8) RMII</b> [Burdea, et al, 1992]	Pneumatic	

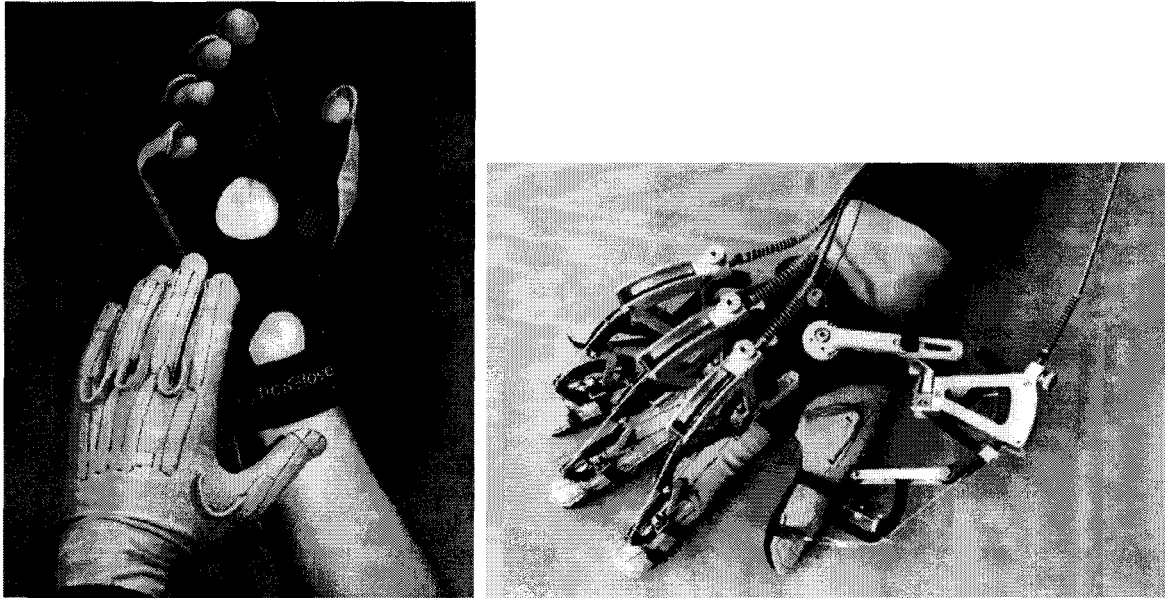
One of the non-portable force-feedback systems that really made an impact from the commercialization point of view is the PHANTOM (Personal Haptic iNterface Mechanism, see Table 1, System 5). This is a 6 degree-of-freedom lightweight manipulator composed of a three degree of freedom arm and a three degree of freedom thimble-gimbal. The arm's three joints are powered by DC motor while the gimbal's orientation is passive. The user is able to feel forces at one point at his/her fingertip or at a stylus that will be held by the user. The Phantom has been used in many applications such as medicine, training and tele-operation [Salisbury and Srinivasan, 1996]. The PenCAT (see Table 1, System 6) is a very similar system with the difference that it features only 4 degrees-of-freedom where force feedback is possible on only two of them, and that any motion is in the horizontal plane. Finally, the 6-degree of freedom magnetic interface developed by Carnegie Mellon University provides a high bandwidth, with only one moving part to the palm of the user [Berkelman, et al., 1996] (see Table 1, System 7).

Work towards improved portability with more freedom of motion of non-portable force feedback systems was done by Luecke and his colleagues at Iowa State University [Luecke, 1995]. Their haptic interface consists of an exoskeleton hand master tracked and supported by a robot. Magnetically-levitated finger attachments produce feedback forces at each phalanx without static friction. The system has higher dexterity and a large work envelope, which makes it more suitable for large volume simulations. The use of large currents near the user's hand (required for the magnetic coils in the exoskeleton), and a powerful supporting robot raise safety concerns. Furthermore, magnetic coil overheating prevents prolonged simulations, while robot kinematic singularities may limit the type of motions the user can perform while wearing the device [Burdea, 1996].

Similar work was done at NASA Jet Propulsion Laboratory (JPL) for a telerobotic application. The scientists retrofitted an older JPL Universal Master [Bejczy and Salisbury, 1980] producing wrist force feedback with a 16 degree-of-freedom hand master [Jau, et al, 1994]. The master-structure weighs about 2.5-lb and can move within a 30x30x30-cm cube. The weight of the master may still pose problems, and complexity is a factor to be considered. There is a need for simpler force feedback devices that are both light (so as to avoid user fatigue), dexterous (to allow independent finger interaction) and portable (to maintain the user's freedom of motion). Once such force feedback interfaces are constructed they could be integrated with a large visual display or an HMD.

Portable systems, are force feedback devices that are *grounded* to the human body. They are distinguished into *arm-exoskeletons* if they are applying forces at the human arm and in *hand-masters* if they are applying forces at the human's wrist and/ or palm. An example of an arm exoskeleton is the "Force ArmMaster" produced by EXOS Co. under a NASA SBIR task [Exos Co., 1993]. It uses three DC motors for the shoulder, one for the elbow and one for the forearm. Arm exoskeletons can reproduce, weight feeling, collisions with the environment and other virtual and remote forces that are applied at locations on the human arm besides the hand. However, portable arm-exoskeletons tend to be heavy (the Force ArmMaster weighs 22-lb), producing user fatigue and discomfort in extended simulations.

Portable hand masters are haptic interfaces that apply forces to the human hand while they are attached at the human operator fore-arm. In most of the cases, these systems look like gloves where the actuators are placed at the human fore-arm and the forces are transmitted to the fingers using cables, tendons and pulleys. An example of such a system is the CyberGrasp. The CyberGrasp is a lightweight, force-reflecting exoskeleton system that fits over a CyberGlove (see Figure 3) and adds resistive force feedback to each finger [Virtual Technologies, 1999].



**Figure 3:** The CyberGlove® and the CyberGrasp® [courtesy of Virtual Technologies, Inc. ([www.virtex.com](http://www.virtex.com))].

The grasp forces are exerted through a network of tendons that are routed to the fingertips via an exoskeleton. The tendon sheaths are specifically designed for low compressibility and low friction. The actuators are high-quality DC motors located in a small enclosure on the desktop. There are five actuators, one for each finger. The device exerts grasp forces that are roughly perpendicular to the fingertips throughout the range of motion, and forces can be specified individually. Due to the tendon/cable network, the remote reaction forces can be emulated very well, however, it is difficult to reproduce the feeling of “remote stiffness”.

A light force feedback hand master designed to retrofit open-loop sensing gloves was proposed by [Burdea, et al, 1992; Gomez, et al, 1995]. The Rutgers RMII (see Table 1, System 8) has low-friction custom graphite-glass actuators, which output up to 16 N/fingertip with very high dynamic range (300). The large dynamic range and the very low friction, make the RMII a powerful and easy-to-use portable master. Non-contact position sensing within the feedback structure was integrated, thus, the RMII does not need a separate sensing glove. However, the palm can not close completely so that it is not possible to feel remote/virtual objects with small dimensions. In addition, it offers a relatively small bandwidth, and there is a need for many out of body supporting equipment such as air-supply and electro-valves.

Currently, a joint JPL and Rutgers University research is underway to determine the potential of using electrorheological fluids [Bar-Cohen, et al, 1999] to produce miniature controlled stiffness elements. These elements are intended to be made miniature and support such remote control

mechanisms as cybergloves and others. To examine the applicability of this Remote MEchanical Mirroring using Controlled stiffness and Actuators (MEMICA) technology, joint efforts are being made to use the NASA Johnson Space Center Robonaut as a testbed.

### ACKNOWLEDGEMENT

The portions of this chapter that were written JPL employees were done at the Jet Propulsion Laboratory, California Institute of Technology, under a contract with the National Aeronautics and Space Administration.

### 10.3.3 REFERENCES

- Bar-Cohen, Y. C. Pfeiffer, C. Mavroidis and B. Dolgin, January 27, 1999, "Remote MEchanical Mirroring using Controlled stiffness and Actuators (MEMICA)," Submitted as a New Technology Report, January 18, 1999, Item No. 0237b, Docket 20642.
- Bejczy, A., and J. Salisbury, 1980, "Kinematic Coupling Between Operator and Remote Manipulator," *Advances in Computer Technology*, Vol. 1, pp. 197--211, ASME.
- Berkelman, P. J., Butler, Z. J., and Hollis, R. L., 1996, "Design of a Hemispherical Magnetic Levitation Haptic Interface Device," *Proceedings of the 1996 ASME IMECE*, Atlanta, November 17-22, 1996, DSC-Vol. 58, pp. 483-488.
- Brown, M. and Reger, B., 1998, "The Haptics Community Web-Page", <http://haptic.mech.nwu.edu/>.
- Burdea G., J. Zhuang, E. Roskos, D. Silver and N. Langrana, 1992, "A portable dexterous master with force feedback," *Presence -- Teleoperators and Virtual Environments*, Vol. 1(1), pp. 18-28.
- Burdea G. and N. Langrana, 1993, "Virtual force feedback: Lessons, Challenges, Future Applications," *Journal of Robotics and Mechatronics*, Vol. 5, No. 2, Japan.
- Burdea, G., 1996, *Force and Touch Feedback for Virtual Reality*, John Wiley & Sons, New York.
- Cybernet Systems Co., 1995, Company brochure, Ann Arbor, MI.
- Exos Co., 1993, *Force ArmMaster Specifications, Company Brochure*, Woburn, MA.
- Gomez D., G. Burdea and N. Langrana (1995), "Integration of the Rutgers Master II in a Virtual Reality Simulation," *IEEE Virtual Reality Annual International Symposium (VRAIS)*, pp. 198-202.
- Haptic Technologies, 1999, <http://www.haptech.com/prod/index.htm>.
- Howe, R., 1998, "Introduction to Haptic Display: Tactile display," *the Haptics Community Web Page*, <http://haptic.mech.nwu.edu/intro/tactile/>.
- Jau, B., A. Lewis and A. Bejczy, 1994, "Anthropomorphic Telemanipulation in Terminus Control Mode," *Proceedings of Ro-ManST'94*.
- Immersion Corp., 1999, <http://www.force-feedback.com/research/research.html>.
- Li, L. 1993, "Virtual Reality and Telepresence Applications in Space Robotics," *Virtual Reality Systems*, Vol. 1, No. 2, pp. 50-56.
- Luecke G., 1995, "Robotic & Magnetic interface for Force Interaction with Virtual Reality," National Science Foundation Grant, Robotics and Machine Intelligence, Washington DC.

Massie T. and K. Salisbury (1994), ``The PHANTOM Haptic Interface: A Device for Probing Virtual Objects," *ASME Winter Annual Meeting*, DSC-Vol. 55-1, pp. 295--300.

Microsoft, 1999, <http://www.microsoft.com/products/hardware/sidewinder/force-feedback/sidewinder1.htm>

Salisbury, K. and Srinivasan, M. (Eds.), 1996, "Proceedings of the First PHANTOM User's Group Workshop," September 1996, MIT, MA.

Sensible Technologies, 1999, <http://www.sensible.com/products/desktop.htm>

US Navy Office of Training Technology (OTT), 1999, "Haptic (Sensory/Touch) Interfaces," [http://www.ott.navy.mil/1\\_3/1\\_3\\_5/](http://www.ott.navy.mil/1_3/1_3_5/)

Virtual Technologies, 1999, <http://www.virtex.com/> .